

**SYNTHESIS AND CHARACTERIZATION OF MIXED ALKALINE
EARTH SULPHIDE PHOSPHORS ACTIVATED BY COPPER FOR
FIBER OPTIC FLUORESCENCE THERMOMETRY**

THESIS

Submitted in partial fulfillment
of the requirements for the degree of
DOCTOR OF PHILOSOPHY

By

KAILASH CHANDRA SATI

Under the supervision

of

Prof. R. P. Khare



**BIRLA INSTITUTE OF TECHNOLOGY AND SCIENCE
PILANI (RAJASTHAN)
2005**

**BIRLA INSTITUTE OF TECHNOLOGY AND SCIENCE
PILANI (RAJASTHAN)**

CERTIFICATE

This is to certify that the thesis entitled “Synthesis and Characterization of Mixed Alkaline Earth Sulphide Phosphors Activated by Copper for Fiber Optic Fluorescence Thermometry” and submitted by Kailash Chandra Sati. ID No. 2001PHXF401 for award of Ph.D. Degree of the Institute embodies the original work done by him under my supervision.

Signature in full of the Supervisor



Name in capital block letters

R. P. Khare

Date: 14.7.2025

Designation

Professor
Engineering Services Division
B. I. T. S., Pilani-333031

Abstract

Thermometry is the science of measuring temperature or the degree of heat of a particular object or body. The importance of this branch of science can be judged from its relevance to most spheres of scientific activity, industry and indeed to daily life. Interest in fiber optic sensors, for temperature sensing, stems from the fundamental differences between an optical fiber and a metal wire for signal transmission. These differences give fiber optic sensors the following valuable characteristics: electrical, magnetic and electromagnetic immunity, small sensor size, safety, capability of remote measurements, simplicity of calibration, etc.

As the sensor can be formed using either the fiber itself as the sensing medium (termed as "intrinsic sensing") or a material of structure attached to the end of the fiber (termed as "extrinsic sensing"). The number of possible fiber optic temperature sensor devices is quite large.

One thermometric technique that is adaptable to the needs of a wide variety of situations is based on fluorescing materials, many of them phosphors. The thermal dependence of phosphor fluorescence may be exploited to provide for a noncontact, emissivity-independent, optical alternative to other more conventional techniques, e.g., those employing pyrometry, thermocouples, or thermistors.

The number of such phosphors, which satisfy the requirement of linearity of response, spectral tunability, stability and ease of synthesis, are indeed very few. Therefore, there is a need to investigate more materials for this application. In this context, copper activated alkaline earth sulphides seem to be promising candidates as these phosphors can be easily synthesized, they are quite stable over long period of time, if protected from moisture and their fluorescence is sensitive to temperature. Although these phosphors have been known for a very long time and their photoluminescence, cathodoluminescence and electroluminescence have been reported by many investigators in single sulphides as well as mixed sulphides, no systematic efforts have been made to study the temperature dependence of fluorescence of this system. Therefore, the present work aims at investigating the fluoro-optic behaviour of copper-activated mixed alkaline earth sulphide phosphors at room temperature and as a function of temperature. The mixed lattice has been chosen because it is possible to tune the peak wavelength of emission by varying the relative fraction of constituent sulphides.

The objectives of the present investigations are:

- (i) To synthesize mixed alkaline earth sulphide phosphors activated by copper
- (ii) To ascertain the crystalline structure of synthesized materials
- (iii) To know the nature of luminescence centres responsible for emission
- (iv) To infer the mechanism of thermal quenching and the nature of other processes involved in the luminescence of these materials; and
- (v) To assess the suitability of these materials for thermographic applications

Consistent with these objectives, three series of mixed alkaline earth sulphides have been synthesized by solid state fusion reaction. They are (Ca, Sr)S:Cu, (Ba, Sr)S:Cu, and (Ca, Ba)S:Cu. The following investigations have been carried out on all the three series of phosphors.

- 1 Recording of X-ray diffraction spectra
- 2 Recording of excitation spectra
3. Recording of fluorescence spectra at RT
- 4 Study of the variation of fluorescence intensity at λ_{\max} (wavelength of maximum emission) with temperature
5. Recording of lifetime of fluorescence at λ_{\max} at RT.
6. Study of the variation of lifetime of fluorescence at λ_{\max} with temperature.

The XRD of (Sr,Ca)S:Cu and (Sr,Ba)S:Cu phosphors exhibit sharp diffraction lines which means that these phosphors are well crystallized in the solid solution with a NaCl type structure. As the XRD is exhibiting only one phase in all the ratios of Ca/Sr and Ba/Sr, it is clear that the solid solution has been formed for the complete range from 0 to 100 mole % for these two series of phosphors. The lattice constant in both the cases increases linearly with increase in x (the fraction of Sr or Ba in the mixed lattice) of $(\text{Ca}_{(1-x)}\text{Sr}_{(x)})\text{S}:\text{Cu}$ and $(\text{Sr}_{(1-x)}\text{Ba}_{(x)})\text{S}:\text{Cu}$ respectively. This means that these two solid solutions obey Vegard's law.

The XRD of (Ca,Ba)S:Cu phosphors show the presence of both the phases for all ratios of CaS/BaS. However the intensities of diffraction lines vary with the change in the content of respective phases.

The excitation spectra of single alkaline earth sulphides i.e SrS:Cu, BaS:Cu and CaS:Cu appear to consist of two peaks that are merged to form a single broad band peaking in the range from 0.30 to 0.40 μm . The peaks are not affected by change in concentration of activator; however the intensity changes. In the case of mixed sulphides, as expected, the peak

wavelength varies with the change in the ratio of constituent sulphides. Consistent with these results, we have used the radiation of 0.3650 μm wavelength for excitation of fluorescence in all the samples.

In the case of $(\text{Sr}_x\text{Ca}_{(1-x)})\text{S}:\text{Cu}$ phosphors, as the value of x varies from 0 (for pure $\text{CaS}:\text{Cu}$) to 1 (for pure $\text{SrS}:\text{Cu}$), the emission peak monotonously shifts from 0.49 μm (for pure $\text{CaS}:\text{Cu}$) to 0.52 μm (for pure $\text{SrS}:\text{Cu}$). Similarly in the case of $(\text{Ba}_x\text{Sr}_{(1-x)})\text{S}:\text{Cu}$ phosphors, as the value of x varies from 0 to 1, the emission peak shifts from 0.52 μm to 0.61 μm . This behavior further confirms the formation of the mixed lattice in these two cases. The shift in the emission peak may be attributed partially to a change in the band gap and partially to a change in the crystal structure. This property of these two series of phosphors is interesting from the point of view of tuning of the emitted fluorescence by simply varying the relative fraction of the constituent sulphides.

The third series of phosphors, namely, $(\text{Ca},\text{Ba})\text{S}:\text{Cu}$ shows phase dominated fluorescence. Thus phosphors with higher fraction of CaS emit 0.49 μm whereas those with higher fraction of BaS emit 0.61 μm . This behavior also shows that the mixed lattice has not been formed.

The record of the variation of fluorescence intensity at λ_{max} (the wavelength of maximum intensity at RT) as a function of temperature for single alkaline earth sulphides activated by copper shows that the fluorescence intensity decreases in all the cases. However the brightness of phosphors is in the following order $\text{SrS}:\text{Cu} > \text{BaS}:\text{Cu} > \text{CaS}:\text{Cu}$. There is no significant variation in the trend with the concentration of dopant i.e copper.

In the case of mixed alkaline earth sulphide phosphors this variation has been found to be much more pronounced for $(\text{Sr},\text{Ba})\text{S}:\text{Cu}$, $(\text{Sr},\text{Ca})\text{S}:\text{Cu}$, $(\text{Ca},\text{Ba})\text{S}:\text{Cu}$ phosphors respectively. No shift in λ_{max} with temperature has been found in any of the phosphors; though all of them exhibited thermal quenching.

At λ_{max} , with pulsed excitation the decay of fluorescence was recorded at different temperatures for all the phosphors. From these records, the lifetime (τ) of fluorescence at different temperature was determined. We utilized these values of τ to calculate the activation energy W involved.

In conclusion, copper activated mixed alkaline earth sulphides seems to be the potential candidates for fiber optic fluorescence thermometry because (i) their fluorescence intensity varies markedly with temperature (at least in the range of investigation from RT to about 150 $^\circ\text{C}$) and (ii) their lifetime also varies with temperature. Furthermore, the peak wavelength of

emission can be tuned in $(\text{Sr}_x\text{Ca}_{(1-x)})\text{S}:\text{Cu}$ and $(\text{Ba}_x\text{Sr}_{(1-x)})\text{S}:\text{Cu}$ phosphors by varying the fraction x . These phosphors may be used in the variety of thermographic applications such as electric machinery, flow tracing, gas centrifuges, heat flux, particle beam characteristics etc.

Key words: Mixed alkaline earth sulphides , fiber optic sensing materials, temperature sensitive fluorescent materials, photoluminescent materials.

Acknowledgement

It gives me immense pleasure to remember his ever smiling face that imparts me the courage to enjoy the cumbersome work and no word could adequately express the deep sense of gratitude I owe to my beloved supervisor, Dr. R. P. Khare, Professor, Engineering Services Division, BITS, Pilani. He has been wonderful, being a consistent source of vast guidance and inspiration throughout the course of this work by sparing his valuable time for numerous discussions on the subject at every stage of its progress.

I am deeply indebted to Professor R. C. D. Kaushik, Director and Dr. B. K. Khan, Principal, BRCM College of Engineering and Technology, Bahal, who motivated and permitted me to register for PhD programme when I was Lecturer there.

I am grateful to Professor S. Venkatesawaran, Vice Chancellor, BITS, Pilani, and Professor L. K. Maheshwari, Director, BITS, Pilani for allowing me to carry out my research work in this Institute.

I am also thankful to Professor Ravi Prakash, Dean, Research and Consultancy Division, BITS, Pilani and Dr. S. D. Pohekar, for their cooperation and encouragement, during various stages of this work.

My special thanks are extended to Prof. K. E. Raman, Deputy Director (Administration), and Mr. R. Purohit, for providing facilities and help for carrying out my research work at BITS, Pilani.

Much appreciation is expressed to Prof. S. Gurunakaran, Prof Surekha Bhanot and Prof. V. K. Chaubey who are the members of Doctoral Advisory Committee (DAC), for their kind suggestions, moral support and assistance.

My sincere thanks also due to Dr. M. Ishwar Bhatt, Librarian, BITS, Pilani for allowing me to use library facility; Dr. P. Srivastava, Assistant Professor, IIT Delhi for providing useful literature and Punctet Arora, Engineer Systems, Jet Blue Airlines, New York, and Himanshu Suyal, Research Scholar, Heriot-Watt University, Edinburgh for supplying various research papers during literature survey.

Further I wish to express my deep gratitude to Anil Kumar Director, Mr. K. S. Jindal, Ex-Director, Mr. V. P. Pande, Divisional Head, and Mr. A. K. Shrivastava, Head, Resonator Group, all from Laser Science & Technology Centre (DRDO), Delhi for providing essential facilities at the center as well as moral support during the course of research.

I am also indebted to Mr. Ramesh Kumar, Rashmi Rai and Mr. Mukesh Kumar for assisting me in recording X-ray diffraction spectra at LASTEC, Delhi.

I also wish to thank Mr. Ramesh Sharma, Om Prakash, and Suresh Kumar for providing necessary facilities for word processing and Mr. K. N. Sharma, (BITS) Mr. Ishar Kumar, and Pradeep (LASTEC) for preparing nice drawings for thesis.

I would like to express gratitude to my close friends, Mr. B. M. Sundriyal, Priti Arora, Mr. Rajendra Khapre, Mr. Satvir Singh and Mr. Pradeep Yadav, Mr. N. R. Das, Mr. A. K. Bahel, Ms. Neena Sati, Mr. Rohit Gupta, Mr. Subodh Kumar, Mr. R. V. Ralegaonkar and all other friends who supported and helped in some way or the other during the course of this work.

Last but not least, this work would not have been completed without the blessings of my parents.



Kailash Chandra Sati

Table of Contents

Abstract	i
Acknowledgment	v
Table of Contents	vii
List of Tables	xi
List of Figures	xii
List of Symbols/Abbreviations	xv
1 Introduction	
1.1 Thermometry: An Overview	1
1.2 Fiber-optic Fluorescence Thermometry	3
1.2.1 The Nature of Fluorescent Materials	3
1.2.2 History of the Technique	4
1.3 Physical Principles of Fluorescence Thermometry	7
1.3.1 The Fluorescence Process	7
1.3.2 Factors Influencing the Fluorescence Process	10
1.3.3 Fluorescence Intensity	16
1.3.4 Fluorescence Lifetime	16
1.3.5 Fluorescence Line Shift	18
1.4. Statement of the Problem	19
References	22
2 Synthesis of Phosphors	
2.1 Introduction	28
2.2 Phosphor Composition	28
2.2.1 Host Material	28
2.2.2 Activator	28
2.2.3 Flux	29
2.2.4 Mixed Lattice Phosphors	30
2.3 Synthesis of Phosphors	31
2.3.1 General Considerations	31

2.3.2 Present method of synthesizing phosphors	31
References	36
3. X- ray Diffraction Spectra	
3.1 Introduction	38
3.2 Powder Method of X-Ray Diffraction	38
3.2.1 Optical Arrangement	40
3.2.2 Choice of Radiation	42
3.2.3 Filtered Radiation	43
3.2.4 Effect of Specific Absorption	44
3.2.5 Effect of Sample Size	44
3.3 Indexing of cubic Crystal	45
3.4 Experimental Setup for Present Investigation	46
3.5 Results	48
References	56
4. Excitation and Emission Spectra	
4.1 Introduction	57
4.2 Theories of Luminescence	57
4.2.1 Configurational Coordinate Model	57
4.2.2 Continuous Dielectric Model	60
4.2.3 Energy Band Model	60
4.3 Processes in Crystalline Phosphors	61
4.3.1 System in Which the Absorption and Emission of Energy Take Place in the Same Centre	61
4.3.2 Systems in Which Absorption Occurs in One Centre and the Luminescence is Emitted by Another Centre and the Transfer of Energy Takes Place without Movement of Charge Carriers	65
4.3.3 Systems in which the transport of energy by charge carriers is the dominant feature	66
4.4 Experimental Setup for Recording Excitation Spectra	66

4.4.1 Xenon Lamp	66
4.4.2 Optical Filters	67
4.4.3 Monochromator	67
4.4.4 Detector and Readout	69
4.5 Experimental Setup for Recording Fluorescence Spectra and Decay of Fluorescence	69
4.6 Results	76
4.6.1 Excitation spectra	76
4.6.2 Emission Spectra	79
References	85
5. Temperature Dependence of Fluorescence	
5.1 Introduction	87
5.2 Theory of Temperature Dependence of Fluorescence	87
5.3 Some Relevant Parameters Related to Thermal Quenching	88
5.3.1 Kinetics and Decay of Luminescence	89
5.4 Results	91
5.4.1 Variation of Fluorescence Intensity with Temperature	91
5.4.2 Calculation of Relevant Parameters	98
5.4.3 Variation of Lifetime of Fluorescence	103
References	110
6. Discussion and Conclusions	
6.1 Introduction	112
6.2 X-Ray Diffraction (XRD) Spectra	113
6.3 Excitation and Emission Spectra	114
6.4 Temperature Dependence of Fluorescence	117
6.5 Conclusions	119
6.5.1 Electrical Machinery	119
6.5.2 Flow Tracing	120
6.5.3 Gas Centrifuges	120
6.5.4 Heat Flux	120

4.4.1 Xenon Lamp	66
4.4.2 Optical Filters	67
4.4.3 Monochromator	67
4.4.4 Detector and Readout	69
4.5 Experimental Setup for Recording Fluorescence Spectra and Decay of Fluorescence	69
4.6 Results	76
4.6.1 Excitation spectra	76
4.6.2 Emission Spectra	79
References	85
5. Temperature Dependence of Fluorescence	
5.1 Introduction	87
5.2 Theory of Temperature Dependence of Fluorescence	87
5.3 Some Relevant Parameters Related to Thermal Quenching	88
5.3.1 Kinetics and Decay of Luminescence	89
5.4 Results	91
5.4.1 Variation of Fluorescence Intensity with Temperature	91
5.4.2 Calculation of Relevant Parameters	98
5.4.3 Variation of Lifetime of Fluorescence	103
References	110
6. Discussion and Conclusions	
6.1 Introduction	112
6.2 X-Ray Diffraction (XRD) Spectra	113
6.3 Excitation and Emission Spectra	114
6.4 Temperature Dependence of Fluorescence	117
6.5 Conclusions	119
6.5.1 Electrical Machinery	119
6.5.2 Flow Tracing	120
6.5.3 Gas Centrifuges	120
6.5.4 Heat Flux	120

6.5.5 Particle Beam Characteristics	120
6.6 Suggestions for Further Research	121
References	123

	35
values of $h^2 + k^2 + l^2$	45
	49
	50
	51
	52
	53
	75
(λ_{\max}) of alkaline	79
h copper	
hing	102
	109
of single alkaline	115
Cu	

List of Tables

Table	Title	Page No.
Table 1.1:	Early phosphors thermometry systems and the applications	5
Table 1.2 :	The dependence of the rise time of the $^5D_0 \rightarrow ^7F_2$ transition on the concentration of Eu^{3+} in $Y_2O_3:Eu^{3+}$	12
Table 1.3:	Experimental band gap energies of alkaline earth sulphide	20
Table 2.1:	Composition of SrS:Cu phosphors	32
Table 2.2:	Composition of BaS:Cu phosphors	33
Table 2.3:	Composition of CaS:Cu phosphors	33
Table 2.4:	Composition of (Ca,Sr)S:Cu phosphors	34
Table 2.5:	Composition of (Sr,Ba)S:Cu phosphors	34
Table 2.6:	Composition of (Ca,Ba)S:Cu phosphors	35
Table 3.1:	Planes (h, k, l) and corresponding values of $h^2 + k^2 + l^2$	45
Table 3.2:	d_{hkl} and 'a' values for SrS: Cu	49
Table 3.3:	d_{hkl} and 'a' values for BaS: Cu	50
Table 3.4:	d_{hkl} and 'a' values for CaS: Cu	51
Table 3.5:	d_{hkl} and 'a' values for (Sr,Ca)S:Cu	52
Table 3.6:	d_{hkl} and 'a' values for (Sr,Ba)S:Cu	53
Table 4.1:	Special features of oscilloscope	75
Table 4.2:	The maximum emission wavelength (λ_{max}) of alkaline earth sulphide phosphors activated with copper	79
Table 5.1:	Parameters relevant to thermal quenching for alkaline earth sulphides phosphors	102
Table 5.2:	Calculation of W	109
Table 6.1:	Summary of emission spectra at RT of single alkaline earth sulphide phosphors activated by Cu	115

Fig 4.2: Scitz model	59
Fig 4.3: Model of Dexter, Klick & Russel	59
Fig. 4.4: Energy band model	61
Fig. 4.5: Modes of excitation and physical picture of absorption processes	62
Fig 1.6 : Jablonski model	64
Fig. 4.7: Block diagram of experimental setup for recording at RT	67
Fig 4.8: Block diagram of experimental setup for recording fluorescence spectra at RT, decay time and temperature dependence of fluorescence	71
Fig.4.9: Optical path in mirror monochromator 'SPM2'	72
Fig 4.10: Excitation spectra of representative samples of S- series of phosphors (SrS:Cu)	76
Fig 4.11: Excitation spectra of representative samples of B- series of phosphors (BaS:Cu)	76
Fig 4.12: Excitation spectra of representative samples of C- series of phosphors (CaS:Cu)	77
Fig 4.13: Variation of peak λ_{exc} with fraction, x for $(Sr_xCa_{(1-x)})S:Cu$ (0.003M)	78
Fig 4.14: Variation of peak λ_{exc} with fraction, x for $(Sr_xBa_{(1-x)})S:Cu$ (0.003M)	78
Fig 4.15: Variation of peak λ_{exc} with fraction, x for $(Ba,Ca)S:Cu$ (0.001M)	79
Fig 4.16: Emission spectra of representative samples of S- series of phosphors (SrS:Cu)	80
Fig 4.17: Emission spectra of representative samples of B- series of phosphors BaS:Cu	80
Fig 4.18: Emission spectra of representative samples of C- series of phosphors (CaS:Cu)	81
Fig 4.19(a): Emission spectra of representative samples of CS- series of phosphors, (Sr, Ca)S:Cu	82
Fig 4.19(b): Plot of λ_{max} as a function of lattice parameter for (Sr,Ca)S:Cu	82
Fig 4.20(a): Emission spectra of representative samples of SB- series of phosphors, (Sr,Ba)S:Cu	83
Fig 4.20(b): Plot of λ_{max} as a function of lattice parameter for (Sr,Ba)S:Cu	83

Fig 4.21: Emission spectra of representative samples of CB- series of phosphors, (Ba,Ca)S:Cu	84
Fig 5.1: Definition of parameters	89
Fig 5.2: Temperature dependence of fluorescence intensity of representative samples of SrS:Cu	92
Fig 5.3: Temperature dependence of fluorescence intensity of representative samples of BaS:Cu	93
Fig 5.4: Temperature dependence of fluorescence intensity of representative samples of CaS:Cu	94
Fig 5.5: Temperature dependence of fluorescence intensity of representative samples of (Sr,Ba)S:Cu	95
Fig 5.6: Temperature dependence of fluorescence intensity of representative samples of (Sr,Ca)S:Cu	96
Fig 5.7: Temperature dependence of fluorescence intensity of representative samples of (Ca,Ba)S:Cu	97
Fig. 5.8: Plots of $\ln(I_0/I)$ versus $1/T$ for representative samples	98
Fig.5.9: Record of Rise and Decay of fluorescence of $(\text{Sr}_{0.9}, \text{Ba}_{0.3})\text{S}:\text{Cu}$ phosphor at different temperatures	103
Fig.5.10: Plots of $\ln(\tau_0/\tau)$ vs. $1/T$ for representative phosphors	106
Fig 6.1: Energy level diagrams of a free Cu^+ ion and a Cu^+ ion in octahedral crystal field	116
Fig 6.2: Schon –Klasens model for thermal quenching of luminescence in sulphide phosphors	118

List of Symbols /Abbreviations

a	Edge of the cubic lattice
a_A	Lattice constant of A
a_B	Lattice constant of B
a_j	Probability rate
a_s	Lattice constant of solid solution
$A_{1,2}$	Radiative spontaneous emission
AEDC	Arnold Engineering Development Center
AR	Analytical reagent
C	Conduction band
CRT	Cathode-ray tube
CT	Charge transfer
CTS	Charge transfer state
Co	Cobalt
Cu	Copper
DC	Direct current
F	Excited state
Fe	Iron
G	Ground state
gm	gram
I	Luminescence intensity
kV	kilo Volt
JCPDS	Joint Committee for Powder Diffraction Standards
L_1	Occupied state of luminescence centre
L_2	Unoccupied state of luminescence centre
L_3	Ground state of luminescence centre
L_4	Excited state of luminescence centre
mV	Milivolt
M	Metastable state

n	Order of diffraction
N	Number of photons
Ni	Nickel
ns	Nanosecond
ORNL	Oak Ridge National Laboratory
PMT	Photomultiplier tube
PWHM	Peak width at half maximum
P_{nr}	Probability of non-radiative transitions
P_r	Probability of radiative transitions
QE	Quantum efficiency
R_0	Critical distance for energy transfer
RF	Radio Frequency
RT	Room temperature
s	Frequency factor
T	Temperature
T_B	Breaking Point Temperature
$T_{1/2}$	Half-Value Temperature
T_Q	Quenching Temperature
UV	Ultraviolet
V	Valence band
W	Thermal activation energy
$W_{1,2}$	Nonradiative spontaneous emission
x	Mole fraction
XRD	X-ray diffraction
YAG	Yttrium Aluminium Garnet
ΔE	Energy
$^{\circ}\text{C}$	Degree centigrade
Å	Angstrom
hkl	Miller indices
τ	Lifetime

n	Order of diffraction
N	Number of photons
Ni	Nickel
ns	Nanosecond
ORNL	Oak Ridge National Laboratory
PMT	Photomultiplier tube
PWHM	Peak width at half maximum
P_{nr}	Probability of non-radiative transitions
P_r	Probability of radiative transitions
Q_E	Quantum efficiency
R_0	Critical distance for energy transfer
RF	Radio Frequency
RT	Room temperature
s	Frequency factor
T	Temperature
T_B	Breaking Point Temperature
T_H	Half-Value Temperature
T_Q	Quenching Temperature
UV	Ultraviolet
V	Valence band
W	Thermal activation energy
$W_{1,2}$	Nonradiative spontaneous emission
x	Mole fraction
XRD	X-ray diffraction
YAG	Yttrium Aluminium Garnet
ΔE	Energy
$^{\circ}C$	Degree centigrade
Å	Angstrom
hkl	Miller indices
τ	Lifetime

κ	Reciprocal of decay rate
μs	Microsecond
μA	Micro ampere
λ_{max}	Wavelength of maximum emission
ψ	Limiting range of the goniometer arc
λ	Wavelength
θ	Angle of diffraction
μ	Linear absorption coefficient
λ_{exc}	Wavelength of excitation
η	Fluorescence efficiency

Chapter 1

Introduction

1.1 Thermometry: An Overview:

Thermometry is the science of measuring temperature or the degree of heat of a particular object or body. The importance of this branch of science can be judged from its relevance to most spheres of scientific activity, industry and indeed to daily life. Almost all chemical processes and reactions are temperature dependant. Not infrequently in chemical plant, temperature is the only indication of the progress of the process, which is occurring. Where the temperature of the operation is critical to the reaction, a considerable loss of efficiency may result from the use of incorrect temperature. In some cases, loss of control of temperature can result in catastrophic plant failure with attendant damage and possible loss of life. There are many other areas of industry where temperature measurement is essential. Such applications include steam raising and electricity generation, plastic and glass manufacturing and moulding, manufacturing processes in metallurgical industries, in milk and dairy products and many other aspects of the food industries. Further in biomedical areas, the taking and regular monitoring of patients' temperature provide a basic diagnostic criterion, and it is essential during the treatment of hyperthermia, for the safety of patients. The importance of temperature measurements can even be seen simplistically by consideration of the financial aspects of the sensors and devices used internationally. Estimates of the world-wide sales of temperature sensors run to several hundred million dollars per year, a figure that could be increased several times when the associated controllers, indicators, and other aspects of measurement systems are added. A comprehensive account of various aspects of temperature measurement has been given by Michalski, Eckersdorf and McGhee[1].

Although a wide range of existing instruments are available for use either in the industry or in the laboratory, or under special industrial conditions, innovation and research and development activities in temperature monitoring continue, due to the ever extending use of thermometers in the industrial and biological research and development spheres. These environments can present a number of real difficulties for the determination of temperature. The region to be measured may be extremely hostile, moving or in a position where access is extremely difficult, or where the physical contact of a sensing probe may even be impossible,

or where the presence of interference from other forms of electromagnetic noise excludes the use of electronic thermometers. For example these situations may be the measurement of the temperature of a rotating blade of a turbine-engine, the monitoring of winding temperature in electrical transformers, and temperature monitoring during clinical RF heat treatment. In order to seek alternative means of temperature sensing, one of the most active research and development areas is in thermometry based on the use of fiber optics.

The primary reason for interest in fiber optic sensors, in most cases, stems from the fundamental differences between an optical fiber and a metal wire for signal transmission. These differences give fiber optic sensors the following valuable characteristics:

- Electrical, magnetic and electromagnetic immunity.
- Small sensor size
- Safety
- Capability of remote measurements
- Simplicity of calibration

There is perhaps most diversity in the techniques that are available for optically based temperature measurement, as a result of the fact that there are essentially as many ways of making a temperature measurement optically as there are temperature-dependant optical properties. As the sensor can either be formed using the fiber itself as the sensing medium (termed as "intrinsic sensing") or form a material of structure attached to the end of the fiber (termed as "extrinsic sensing"), the number of possible fiber optical temperature sensor devices is quite large. Indeed, there has been something of the explosion of device proposals seen in the literature. Extensive reviews on various proposed sensor schemes can be found in literature [2,3].

In addition, a variety of simpler optomechanical schemes, such as those employing changes in the intensity of reflected light, due to displacement of a reflecting surface, or grating displacement which have been proposed for pressure measurement, have been considered [4,5]. At the other extreme, highly sophisticated interferometric systems, such as the dual wavelength device which can significantly extend the usual range of a normal interferometric system, and those using white light interferometry which would be free of 'switch-on' recalibration, have been suggested [6].

The optimum selection for development among the wide choices of potentially usable sensor schemes listed above would rely strongly on matching the intended application. For industrial applications, system cost, range, ease of calibration, stability and durability would

be the primary considerations; for bio-medical purposes, probe size, sterilizability, biocompatibility and precision as well as the cost implications of disposability are of importance. If the application requires multi-point sensing then distributed sensing schemes, such as those using optical scattering properties, may be the best answer, whereas if the temperatures are very high, as in an aircraft engine, the radiometric approach may be the best. At a more basic level, there are several fundamental considerations, which need to be taken into account as well. Sensor fabrication should, as far as possible, be simple. The performance of the instrument should not depend on which individual sensor is being used. Substitution of sensors should be quick and easy and ideally, the system should not require calibration before use or after sensor replacement. If a calibration is required, it should be very simple to perform, preferably by the user, *in situ*. The sensor materials or structure should be very stable over time, with repeated thermal excursions.

Most importantly, the performance of the system has to be insensitive to optical signal changes such as those caused by fiber bending, light source degradation, variable connector losses, or changes in fiber transmission over time. Many of the early sensor designs were based on the detection of a simple change of light intensity with temperature. In these systems it was often impossible to separate the effects of thermally induced changes in intensity from other non-thermal sources of signal changes such as those discussed. Therefore, in the most successful systems available today, some type of intensity ratioing is employed or a temperature-sensitive parameter other than intensity is detected.

1.2. Fiber-optic Fluorescence Thermometry:

One thermometric technique that is adaptable to the needs of a wide variety of situations is based on fluorescing materials, many of them phosphors. The thermal dependence of phosphor fluorescence may be exploited to provide for a noncontact, emissivity-independent, optical alternative to other more conventional techniques, e.g., those employing pyrometry, thermocouples, or thermistors. In fact, as discussed below, there are certain situations in which the advantages fluorescence-based thermometry has over other methods make it the only useful approach.

1.2.1 The Nature of Fluorescent Materials:

Prior to discussing those properties of phosphors important to thermometry, some relevant terminology should be introduced. Luminescence refers to the absorption of energy by a material, with the subsequent emission of light. This is a phenomenon distinct from blackbody radiation, incandescence, or other such effects that cause materials to glow at high

temperature. Fluorescence refers to the same process as luminescence, but with the qualification that the emission is usually in the visible band and has a duration of typically 10^{-9} - 10^{-3} s. Phosphorescence is a type of luminescence of greater duration, $\approx 10^{-1}$ - 10^3 s. Emission, luminescence, phosphorescence, and fluorescence are closely related terms and sometimes are used interchangeably [7]

A phosphor is a fine white, or slightly colored, powder designed to fluoresce very efficiently. Color television and cathode-ray tube (CRT) displays employ phosphor screens that emit visible light then seen by the viewer. The source of energy that excites this fluorescence is a beam of electrons. Other examples of phosphor uses are in fluorescent spray paints, fluorescent lighting, photocopy lamps, scintillators and x-ray conversion screens. For the last, a beam of x rays provides the excitation. Other excitation sources are neutrons, gamma rays, ultraviolet (UV) light and, in some cases, visible light. Many different phosphors are manufactured for these and other applications. The lighting and display industries have provided the impetus for the study of thousands of phosphor materials over the last several decades, and much is known about them [8-10].

In terms of their composition, phosphors may be divided into two classes; organic and inorganic. It is the latter that have primarily but not exclusively found use in thermometry. Inorganic phosphors consist of two components; a host inorganic compound and an activator (or doping agent) from which the light is emitted. Such materials do not have to be in the powdered form to be useful. Some phosphors are fabricated into macroscopic pieces of crystal or glass. In this form, certain of them are useful as solid-state laser media, and can be thought of as phosphors having a singular particle size and number density [11-14].

1.2.3 History of the Technique:

Research on luminescing materials was largely the domain of academia until the introduction of the fluorescent lamp in 1938 [9]. After this, industrial laboratories were spurred into action by the growing need for commercial and domestic lighting, and also by the need for improved cathode ray tubes. The degradation of luminescent output with increasing temperature can be detrimental in lamp applications. Therefore, thermal characterization was an important task for those studying phosphors. Neubert suggested phosphor use thermometry as early as 1937 [15]. Urbach [16, 17] contributed, to early phosphor thermometry approaches and applications. Table 1.1 surveys some of the developments important to phosphor thermometry from that time through the early 1980s.

Table 1.1 Early phosphors thermometry systems and the applications

Author(s)	Application	Phosphor/method	Design features	Range/uncertainty	(year/Ref.)
Bradley	Measurement of temperature distributions on a flat plate in supersonic flow	ZnCdS:Ag,Cu(New Jersey Zinc Co.), intensity shift	Excitation at 365 nm, With fluorescence signal passed through a Wratten 2A filter	$\approx 8-25^{\circ}\text{C}$ $\Delta T = \pm 0.2^{\circ}\text{C}$	1953 [15]
Gross et al.	Development of phosphor based detectors of thermal radiation	ZnS:Ag:Cl. CdS:Ag, intensity change and wavelength shift	Spectrometer used to monitor intensity variations and wavelength shift of heated target	$\approx 10-40^{\circ}\text{C}$ No error estimate presented by author	1960 [43] 1963 [44]
Czysz and Dixon	Thermal mapping of models in wind tunnels for heat transfer measurements	Radel in phosphors (US Radium Co.) intensity shift	Surface thermocouple heat transfer gauges used to eliminate the absolute intensity measurements	Range unspecified $\Delta T = \pm 0.2^{\circ}\text{C}$	1966 [26 -28]
Brenner	Measurement of collector junction temperatures in power transistors	Radel in No 2090 (US Radium Co.) intensity shift	ASA 400 B&W film used to sense fluorescence intensities with readout via microdensitometry	$170-210^{\circ}\text{C}$ $\Delta T = 2.0^{\circ}\text{C}$	1971 [45]
Fry	Integrated circuit	Radel in No. 3251	Fiberoptic conveys fluorescence from the IC to the detector	$60-100^{\circ}\text{C}$	1971 [46]
Kusama et al.	Determination of the temperature of color television screens	$\text{Y}_2\text{O}_2\text{S}:\text{Eu}$, line shift of the $^5\text{D}_0 \rightarrow ^7\text{F}_2$ transition	Sony Trinitron™ color CRT used, with beam currents varied from $100\mu\text{A}$ to 1 mA per RGB channel	$25-50^{\circ}\text{C}$ $\Delta T = 1.0^{\circ}\text{C}$	1976 [34]
Pattison	Measurement of surface temperature on rotating turbo generators	Levy West W800 in transparent lacquer, intensity shift	Fiberoptic cables used to convey excitation and emission signals through the generator housing	No specific range or error estimate presented by author	1977 [47]
Wickersheim and Alves	Measurements of requiring isolation from or immunity to electromagnetic fields	Eu^{3+} -doped, rare-earth oxysulfides, line-intensity ratios	Prefiltration of UV excitation radiation by reflection from series of dichroic mirrors	$9-250^{\circ}\text{C}$ Noise equivalent temp. $= 0.025^{\circ}\text{C}$	1979 [18]
Sholes and small	Thermal dosimetry during rf-hyperthermia treatments of malignant tumors	$\text{Al}_2\text{O}_3:\text{Cr}^{3+}$ (0.05%), decay lifetime of R lines	Mechanical shutter exposes the ruby sample to the excitation source for 10 ms intervals	$35-46^{\circ}\text{C}$ (Partial range) $\Delta T = 0.3^{\circ}\text{C}$	1980 [22]
Samulski and Shrivastava	Thermal dosimetry during rf-hyperthermia treatments of malignant tumors	Calcium and Zinc-cadmium sulfides, integrated response	0.75 ms pulses from xenon lamp used as excitation; data were taken at 1 min intervals	$20-50^{\circ}\text{C}$ Probe resolution $= 0.3-0.4^{\circ}\text{C}$	1980 [40,41]
McCormack	Measurements requiring electrically insulating and chemically inert probes	$\text{BaClF}:\text{Sm}^{2+}$ decay lifetime of the $^5\text{D}_0 \rightarrow ^7\text{F}_0$ transition	Plastic-clad silica fiber with $\text{NA} = 0.25$ was used to maximize the optical power collected	$25-200^{\circ}\text{C}$ $\Delta T = \pm 5^{\circ}\text{C}$	1981 [42]

In 1950, magnesium fluorogermanate was synthesized and used widely as a lamp phosphor [8]. Eventually, in the 1980s, it became the basis of commercial phosphor thermometry products [18,19].

One of the first thermometric applications of a phosphor known to us was by Bradley [20] who, in 1952, measured the temperature distribution on a flat wedge in a supersonic flow field using a phosphor provided by Urbach. Fluorescence thermometry in the 1950s is surveyed in a paper by Byler and Hays [21] of U.S. Radium Corporation (now USR Optonix, Inc.) which marketed the phosphors identified by Urbach. In 1960, Maiman invented the ruby laser, making use of the efficient fluorescence of ruby, in which Cr^{+3} is the activator in an Al_2O_3 host. Its temperature-dependent fluorescence properties have also been used for thermometry [22-24]. Trivalent rare earth activators are now widely used, particularly Tb^{3+} , Eu^{3+} , and Dy^{3+} , in a variety of hosts. Interestingly, their use as laser media predates their use in television picture tubes. For example, Chang [25] operated a $\text{Y}_2\text{O}_3:\text{Eu}$ laser in 1963. Renowned for its relative insensitivity to temperature changes, we shall describe below situations wherein this material has nevertheless found use in practical high temperature ($> 600^\circ\text{C}$) thermometry systems. Also in the 1960s, Cysz et al [26-28] carried out phosphor thermometry on models in wind tunnels at the Arnold Engineering Development Center (AEDC), and this work has continued up to the present at this facility. They use phosphors originally investigated by Urbach. Wickersheim and colleagues [29-33] explored the possible use of rare-earth activated materials in a variety of applications, including lasers, scintillators, neutron detectors, x-ray detectors, etc. Their efforts at determining the temperature sensitivity of phosphors were fruitful, and this work eventually led to the commercialization of thermometry systems based on fluorescence. In 1977, Kusama et al [34] exploited the thermal dependence of cathode ray tube phosphors to study electron-beam heating effects in color television applications.

It was not until the 1970s that the technological tools became generally available for exploiting the thermal properties of phosphor emission in a broader range of applications. For instance, high quality optical fibers capable of ultraviolet transmission appeared at that time. A group led by Leroux developed approaches based on utilizing the temperature dependence of fluorescence intensity and temporal response [35-38] for surface thermometry purposes. By applying phosphor to the tip of an optical fiber, Wickersheim and Alves [18] produced the optical analog of a thermocouple. In 1979, James et al [39] mentioned several methods for extracting temperature from phosphor fluorescence measurements, including

phosphor time decay determination. Also pursuing this approach were Samulski and colleagues [40,41] in 1980 and McCormack [42] in 1981.

Also, from the beginning, lasers have been useful in studying and characterizing phosphors. In many situations, a laser is the most appropriate source of illumination for phosphor-based thermography, even over relatively large surfaces. Moreover, the introduction of new types of lasers makes possible new classes of thermal phosphor applications. For instance, significant advances in phosphor thermometry in the 1980s were made possible by the advent of short-pulse UV lasers.

Finally, over the past 22 years, the many advances in electro-optics and solid state electronics have enabled measurements of fluorescence decay times at the nanosecond level. Prior to this, the capture and analysis of such fast pulses lay mostly in the domain of experimental nuclear and particle physics and required expensive, sophisticated instrumentation.

Histories and reviews of phosphor-based thermometry have been written by Dowell [48] and Baumann [38]. Thorough bibliographies of the literature covering the research on thermographic phosphors carried out in the 1980s have been assembled [49, 50] and described [51] elsewhere.

1.3 Physical Principles of Fluorescence Thermometry:

It has long been generally known that the brightness or energy-to-light conversion efficiency of fluorescent materials is temperature dependent. There are several ways this temperature dependence is manifested. Since a number of factors underlies the intrinsic nature of the fluorescence process, we begin with an overview of it.

1.3.1 The Fluorescence Process:

The fundamental aspects of the fluorescence of solid materials are well understood. Prior to excitation, the material's electronic levels are populated in the ground state. A means to deposit energy in the material is required in order to excite a higher electronic state. This may be accomplished by exposure to electromagnetic radiation (visible or ultraviolet light, or X-ray or gamma rays), particle beams (electrons, neutrons, or ions), or, as is the case for semiconductors, electrical current. The atomic configuration will not typically remain permanently excited but will either return to its ground state or assume an intermediate level. Conservation principles dictate that the amount of energy absorbed must also be released. This may be manifested by emission of a photon with energy equal to that of the energy-level difference, by transfer of energy via quantized vibrational (phonon) exchange in the material, or by other more complicated energy exchange mechanisms. Generally the lifetime of the

phosphor time decay determination. Also pursuing this approach were Samulski and colleagues [40,41] in 1980 and McCormack [42] in 1981.

Also, from the beginning, lasers have been useful in studying and characterizing phosphors. In many situations, a laser is the most appropriate source of illumination for phosphor-based thermography, even over relatively large surfaces. Moreover, the introduction of new types of lasers makes possible new classes of thermal phosphor applications. For instance, significant advances in phosphor thermometry in the 1980s were made possible by the advent of short-pulse UV lasers.

Finally, over the past 22 years, the many advances in electro-optics and solid state electronics have enabled measurements of fluorescence decay times at the nanosecond level. Prior to this, the capture and analysis of such fast pulses lay mostly in the domain of experimental nuclear and particle physics and required expensive, sophisticated instrumentation.

Histories and reviews of phosphor-based thermometry have been written by Dowell [48] and Baumann [38]. Thorough bibliographies of the literature covering the research on thermographic phosphors carried out in the 1980s have been assembled [49, 50] and described [51] elsewhere.

1.3 Physical Principles of Fluorescence Thermometry:

It has long been generally known that the brightness or energy-to-light conversion efficiency of fluorescent materials is temperature dependent. There are several ways this temperature dependence is manifested. Since a number of factors underlies the intrinsic nature of the fluorescence process, we begin with an overview of it.

1.3.1 The Fluorescence Process:

The fundamental aspects of the fluorescence of solid materials are well understood. Prior to excitation, the material's electronic levels are populated in the ground state. A means to deposit energy in the material is required in order to excite a higher electronic state. This may be accomplished by exposure to electromagnetic radiation (visible or ultraviolet light, or X-ray or gamma rays), particle beams (electrons, neutrons, or ions), or, as is the case for semiconductors, electrical current. The atomic configuration will not typically remain permanently excited but will either return to its ground state or assume an intermediate level. Conservation principles dictate that the amount of energy absorbed must also be released. This may be manifested by emission of a photon with energy equal to that of the energy-level difference, by transfer of energy via quantized vibrational (phonon) exchange in the material, or by other more complicated energy exchange mechanisms. Generally the lifetime of the

excited state is short, on the order of only a few milliseconds. Neither the longer lived phosphorescent states nor the electron traps that may be present in some phosphors to varying degrees have typically been utilized for fluorescence thermometry. (Curie [52] presents additional discussion of the processes involved in these phenomena.)

Many of the materials that fluoresce efficiently and that have been found useful for a variety of laser, display, lighting, fluorographic, and thermographic applications are those for which the luminescence originates from a deliberately added impurity. As an example, a host material such as Al_2O_3 is transparent and nonfluorescent until Cr^{+3} is added. It then becomes red and fluoresces with properties that make it useful in the design of lasers and thermometry systems. The dopant concentration is usually a few percent or less so that nonradiative deexcitation exchange is minimized between the atoms (i.e., the luminescent centers are said to be isolated). Fluorescence as referred to here is the emission occurring from electronic transitions and is usually in the visible region of the spectrum, but may also be in the near infrared (IR), as from Nd, or in the UV, as is typical for Gd. Dieke and Cross [53] have given the energy-level diagrams for various well-known states of some rare earths that are commonly used as the luminescent center in a thermometry application.

It is generally true that the fluorescence spectral properties of any material will change with temperature. This is so in part because the Boltzmann distribution governs the partitioning of the populations in the various participating vibrational levels of the ground, excited, and emitting states. A change in intensity distribution (including width and position of spectral lines) results since individual oscillator strengths vary in accordance with the selection rules and the Franck-Condon principle. Kusama et al. [34] explored this for $\text{Y}_2\text{O}_2\text{S}:\text{Eu}$. They measured the temperatures of a commercially available CRT using cathode ray stimulation and subsequent observation of the line shifts.

The temperature dependence of these processes can be striking when there is competition with states which contend for nonradiative deexcitation pathways. The rate of change of the population of an emitting state, 2, to a ground state, 1, is the sum of a constant, purely radiative spontaneous emission, $A_{1,2}$, and a nonradiative component, $W_{1,2}$, which is temperature dependent.

$$\kappa = 1/\tau = A_{1,2} + W_{1,2} \quad (1.1)$$

The measured lifetime, τ is the reciprocal of decay rate, κ . One model for temperature dependence for some fluorescence materials used for thermometry is based on thermal promotion to a nonemitting electronic state followed by nonradiative relaxation. For

europium phosphors, this is cited as a charge transfer state (CTS). This is illustrated in Fig.1.1 which shows an energy level diagram based on the model that Fonger and Struck used to describe the thermal quenching of oxysulfides [54, 55].

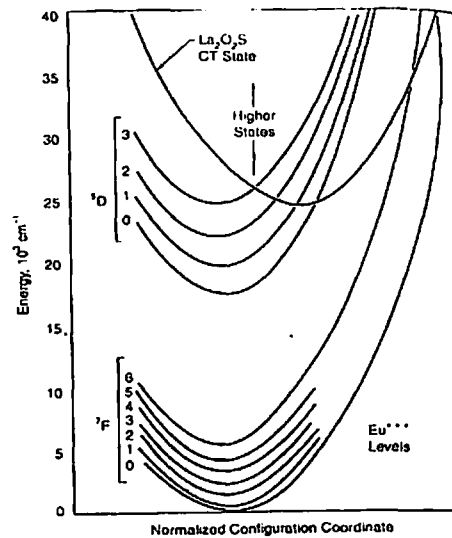


Fig 1.1: The configuration coordinate diagram for $\text{La}_2\text{O}_2\text{S}:\text{Eu}$

The excited electronic states of this atom are designated by $5 D_j$ where $j = 0, 1, 2,$ and 3 . Once the particular $5 D_j$ state is excited, by whatever means, its population may be increased or decreased via several energy transfer pathways. A radiative transition to the ground state is possible with a probability rate of a_j . Note that this is the reciprocal of the spontaneous, unquenched lifetime. Depending on the temperature, the vibrational distribution in the excited state will be given by a Boltzmann distribution. At low temperature, states in resonance with the CTS seen in Fig.1.1 are improbable. However, at higher temperature a significant fraction of the distribution will be at energies corresponding to the CTS and the transition to the CTS becomes likely. The rate is therefore proportional to $e^{(-\Delta E/kT)}$ where ΔE is the energy difference between the $5 D_j$ and the CT states and the constant of proportionality is $a_{\text{CTS},j}$. Feeding from the CTS down to the $5 D_j$ is possible. Deactivation from the CTS, is nonradiative with a rate of a_{CTS} . The rates from the CTS, according to Fonger and Struck [54, 55] are about $10^{11} - 10^{12} \text{ s}^{-1}$, i.e., on the order of a lattice vibration rate. For continuous illumination, they note that the intensity is given by

$$I(T) = [a_j + a_j A \exp(-\Delta E/kT)]^{-1}, \quad (1.2)$$

where A is related to a_{CTS} and $a_{\text{CTS},j}$, T is temperature, ΔE is energy, and k is the Boltzmann constant. Other models for some phosphors have a similar dependence.

europium phosphors, this is cited as a charge transfer state (CTS). This is illustrated in Fig.1.1 which shows an energy level diagram based on the model that Fonger and Struck used to describe the thermal quenching of oxysulfides [54, 55].

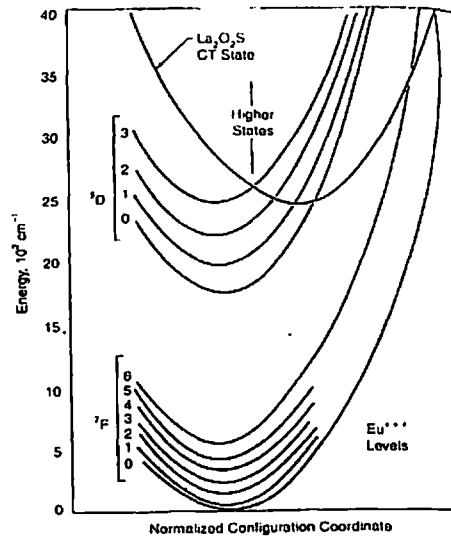


Fig 1.1: The configuration coordinate diagram for $La_2O_2S:Eu$

The excited electronic states of this atom are designated by $5D_j$ where $j = 0, 1, 2,$ and 3 . Once the particular $5D_j$ state is excited, by whatever means, its population may be increased or decreased via several energy transfer pathways. A radiative transition to the ground state is possible with a probability rate of a_j . Note that this is the reciprocal of the spontaneous, unquenched lifetime. Depending on the temperature, the vibrational distribution in the excited state will be given by a Boltzmann distribution. At low temperature, states in resonance with the CTS seen in Fig.1.1 are improbable. However, at higher temperature a significant fraction of the distribution will be at energies corresponding to the CTS and the transition to the CTS becomes likely. The rate is therefore proportional to $e^{(-\Delta E/kT)}$ where ΔE is the energy difference between the $5D_j$ and the CT states and the constant of proportionality is a_{CTSj} . Feeding from the CTS down to the $5D_j$ is possible. Deactivation from the CTS, is nonradiative with a rate of a_{CTS} . The rates from the CTS, according to Fonger and Struck [54, 55] are about $10^{11} - 10^{12} s^{-1}$, i.e., on the order of a lattice vibration rate. For continuous illumination, they note that the intensity is given by

$$I(T) = [a_j + a_i A \exp(-\Delta E/kT)]^{-1}, \quad (1.2)$$

where A is related to a_{CTS} and a_{CTSj} , T is temperature, ΔE is energy, and k is the Boltzmann constant. Other models for some phosphors have a similar dependence.

For some materials, a temperature-dependent deexcitation pathway based on multiphonon emission [56] exists. The multiphonon decay rate is

$$W_m = G [(1 - e^{-h\nu/kT})]^{-N} e^{-\gamma N E}, \quad (1.3)$$

where N is the number of photons required to reach the energy of the transition ΔE , and G and γ are characteristics of the material. This explanation has been applied to YAG hosts, [57-61] among others. If the energy difference between the ground and emitting states is four to five times the highest vibrational frequency of the surrounding lattice, then at sufficiently high temperatures a multiphonon transition is allowed and the transition probability is temperature dependent.

1.3.2. Factors Influencing the Fluorescence Process:

(a) Dopant Concentration:

The parameters describing the luminescence characteristics of any given phosphor are dependent on the concentration of the activating impurity. Overall intensity, relative spectral distribution, decay time, rise time, and response to temperature are all affected to some degree. It is standard practice when characterizing the thermal response of a given phosphor to measure its brightness as a function of dopant concentration. A representative case [62] is shown in Fig. 1.2. These data illustrate that a high dopant concentration of Eu in a host of Y_2O_3 results in most of the luminescence being concentrated into the 5D_0 emission line (at 611 nm) that is of importance to color televisions.

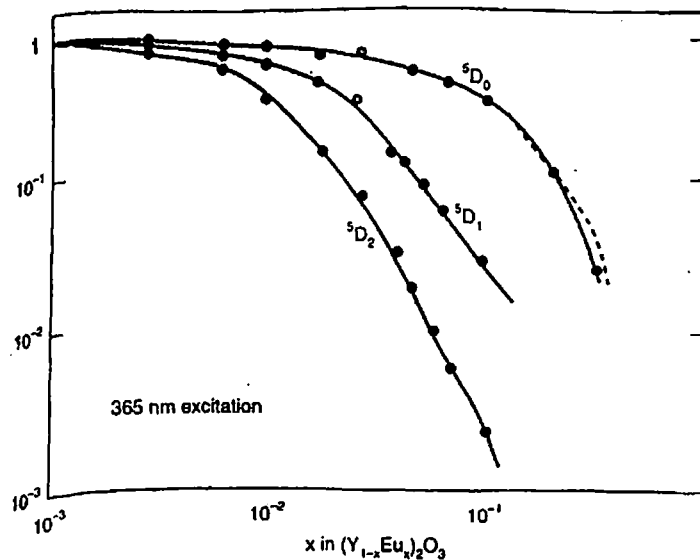


Fig 1.2: Fluorescence intensity vs dopant concentration for Eu in a host of Y_2O_3

They further illustrate that the more activator centers there are in a phosphor, the more it will fluoresce, up to a point. However, when the concentration levels reach a certain point, another nonradiative deexcitation pathway becomes important. As the activator density is increased, the probability that an excited activator will transfer energy non-radiatively to a neighboring dopant ion increases. The arrival at a cutoff in this process is usually referred to as concentration quenching. For other dopants, even when in the same host, the concentration that produces the maximum brightness will be different. For example, the optimum concentration of Sm or Dy in Y_2O_3 is 0.5% [9, 63].

Generally, one seeks to maximize the brightness of the phosphor. With respect to thermometry applications, however, there are other considerations that may warrant the use of different strategies. For instance, at high concentrations the fluorescence decay profile may not be that of simple single-exponential decay. This is important for decay-time-based approaches since multiexponential and nonexponential decay profiles are more difficult to model. (Multiexponential decay is not necessarily a problem if measurements based on continuous line intensities are being made though.) These more complex wave forms can make calibration and data analysis difficult but not intractable. An example of this phenomenon arises in the use of YAG:Tb, which is a good phosphor for high temperature thermometry. At low concentrations, about 516 of the excitation energy drives the 5D_3 states (blue bands between 350 and 450 nm) while the remainder excites the 5D_4 states (blue-green and green bands at 488 and 544 nm). At sufficiently high dopant levels, there is an energy transfer from the higher to the lower states. Whereas the latter states exhibit exponential decay at up to 3% dopant concentration, the former appear to follow the Forster model, [64,65] the decay function for which is

$$x(t)/x(0) = \exp[-t/\tau - N/N_0 (\pi t/\tau)^{1/2}] \quad (1.4)$$

where $N_0 = 3/(4\pi R_0^3)$ with R_0 being the critical distance for energy transfer (≥ 1 nm), N is the dopant concentration in number of atoms per cm^3 , and τ is the unquenched spontaneous lifetime. The implications and role of the Forster model with respect to fluorescence thermometry are discussed by Dowell [65, 66]. The spectral emission distribution can be a sensitive function of dopant concentration. An example of this is illustrated in Fig. 1.3 for $Y_2O_2S:Eu$ [67]. At low Eu concentrations, the shorter wavelength lines are stronger than they are at higher concentrations. Kusama et al.[34] noted that this is particularly important for intensity based thermometry. They indicate that the 5D_2 emission of $Y_2O_2S:Eu$ is especially sensitive to Eu concentrations. In comparing temperature dependent ratios of this line to a

They further illustrate that the more activator centers there are in a phosphor, the more it will fluoresce, up to a point. However, when the concentration levels reach a certain point, another nonradiative deexcitation pathway becomes important. As the activator density is increased, the probability that an excited activator will transfer energy non-radiatively to a neighboring dopant ion increases. The arrival at a cutoff in this process is usually referred to as concentration quenching. For other dopants, even when in the same host, the concentration that produces the maximum brightness will be different. For example, the optimum concentration of Sm or Dy in Y_2O_3 is 0.5% [9, 63].

Generally, one seeks to maximize the brightness of the phosphor. With respect to thermometry applications, however, there are other considerations that may warrant the use of different strategies. For instance, at high concentrations the fluorescence decay profile may not be that of simple single-exponential decay. This is important for decay-time-based approaches since multiexponential and nonexponential decay profiles are more difficult to model. (Multiexponential decay is not necessarily a problem if measurements based on continuous line intensities are being made though.) These more complex wave forms can make calibration and data analysis difficult but not intractable. An example of this phenomenon arises in the use of YAG:Tb, which is a good phosphor for high temperature thermometry. At low concentrations, about 516 of the excitation energy drives the 5D_3 states (blue bands between 350 and 450 nm) while the remainder excites the 5D_4 states (blue-green and green bands at 488 and 544 nm). At sufficiently high dopant levels, there is an energy transfer from the higher to the lower states. Whereas the latter states exhibit exponential decay at up to 3% dopant concentration, the former appear to follow the Forster model, [64,65] the decay function for which is

$$x(t)/x(0) = \exp[-t/\tau - N/N_0 (\pi t/\tau)^{1/2}] \quad (1.4)$$

where $N_0 = 3/(4\pi R_0^3)$ with R_0 being the critical distance for energy transfer (≥ 1 nm), N is the dopant concentration in number of atoms per cm^3 , and τ is the unquenched spontaneous lifetime. The implications and role of the Forster model with respect to fluorescence thermometry are discussed by Dowell [65, 66]. The spectral emission distribution can be a sensitive function of dopant concentration. An example of this is illustrated in Fig. 1.3 for $Y_2O_2S:Eu$ [67]. At low Eu concentrations, the shorter wavelength lines are stronger than they are at higher concentrations. Kusama et al.[34] noted that this is particularly important for intensity based thermometry. They indicate that the 5D_2 emission of $Y_2O_2S:Eu$ is especially sensitive to Eu concentrations. In comparing temperature dependent ratios of this line to a

5D_0 emission line, a difference of 0.1 mol % between samples will vary the ratio by about 5% and lead to an estimated error of 15 °C.

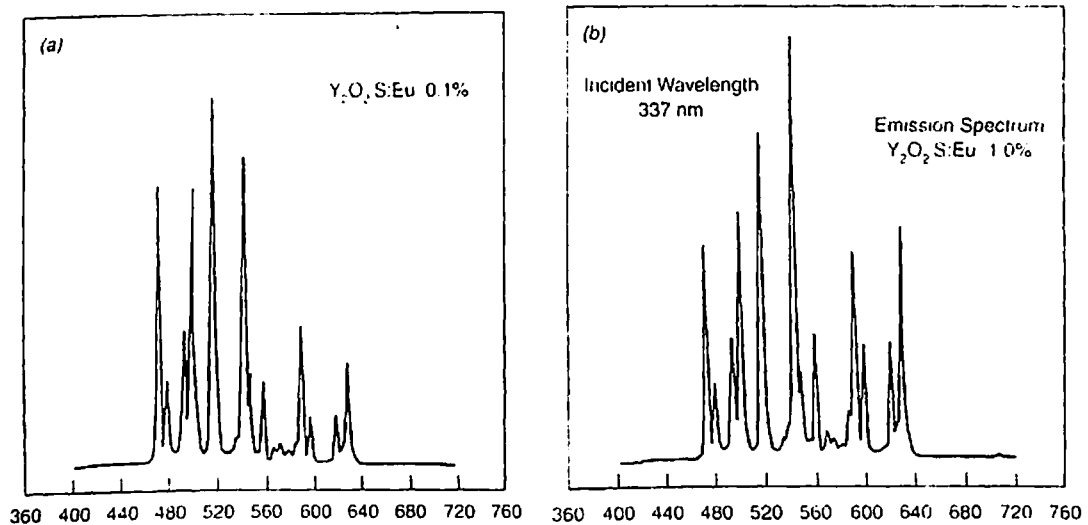


Fig1.3: Spectral emission distribution for $Y_2O_2S:Eu$ at dopant concentration of (a) 0.1% and (b) 1.0 %

Finally, rise times are affected by dopant levels. This occurs especially when one level feeds another as noted by Hellier [68] and Rhys-Williams and Fuller [69]. Table II contains the results of measurements of rise time versus Eu concentration in Y_2O_3 .

Table 1.2: The dependence of the rise time of the $^5D_0 \rightarrow ^7F_2$ transition on the concentration of Eu^{3+} in $Y_2O_3:Eu^{3+}$ (after Ref. 69).

Eu^{3+} (mole%)	Rise time (ms)
0.27	0.320
1.00	0.267
2.20	0.189
3.30	0.130
5.56	0.060
11.10	0.020

(b) Saturation Effects:

Saturation effects on YAG:Tb, another phosphor of interest in thermometry, are discussed by de Leeuw and 't Hooft [70]. A survey of the study of saturation effects is given there.

High incident fluxes, whether from laser, particle beam, or any other excitation source, can lead to luminescence saturation effects. When this occurs, phosphor efficiency changes as a function of the incident flux. In typical applications, this would manifest itself as a spurious temperature change if the flux were to increase to the point of causing saturation. An illustrative example arises in the description of saturation of $Y_2O_3S:Eu$ by Imanaga *et al.* [71] where the relative dopant concentrations were 0.1% and 4%. A nitrogen laser (337 nm) focused to a spot size of about 1 mm^2 was used for short duration (4 ns) photon excitation. For cathode ray excitation a 10 kV electron beam of 5 μs duration was used and a number of effects were noted. With the latter form of excitation, the spectral distribution changed as a function of input fluence beginning at about $0.1 \mu\text{A}/\text{cm}^2$. The effect was more pronounced at higher concentrations. Above a certain threshold value, overall intensity decreases, but for the lower concentration, this threshold value itself is lower and the rate of decrease is faster than at higher concentrations. Increasing the beam voltage, independently of beam current, will degrade the saturation of this phosphor according to Yamamoto and Kano [72]. Conversely, the situation may improve for some phosphors over a certain range, as observed in the case of ZnS and Zn_2SiO_4 by Dowling and Sewell [73]. For short-pulse excitation via nitrogen laser, the saturation effects are even more complex. Moreover, saturation is itself a temperature dependent phenomenon. Generally, for all concentrations, the saturation thresholds are lower at higher temperatures. Saturation is enhanced at higher concentrations, but the rates will be different from one emission line to another. There is evidence for a decrease in fluorescence decay time with increasing laser fluence. Imanaga *et al.* [71] suggest several possible mechanisms that may cause luminescence saturation behavior in this case. Beam-induced temperature rise was ruled out as a possible cause since saturation was less pronounced for the most temperature-dependent emission lines, as well as for other reasons [71], although this might be the dominant mechanism at work in other cases. Thermodynamic considerations, coupled with experimental studies, can help determine if beam-related effects will be a problem in a given situation. The results found by Imanaga *et al.* [71] may likely be due to the increased probability of having two excited dopant atoms in close proximity to each other. Evidently, when this occurs, an additional nonradiative de-excitation path is allowed. For instance, one of the excited atoms might transfer its energy to its neighbor, thus creating a doubly excited atom which nonetheless can emit only one fluorescence photon rather than two, thus decreasing the emission rate.

In most applications, one does not have the opportunity to deliver a surfeit of laser excitation due to the necessity for transporting beams long distances, usually over optical fibers which have limited fluence-handling capacity. Saturation becomes a relatively important problem during laboratory calibrations, however, when a more nearly ideal optical arrangement is employed, i.e., one having higher available laser power and finer focusing.

Finally, we note that Raue et al. [74] have studied saturation effects in Tb-doped phosphors excited by cathode beams. They have developed a model that is consistent with the results of excited state absorption experiments carried out on a variety of these materials.

(c) Impurities:

There are inevitably small amounts of undesired species in solid solution in the host material, and these change the atomic electronic environment experienced by the activators so as to either augment or hinder phosphor performance. For instance, at concentrations greater than 1ppm, transition metal impurities will decrease phosphor brightness. This is because they absorb at wavelengths similar to those of the typical activators, thus effectively stealing excitation energy and decreasing the number of excited fluorescence centers. Moreover, nonradiative energy transfer from an excited activator to such impurities is efficient, thus increasing the decay rate and quenching the emission.

Even so, it is possible to mix powdered phosphors with great variety of substances, from epoxies to inorganic binders, without affecting emission characteristics. In fact, ceramic binders can be flame sprayed, plasma sprayed, etc., as long as the result is a suspension of mixed materials. Properly chosen additives can also play a positive role. For example, addition of small amounts of Dy and Tb or Pr to $Y_2O_3:Eu$ has the effect of decreasing the lifetime by as much as a factor of 3 with little or no change in quantum efficiency [75]. Having a faster response can be important when using phosphor thermometry to interrogate, e.g., a high speed rotating shaft that has a "viewing time", that is limited [76,77].

(d) Sensitizers:

A sensitizer is a material that, when added to a phosphor, increases the fluorescence output. Weber [14], in a survey of rare-earth laser research, formulated a table of rare-earth ions that have been used as active laser media, and included in it the corresponding rare earths used as sensitizers for each. The sensitizing dopant will absorb energy and, rather than emitting fluorescence, it transfers its energy to the main dopant from which an optical transition occurs. For example, he notes that erbium has been found to be a sensitizer for dysprosium, while gadolinium is a sensitizer for terbium: A prospective sensitizer must

exhibit no absorption at the emission wavelength of interest. It must also have absorption bands that do not steal excitation energy from the activator. Finally, it must have energy levels that are above the fluorescing line which feed the activator but which do not quench it [78].

(e) Quantum Efficiency:

Quantum efficiency, Q_E , is a parameter often used to help scale a phosphor's ability to produce bright light. Knowledge of the approximate quantum efficiency of a phosphor can aid in determining expected signal levels. Numerically, the quantum efficiency is the ratio of the number of photons absorbed by the phosphor to the number that are emitted. If $Q_E \geq 0.8$, a material is considered to be an efficient phosphor. Q_E is not as dominant a criterion for fluorescence thermometry as it is for lighting and display applications. Figure 1.4 presents the emission intensities for a variety of activators [9] in YVO_4 . With Eu as an activator, the resulting phosphor is most efficient and useful in thermometry only above the quenching temperature of $\approx 500^\circ C$. On the other hand, a Dy activator in this host will produce decay times that make the phosphor [67] useful in the range from 300 to $500^\circ C$. (The ratio of two emitting lines in this case can also be used to make measurements at somewhat lower temperatures.) It is interesting to note that $YVO_4:Nd$ is being used as a laser medium despite its low efficiency. For $YVO_4:Eu$, $Q_E = 68\%$ at the optimum concentration of 0.05 mol % (253.7 nm excitation) whereas $Q_E = 88\%$ for $YVO_4:Dy$ at a concentration of 0.003 mol %. The latter is clearly a more efficient phosphor, except for the fact that the concentration dependence is more pronounced.

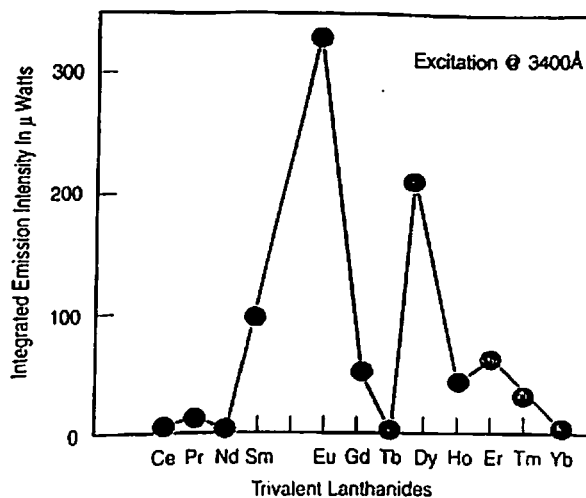


Fig. 1.4: The emission intensities for various rare-earth activators in YVO_4

Efficiency is a wavelength-dependent phenomenon. Therefore, if, e.g., instrumentation availability prevents the use of mid-UV excitation with a phosphor that happens to be efficient in that band, then a substitute material better suited to the wavelength of the excitation source should be used instead.

1.3.3. Fluorescence Intensity:

A comparison of the two spectra of $\text{La}_2\text{O}_2\text{S}:\text{Eu}$ presented in Fig.1.5 shows that the relative intensities of the lines near 465 and 512 nm are temperature dependent. In fact, it is generally the case that certain of the lines in these phosphors get weaker, i.e, become less bright, as the temperature of the material is increased. A plot of intensity versus temperature is shown in Fig.1.6. Clearly, for this material, there is a region where the selected emission line is no longer sensitive to temperature change. At a particular value, viz., the "quenching temperature", the strength of the emission line falls off drastically. The quenching temperatures and the slopes of the temperature dependencies usually differ for each type of phosphor and for each of the emission lines within the spectrum of a given phosphor. In some cases there may be an increase in intensity with temperature over a given range of temperatures, although the opposite is more typical.

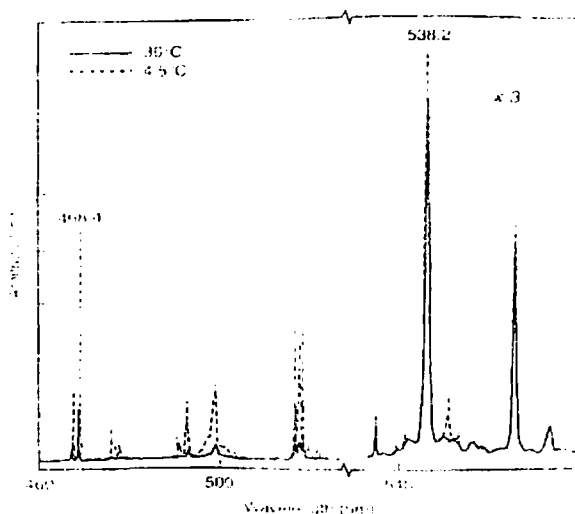


Fig1.5: Temperature dependence of $\text{La}_2\text{O}_2\text{S}:\text{Eu}$ spectra

Temperature dependence of excitation spectra [79,80] and absorption spectra [81] have also been studied.

1.3.4. Fluorescence Lifetime:

When a phosphor is excited by a pulsed source, the persistence of the resulting fluorescence can be observed providing that the length of the source pulse is much shorter

than the persistence time of the phosphor's fluorescence. This is illustrated in Fig.1.7 for the 514 nm line of $\text{La}_2\text{O}_2\text{S}:\text{Eu}$ monitored at two different temperatures. The luminescence intensity decays exponentially in this case, according to the relation:

$$I = I_0 e^{-t/\tau} \quad (1.5)$$

where τ (the lifetime or decay time) is the standard $1/e$ ($\approx 37\%$) folding time for the fluorescence. The decay time is often a very sensitive function of temperature and, therefore, a determination of its value constitutes a very useful method of thermometry. A portion of a calibration curve for $\text{La}_2\text{O}_2\text{S}:\text{Eu}$ is shown in Fig.1.8 for three of its emission lines.

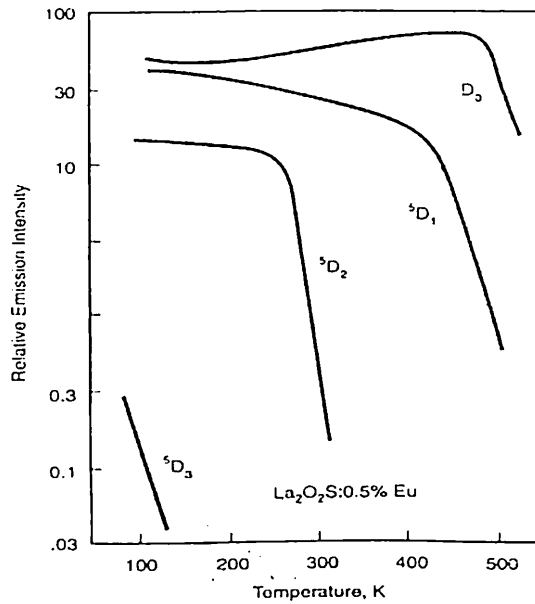


Fig 1.6: Emission intensity vs temperature for $\text{La}_2\text{O}_2\text{S}:\text{Eu}$ spectra

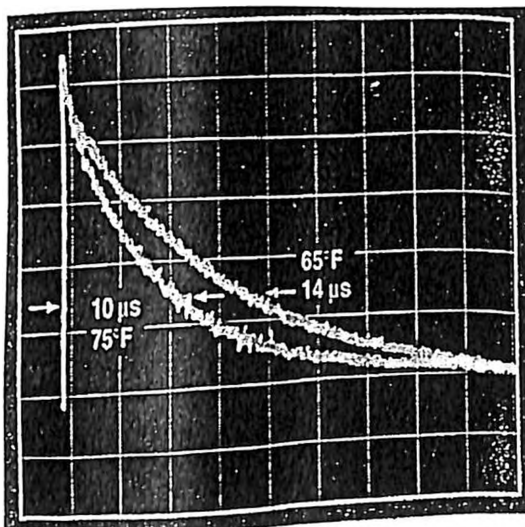


Fig 1.7: Phosphors decay characteristics at 65 and 75 F

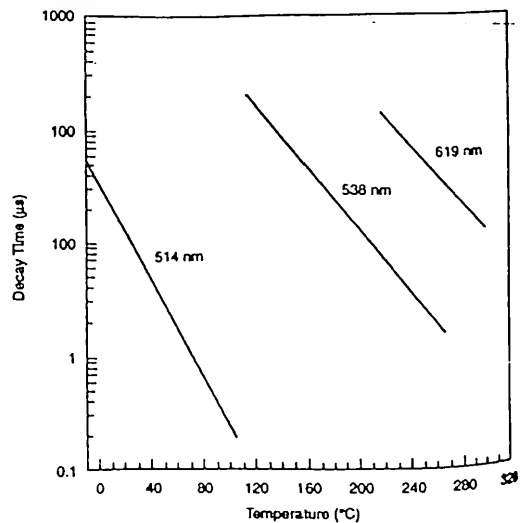


Fig 1.8: Fluorescence decay time vs temperature for $\text{La}_2\text{O}_2\text{S}:\text{Eu}$

Figure 1.9 shows lifetime versus temperature for several materials that have been tested at Oak Ridge National Laboratory (ORNL) and collaborating institution [82].

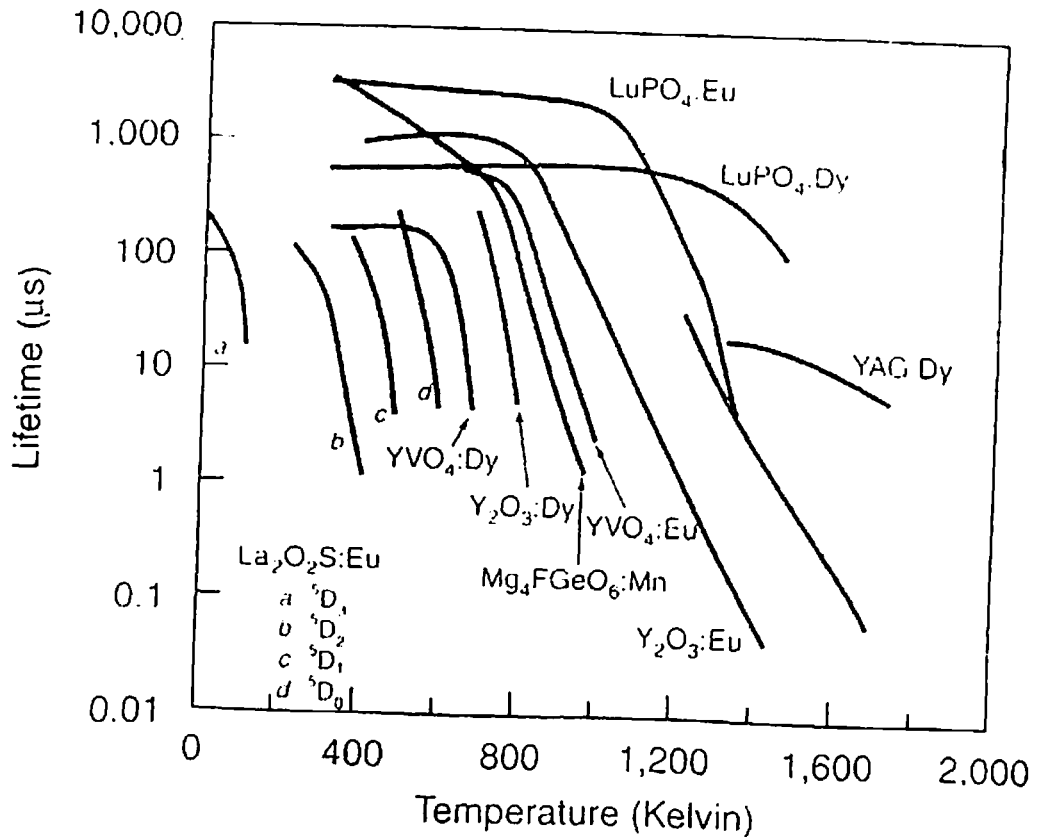


Fig 1.9: Life time vs temperature of selected phosphors

The choice of phosphor for a given application will clearly depend on the temperature range that must be spanned. However, there are additional considerations: chemical compatibility between phosphor, substrate and the surrounding environment, for instance, is one such concern. Fortunately, many of the most efficiently fluorescing materials are very inert; in fact some are ceramics. As another example, the optical background in a given situation may make the wavelength of the phosphors emission an important consideration. In response, however, we note that one can select from among phosphors that emit anywhere between the infrared and the ultraviolet.

1.3.5. Fluorescence Line Shift:

Each emission line is characterized by a wavelength for which the intensity is maximum. Its value may change slightly with temperature, and this is termed a line shift. Also, an emission line has a finite width, called the line width, which is often designated by the spectral width at half the maximum line intensity. Linewidth and line shift changes as a

function of temperature are generally small, and are not often used in fluorescence thermometry. However, as previously mentioned, Kusama et al [34] utilized this approach for cathode-ray-tube thermometry. As shown in Fig.1.10 they observed a shift to the blue of about 0.2 nm in going from -15 to 72 °C. The data they presented indicate that the line shift has an approximately quadratic dependence on frequency.

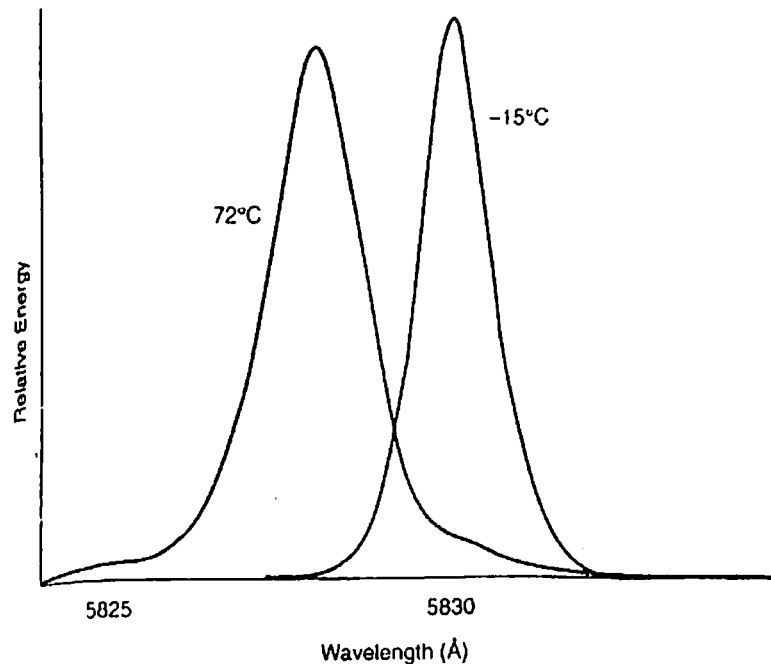


Fig 1.10: Line width and line position at -15 and 72^oC for Y₂O₂S:Eu

1.4. Statement of the Problem:

In the preceding sections we have already discussed that the temperature sensitive fluorescence of some specific phosphors have been used for remote as well as direct measurement of temperature of both static and moving objects. The state of art of these thermographic phosphors and related techniques of measurement have been recently reviewed by Allison & Gillies [83] and Grattan & Zhang [84]. The number of such phosphors, which satisfy the requirement of linearity of response, spectral tunability, stability and ease of synthesis, are indeed very few. Therefore, there is a need to investigate more materials for this application. In this context, copper activated alkaline earth sulphides seem to be promising candidates as these phosphors can be easily synthesized, they are quite stable over long period of time (ten to fifteen years), if protected from moisture and their fluorescence is sensitive to temperature. Although these phosphors have been known for a

very long time [85] and their photoluminescence, cathodoluminescence and electroluminescence have been reported by many investigators in single sulphides [86 - 113] as well as mixed sulphides [114 - 119], no systematic efforts have been made to study the temperature dependence of fluorescence of this system. Further, there is no reliable report about the fluoro-optic behaviour of (Sr, Ba)S:Cu phosphors. A summary of the important results reported so far is given as follows. Alkaline earth sulphides are one of the oldest luminescent materials, studied first by Lenard et al. in 1928 primarily for infra-red applications. First detailed and systematic investigation on CaS was reported by Lehmann and Ryan and Lehmann [91, 92]. They concluded that it is an excellent host material for efficient cathode-ray tube phosphors when activated with rare earths. Since then a number of reports have appeared describing spectroscopic properties of pure and activated sulphides and revealing applications of BaS, SrS and MgS in alloy semiconductors [120], radiation dosimetry [121] and fast high resolution optically stimulated luminescence imaging [122]. Experimental band gap energies of sulphides determined from the optical reflection spectra by various workers [92, 123, 124] are listed in Table 1.3.

Table 1.3 Experimental band gap energies of alkaline earth sulphides

	MgS	CaS	SrS	BaS
Band-gap(eV)				
Polycrystalline, 300K(*)	5.4	4.8	4.4	3.8
Single crystal, 77K(Ξ)	-	5.3	-	-
Single crystal, 2K(∂)	-	5.343	4.831	3.941
Lattice constant (a)	5.204(!)	5.6975(Î)	6.0190(Î)	6.3842(Î)

(*) Lehmann and Ryan [91] (∂) Kaneko and Koda [123] (Ξ) Realo and Jaek [124]

(Î) Kaneko et al. [125]

(!) Quoted by Thakur and Pandey [126]

The work so far reported on Cu-activated sulphides is limited to emission studies. The emission spectrum strongly depends on the presence of a co-activator in the lattice influencing the peak positions of the emission band [94]. However, no systematic trend in the peak-shift has been observed as either the host lattice or co-activators are varied [90].

The Cu emission also depends on the Cu concentration in the lattice and shows concentration quenching at higher Cu concentrations. In CaS the spectrum consists of two bands at about 442 and 493 nm disappearing at high Cu concentration (>0.5 mol%) when a broad band appears at about 530 nm [90]. In SrS the spectrum consists of three bands at about 471, 517, and 548 nm at low Cu concentration (~0.01 mol%) [90]. In BaS the main emission band at 568 nm shifts to 570.5 nm for high Cu concentration. In mixed sulphides, SrS-BaS, a gradual shift of emission spectra to longer wavelengths with increasing BaS content was observed as

expected [117]. A similar shift has been reported by Yamashita et. al [119] in CaS-SrS mixed sulphides.

Therefore, the present work aims at investigating the fluoro-optic behaviour of copper-activated mixed alkaline earth sulphide phosphors at room temperature and as a function of temperature. The mixed lattice has been chosen because it is possible to tune the peak wavelength of emission by varying the relative fraction of constituent sulphides.

The objectives of the present investigations are:

- (i) To synthesize mixed alkaline earth sulphide phosphors activated by copper
- (ii) To ascertain the crystalline structure of synthesized materials
- (iii) To know the nature of luminescence centres responsible for emission
- (iv) To infer the mechanism of thermal quenching and the nature of other processes involved in the luminescence of these materials; and
- (v) To assess the suitability of these materials for thermographic applications

Consistent with these objectives, three series of mixed alkaline earth sulphides have been synthesized by solid state fusion reaction. They are (Ca, Sr)S:Cu, (Ba, Sr)S:Cu, and (Ca, Ba)S:Cu. The following investigations have been carried out on all the three series of phosphors.

- 1 Recording of X- ray diffraction spectra
- 2 Recording of excitation spectra
3. Recording of fluorescence spectra at RT
- 4 Study of the variation of fluorescence intensity at λ_{\max} (wavelength of maximum emission) with temperature
5. Recording of lifetime of fluorescence at λ_{\max} at RT.
6. Study of the variation of lifetime of fluorescence at λ_{\max} with temperature.

Finally the results of all the experiments have been correlated and suitability of these materials for thermographic applications has been discussed.

References:

1. L Michalaki, K Eckersdorf and J Mc Ghee, "Temperature measurement", John Wiley & Sons, Chichester (1991).
2. B Culshaw and J Dakin Eds, Optical Fiber Sensors- System and Applications I& II Artech House Inc., Norwood (1989).
3. B P Pal Ed, "Fundamentals of fiber optic in telecommunications and sensor systems" –Part III, Wiley Eastern Ltd., New Delhi (1992).
4. R P Khare, Aditi Sharma, Sartaj Singh, Indian J. of Engg. & Mater. Sci., 2, 58, (1995).
5. R P Khare, Vandana Prabhu, T V Jaishankar, Indian J. Pure & Appl. Phys., 34, 823 (1996).
6. B T Meggitt, A W Palmer & K T V Gratton, Int. J. Optoelec., 3, 451, (1988).
7. P. Pringsheim, "Fluorescence and Phosphorescence", Interscience, New York. 1 (1949).
8. K. H. Butler, "Fluorescent Lamp phosphors", Pennsylvania State University press, University Park, PA, (1980).
9. R. C. Ropp, "Luminescence and the Solid State", Studies in Inorganic Chemistry 12 Elsevier, Amsterdam, (1991).
10. R. C. Ropp, "The Chemistry of Artificial Lighting Devices: Lamps Phosphors and Cathode Ray Tubes", Studies in Inorganic Chemistry 17, Elsevier, Amsterdam, (1993).
11. R. H. Hoskins and B. H. Soffer, US Patent No. 3,49,6,482 (1963).
12. P. N. Yacom, "Proceedings of the 6th Rare Earth Research Conference", Oak Ridge National Laboratory, Oak Ridge, TN, (1967).
13. C. Greskovich and J. P. Chernach, J. Appl. Phys. 44, 4599 (1973).
14. M. J. Weber, in "The Handbook on the Physics and Chemistry of Rare Earths", edited by K. A. Gschneidner, Jr. and L. Eyring, North-Holland, Amsterdam, , Chap. 35, 275 (1979).
15. Neubert, US Patent No. 2,071,471 (1937).
16. F. Urbach, N. R. Nail, and D. Pearlman, J. Opt. Soc. Am. 39, 1011 (1949).
17. F. Urbach, US Patent No. 2,551,650 (8 May 1951).
18. K. Wickersheim and R. Alves, Ind. Res. Dev. 21, 82 (1979).
19. K. Wickersheim and M. Sun, Res. Dev. 27, 114 (1985).

20. L. C. Bradley III, *Rev. Sci. Instrum.* **24**, 219 (1953).
21. W. H. Byler and F. R. Hays, *Nondestr. Test.* **19**, 177 (1961).
22. R. R. Sholes and J. G. Small, *Rev. Sci. Instrum.* **51**, 692 (1980).
23. T. Bosselmann, A. Reule, and J. Schroeder, *Proc. SPIE* **514**, 151 (1984).
24. K. T. V. Grattan, R. K. Selli, and A. W. Palmer, *Rev. Sci. Instrum.* **59**, 1328 (1988).
25. N. C. Chang, *J. Appl. Phys.* **34**, 3500 (1963).
26. P. A. Czysz and D. N. Kendall, McDonnell Company Technical Report No. F 938, (April 1968).
27. P. A. Czysz and W. P. Dixon, *SPIE J.* **7**, 77 (1969).
28. P. A. Czysz and W. P. Dixon, *Instrum. Control Syst.* **41**, 71 (1968).
29. K. A. Wickersheim, R. A. Buchanan, L. E. Sobon, R. V. Alves, and J. J. Pearson, Lockheed Missiles & Space Company; Third Annual Report No. 4-17-69-1, (1969).
30. K. A. Wickersheim, R. V. Alves, and R. A. Buchanan, *IEEE Trans. Nucl. Sci.* **NS-17**, 57 (1970).
31. R. V. Alves and R. A. Buchanan, *IEEE Trans. Nucl. Sci.* **NS-20**, 415 (1973).
32. R. V. Alves, R. A. Buchanan, K. A. Wickersheim, and E. A. C. Yates, *J. Appl. Phys.* **42**, 3043 (1971).
33. L. E. Sobon, K. A. Wickersheim, R. A. Buchanan, and R. V. Alves, *J. Appl. Phys.* **42**, 3049 (1971).
34. H. Kusama, O. J. Sovers, and T. Yoshioka, *Jpn. J. Appl. Phys.* **15**, 2349, (1976).
35. J. P. Leroux and R. Taboue, *Societe Francaise des Thermiciens, Rencontre annuelle, La Baule* **5, 6**, (7 May 1975).
36. J. P. Leroux, *Publications Scientifiques et Techniques du Ministere de Air*, NT No.119, (1962).
37. J. P. Leroux, G. Blanc, M. Delisee, P. Coppolani, R. Taboue, *Cahiers de la Thennique (I. F.C.E. Paris)*, cahier No. 3 Ser. A, March 1973, IV. 1 a IV. 55.
38. P. Baumann, *Rech. Aerosp.* (5), 29 (1993).
39. K. A. James, W. H. Quick, and V. H. Strahan, *Control Eng.* **26**, 30 (1979).
40. T. Samulski and P. K. Shrivastava, *Science* **208**, 193 (1980).
41. T. Samulski and P. K. Shrivastava, *Phys. Med. Biol.* **27**, 107 (1982).
42. J. S. McCormack, *Electron. Lett.* **17**, 630 (1981).
43. G. E. Gross, *Midwest Research Institute Final Report (M.R.I. Project No. 2300-P)*, (June 1960).

20. L. C. Bradley III, *Rev. Sci. Instrum.* **24**, 219 (1953).
21. W. H. Byler and F. R. Hays, *Nondestr. Test.* **19**, 177 (1961).
22. R. R. Sholes and J. G. Small, *Rev. Sci. Instrum.* **51**, 692 (1980).
23. T. Bosselmann, A. Reule, and J. Schroeder, *Proc. SPIE* **514**, 151 (1984).
24. K. T. V. Grattan, R. K. Selli, and A. W. Palmer, *Rev. Sci. Instrum.* **59**, 1328 (1988).
25. N. C. Chang, *J. Appl. Phys.* **34**, 3500 (1963).
26. P. A. Czysz and D. N. Kendall, McDonnell Company Technical Report No. F 938, (April 1968).
27. P. A. Czysz and W. P. Dixon, *SPIE J.* **7**, 77 (1969).
28. P. A. Czysz and W. P. Dixon, *Instrum. Control Syst.* **41**, 71 (1968).
29. K. A. Wickersheim, R. A. Buchanan, L. E. Sobon, R. V. Alves, and J. J. Pearson, Lockheed Missiles & Space Company; Third Annual Report No. 4-17-69-1, (1969).
30. K. A. Wickersheim, R. V. Alves, and R. A. Buchanan, *IEEE Trans. Nucl. Sci.* **NS-17**, 57 (1970).
31. R. V. Alves and R. A. Buchanan, *IEEE Trans. Nucl. Sci.* **NS-20**, 415 (1973).
32. R. V. Alves, R. A. Buchanan, K. A. Wickersheim, and E. A. C. Yates, *J. Appl. Phys.* **42**, 3043 (1971).
33. L. E. Sobon, K. A. Wickersheim, R. A. Buchanan, and R. V. Alves, *J. Appl. Phys.* **42**, 3049 (1971).
34. H. Kusama, O. J. Sovers, and T. Yoshioka, *Jpn. J. Appl. Phys.* **15**, 2349, (1976).
35. J. P. Leroux and R. Taboue, *Societe Francaise des Thermiciens, Rencontre annuelle, La Baule* **5, 6**, (7 May 1975).
36. J. P. Leroux, *Publications Scientifiques et Techniques du Ministere de Air*, NT No.119, (1962).
37. J. P. Leroux, G. Blanc, M. Delisee, P. Coppolani, R. Taboue, *Cahiers de la Thennique (I. F.C.E. Paris)*, cahier No. 3 Ser. A, March 1973, IV. 1 a IV. 55.
38. P. Baumann, *Rech. Aerosp.* (5), 29 (1993).
39. K. A. James, W. H. Quick, and V. H. Strahan, *Control Eng.* **26**, 30 (1979).
40. T. Samulski and P. K. Shrivastava, *Science* **208**, 193 (1980).
41. T. Samulski and P. K. Shrivastava, *Phys. Med. Biol.* **27**, 107 (1982).
42. J. S. McCormack, *Electron. Lett.* **17**, 630 (1981).
43. G. E. Gross, *Midwest Research Institute Final Report (M.R.I. Project No. 2300-P)*, (June 1960).

44. J. C. Garavitt, G. E. Gross, J. E. Beachy, and W. E. McAllum, Midwest Research Institute Final Report (M.R.I. Project No.2423 P), (June 1963).
45. D. J. Brenner, National Bureau of Standards (U.S.) Technical Note No.591, (July 1971).
46. E. M. Fry, Temperature: Its Measurement and Control in Science and Industry, Instrument Society of America, Research Triangle Park, NC, 4, 577 (1971).
47. R. J. D. Pattison, UK Patent No.1, 480, 583 (20 July 1977).
48. L. J. Dowell, Appl. Mech. Rev. 45, 253 (1992).
49. L. J. Dowell, G. T. Gillies, S. W. Allison, and M. R. Cates, Martin Marietta Energy Systems, Inc., Technical Report No. K/TS-11, 771, (July 1986).
50. L. J. Dowell and G. T. Gillies, University of Virginia Technical Report No. UVA/640419/NEEP89/102, (April 1989).
51. L. J. Dowell, G.T. Gillies, S. W. Allison, and M. R. Cates, J. Lumin. 36, 375 (1987).
52. D. Curie, "Luminescence in crystals" (Methuen & Co.) 1963.
53. G. H. Dieke and H. M. Cross white, Appl. Opt. 2, 675 (1963).
54. W. H. Fonger and C. W. Struck, J. Chem. Phys. 52, 6364 (1970).
55. C. W. Struck and W. H. Fonger, J. Appl. Phys. 42, 4515 (1971).
56. G. Blasse, Prog. Solid State Chem. 18, 79 (1988).
57. M. J. Weber, Phys. Rev. B 8, 54 (1973).
58. D. J. Robbins, B. Cockayne, B. Lent, C. N. Duckworth, and J. L. Glasper, Phys. Rev. B 19, 1254 (1979).
59. D. J. Robbins, B. Cockayne, J. L. Glasper, and B. Lent, J. Electrochem. Soc. 126, 1213 (1979).
60. D. J. Robbins, B. Cockayne, J. L. Glasper, and B. Lent, J. Electrochem. Soc. 126, 1221 (1979).
61. D. J. Robbins, B. Cockayne, B. Lent, and J. L. Glasper, J. Electrochem. Soc. 126, 1556 (1979).
62. L. Ozawa and P. M. Jaffe, J. Electrochem. Soc. 118, 1678 (1971).
63. J. L. Sommerdijk and A. Bril, J. Electrochem. Soc. 122, 952 (1975).
64. W. F. van der Weg, T. J. A. Popma, and A. T. Vink, J. Appl. Phys. 57, 5450 (1985).
65. L. J. Dowell, Los Alamos National Laboratory Technical Report No.LA- 11873-MS, (August 1990).
66. L. J. Dowell, J. Laser Appl. 3, 27 (1991).

67. S. W. Allison, M. R. Cates, L. A. Franks, H. M. Borella, S. S. Lutz, W. D. Turley, B. W. Noel, and A. Beasley, Martin Marietta Energy Systems, Inc., Report No. ORNL/ATD-12, (April 1989).
68. R. G. Hellier, Jr., M.Sc. thesis, University of Virginia, (1992).
69. A. T. Rhys-Williams and M. J. Fuller, *Comput. Enhanced Spectrosc.* **1**, 145 (1983).
70. D. M. de Leeuw and G. W. 't Hooft, *J. Lumin.* **28**, 275 (1983).
71. S. Imanaga, S. Yokono, and T. Hoshima, *Jpn. J. Appl. Phys.* **19**, 41 (1980):
72. H. Yamamoto and T. Kano, *J. Electrochem. Soc.* **126**,305 (1979).
73. P. H. Dowling and J. R. Sewell, *J. Electrochem. Soc.* **100**, 22 (1953).
74. R. Raue, K. Nieuwesteeg, and W. Busselt, *J. Lumin.* **48&49**, 485 (1991).
75. J. L. Ferri and J. E. Mathers, US Patent No. 3,639,932 (8 February 1972).
76. S. S. Lutz, W. D. Turley, H. M. Borella, B. W. Noel, M. R. Cates, and M. R. Probert, Proceedings of the 34th International Instrumentation Symposium: Instrumentation for the Aerospace Industry, Instrument Society of America, Research Triangle Park, NC, 217 (1988).
77. S. W. Allison, M. R. Cates, B. W. Noel, and G. T. Gillies, *IEEE Trans. Instrum. Meas.* **37**, 637 (1988).
78. Guo Chang-Xin, Zhang Wei-Ping, and Shi Chao-Shu, *J. Lumin.* **24-25**, 297 (1981).
79. A. R. Bugos, M.Sc. thesis, University of Tennessee, (1989).
80. A. R. Bugos, S. W. Allison, D. L. Beshears, and M. R. Cates, in Proceedings of the IEEE Southeastcon Conference, IEEE, New York, 228 (1988).
81. W. D. Turley, C. E. Iverson, S. S. Lutz, R. L. Flurer, J. R. Schaub, S. W. Allison, J. S. Ladish, and S. E. Caldwell, *Proc. SPIE* **1172**, 27 (1989).
82. S. W. Allison, M. A. Abraham. L. A. Boatner, M. R. Cates, D. L. Beshears, K. W. Tobin, B. W. Noel, and W. D. Tureley, Technical Digest of the Eleventh International Congress on Lasers & Electro-Optics, Laser Institute of America, Anaheim, CA., (1992).
83. S.W. Allison and G.T. Gillies, *Rev. Sci. Instrum.* **68**, 2615 (1997).
84. K.T.V. Grattan and Z.Y. Zhang, "Fiber Optic Fluorescence Thermometry" .Chapman & Hall, London (1995).
85. F. Urbach, D. Pearlman and H. Hemmendinger , *J Opt. Soc. Am*, **36** 372 (1946).
86. A. Wachtel , *J. Electrochem. Soc.* **107**, 199 (1960).
87. M. Avinor, A. Carmi and Z. Weinberger : *J. Chem. Phys.* **35**, 1978 (1961).

67. S. W. Allison, M. R. Cates, L. A. Franks, H. M. Borella, S. S. Lutz, W. D. Turley, B. W. Noel, and A. Beasley, Martin Marietta Energy Systems, Inc., Report No. ORNL/ATD-12, (April 1989).
68. R. G. Hellier, Jr., M.Sc. thesis, University of Virginia, (1992).
69. A. T. Rhys-Williams and M. J. Fuller, *Comput. Enhanced Spectrosc.* **1**, 145 (1983).
70. D. M. de Leeuw and G. W. 't Hooft, *J. Lumin.* **28**, 275 (1983).
71. S. Imanaga, S. Yokono, and T. Hoshima, *Jpn. J. Appl. Phys.* **19**, 41 (1980):
72. H. Yamamoto and T. Kano, *J. Electrochem. Soc.* **126**,305 (1979).
73. P. H. Dowling and J. R. Sewell, *J. Electrochem. Soc.* **100**, 22 (1953).
74. R. Raue, K. Nieuwesteeg, and W. Busselt, *J. Lumin.* **48&49**, 485 (1991).
75. J. L. Ferri and J. E. Mathers, US Patent No. 3,639,932 (8 February 1972).
76. S. S. Lutz, W. D. Turley, H. M. Borella, B. W. Noel, M. R. Cates, and M. R. Probert, *Proceedings of the 34th International Instrumentation Symposium: Instrumentation for the Aerospace Industry*, Instrument Society of America, Research Triangle Park, NC, 217 (1988).
77. S. W. Allison, M. R. Cates, B. W. Noel, and G. T. Gillies, *IEEE Trans. Instrum. Meas.* **37**, 637 (1988).
78. Guo Chang-Xin, Zhang Wei-Ping, and Shi Chao-Shu, *J. Lumin.* **24-25**, 297 (1981).
79. A. R. Bugos, M.Sc. thesis, University of Tennessee, (1989).
80. A. R. Bugos, S. W. Allison, D. L. Beshears, and M. R. Cates, in *Proceedings of the IEEE Southeastcon Conference*, IEEE, New York, 228 (1988).
81. W. D. Turley, C. E. Iverson, S. S. Lutz, R. L. Flurer, J. R. Schaub, S. W. Allison, J. S. Ladish, and S. E. Caldwell, *Proc. SPIE* **1172**, 27 (1989).
82. S. W. Allison, M. A. Abraham. L. A. Boatner, M. R. Cates, D. L. Beshears, K. W. Tobin, B. W. Noel, and W. D. Tureley, *Technical Digest of the Eleventh International Congress on Lasers & Electro-Optics*, Laser Institute of America, Anaheim, CA., (1992).
83. S.W. Allison and G.T. Gillies, *Rev. Sci. Instrum.* **68**, 2615 (1997).
84. K.T.V. Grattan and Z.Y. Zhang, "Fiber Optic Fluorescence Thermometry" .Chapman & Hall, London (1995).
85. F. Urbach, D. Pearlman and H. Hemmendinger , *J Opt. Soc. Am*, **36** 372 (1946).
86. A. Wachtel , *J. Electrochem. Soc.* **107**, 199 (1960).
87. M. Avinor, A. Carmi and Z. Weinberger : *J. Chem. Phys.* **35**, 1978 (1961).

88. D. Sharma and A. Singh, *Indian J Pure & Appl. Phys.* **7**, 310 (1969).
89. D. Sharma and A. Singh, *Indian J Pure & Appl. Phys.* **9**, 810 (1971).
90. W. Lehman, *J Electrochem. Soc.* **117**, 1389 (1970).
91. W. Lehmann and M. F. Ryan, *J. Electrochem. Soc.* **118**, 477 (1971).
92. W. Lehman, *J Lumin.*, **5**, 87 (1972).
93. N. Singh, G.L. Marwaha and V.K. Mathur, *Phys Status Solidi (a)* **66**, 761 (1981).
94. R. Pandey and S. Sivaraman, *J Phys. Chem. Solids*, **52**, 211 (1991).
95. N. Yamashita, *Jpn. J. Appl. Phys* **30**, 3335 (1991).
96. W. M. Li, et al. *J Appl. Phys.* **86**, 5017 (1999).
97. C. Barthou, J. Benoit, P. Benalloul, K. Polamo and E. Soininen, *J. Appl. Phys.* **88**, 1061, (2000).
98. D. Jia, W. Jia, D. R. Evans, W. M. Dennis, H. Liu, J. Zhu and W. M. Yen, *J. Appl. Phys.*, **88**, 3402, (2000).
99. C. J. Summers, B. K. Wagner, W. Tong, W. Park, M. Chaichimansour, Y. B. Xin, *J. Cryst. Growth*, **214**, 918 (2000).
100. M. Peter, M. Murayama, S. Nishimura, K. Ohmi, S. Tanaka and H. Kobayashi, *J. Appl. Phys.*, **90**, 1992 (2001).
101. C. S. Gupta, *Indian J. Phys A*, **75**, 535 (2001).
102. D. C. Morton, E. W. Forsythe, S. S. Sun, M. C. Wood, M. H. Ervin and K. Kirchner, *Appl. Phys. Lett.* **78**, 1400, (2001).
103. H. Z. Yi, W. Y. Sheng, S. Li, X. X. Rong, *J. Phys: Condens. Matter.*, **13**, 3665 (2001).
104. J. Wu, D. Newman, Ian V. F. Viney, *J. Phys. D: Appl. Phys.* **35**, 968 (2002).
105. V. G. Kravets, A. A. Kryuchin, V. A. Ataev, V. M. Shershukov, *Optic. Matter.*, **19**, 421, (2002).
106. D. Wruck, R. Boyn, M. Wienecke, F. Henneberger, U. Troppenz, B. Huttl, W. Bohne, B. Reinhold, H. E. Mahnke, *J. Appl. Phys.*, **91**, 2847 (2002).
107. P. F. Smet, J. V. Gheluwe, D. Poleman, R. L. V. Meirhaeghe, *J. Lumin.* **104**, 145 (2003).
108. J. M. Fitzgerald, J. G. Hoekstra, R. K. Bansal, J. D. Fowlkes, P. D. Rack, *Mat. Res. Soc. Symp. Proc.*, **780**, Y1.4.1, (2003).

109. J. Ihanus, M. Ritala, M. Leskela, E. Soininen, W. Park, A. E. Kaloyeros, W. Harris, K. W. Barth, A. W. Topol, T. Sajavaara and J. Keinonen, *J. Appl. Phys.*, **94**, 3862 (2003).
110. S. J. Yun, S. H. Ko Park, *Electrochem. Solid State Lett.*, **6**, C30 (2003).
111. J. Wu, D. Newman and I. Viney, *J. Phys. D: Appl. Phys.* **37**, 1371 (2004).
112. Y. S. Kim, S. J. Yun, *J. Phys. : Condens. Matter.*, **16**, 569, (2004).
113. P. F. Smet, D. Poelman and R. L. Meirhaeghe, *J. Appl. Phys.*, **95**, 184 (2004).
114. U.K. Mishra, S.L. Mor and J.D. Ranade, *Indian J Pure & Appl. Phys.*, **18**, 6 (1980).
115. A.M. Rastogi and S.L. Mor, *Indian J Pure & Appl. Phys.*, **19**, 1019 (1981).
116. A.M. Rastogi and S.L. Mor, *Phys. Status Solidi(b)*, **63**, 75 (1981).
117. B.B.Laud and V. W. Kuikarni, *Phys. Status Solidi(a)*, **51**, 269 (1979).
118. N. Yarnashita, K. Ebisumori and K. Nakamura, *Jpn. J. Appl Phys.* **32**, 3846 (1993).
119. N. Yarnashita, K. Ebisumori and K. Nakamura, *J Lumin.*, **62**, 25 (1994).
120. H. Hollway and G. Jesion, *Phys. Rev.* **B26**, 5617, (1982).
121. R. P. Rao and D. R. Rao, *Hlth. Phys.* **45**, 1001, (1983).
122. J. Gaslot, P. Braunlich and J.P. Fillard, *Appl. Phys. Lett.* **40**, 376 (1982).
123. Y. Kaneko and T. Koda, *J. Cryst. Growth* **86**, 72, (1988).
124. K. Realo and I. Jaek Eesti NSV Teaduste Akad. Toimetised Fuus Mat, **27**, 79 (1978).
125. Y. Kaneko., K. Morimoto and T. Koda, *J. Phys. Soc. Japan* **51**, 2247 (1982).
126. K. P. Thakur, J. D. Pandey, *J. Inog. Nucl. Chem.* **37**, 645 (1975).

Chapter 2

Synthesis of Phosphors

2.1 Introduction:

An inorganic solid may be made to luminesce either by the 'built in' traces of beneficial impurity and / or by structural defects foreign to the general pattern of its composition. Impurity-activated phosphors, thus, essentially consist of a bulk material which has a normal crystal structure, and an activating impurity which is incorporated in the host lattice by heating an intimate mixture of phosphor components to high temperatures. In some cases, certain low melting salts, called fluxes, are mixed with the charge to obtain efficient phosphors. The characteristics of a phosphor are jointly determined by these three components which play different roles and have, therefore, different requirements.

Phosphors can be prepared in different forms according to the experimental needs or practical utility of the various forms such as single crystals [1], thin films [2,3] and microcrystalline powder phosphors [4,5]; the latter are the simplest and most commonly used.

2.2 Phosphor Composition:

The basic ingredients of activated phosphors are, in general, as follows:

2.2.1 Host Material:

The pure insulating crystalline material forms the base or host, which primarily functions as a suspension for activator or imperfections and also as an energy transfer medium which surrounds the activator atoms [6]. It promotes luminescence by favourably altering the energy levels under the perturbing influence of the activator so that storage and radiative transitions are possible.

2.2.2 Activator:

In general, the role of activator is to create a domain in the host lattice where electron and hole can recombine with the emission of radiation [7]. More specifically, activator may promote luminescence by (i) intensifying the latent emission bands of the host crystal; e.g., Ti enhances the violet-blue emission of pure silicates [6], (ii) originating a new line or band emission, e.g., rare earth ions in CaO [8], (iii) sensitizing a luminescence emission attributable to another activator as in the case of Pb, Tl and Ce which individually sensitize manganese activated calcite and calcium silicate to u.v. excitation [9-11]. Furthermore activator may introduce electron and hole trapping states [12,13] and may act predominantly

as poison (i) when present in excess and (ii) when incorporated in small proportion in certain phosphors in which it is incompatible. Fe, Ni and Co usually act as poisons or quenchers [14-16] of luminescence, though Ni appears to act as an activator and intensifier sometimes [17,18].

The site that an activator occupies within the host crystal depends upon the ionic radii of the activator and host crystal cation. Thus, if they are within 15% of each other, the activator atom occupies substitutional sites in place of regular host crystal atoms thereby forming s-centre, otherwise, it occupies interstitial sites between regular host crystal ions leading to an i-centre [6]. Rare earths and transition as well as post – transition metals are usual activators.

2.2.3 Flux:

These are salts that readily fuse below the firing temperature. The commonly used fluxes are alkali or alkaline earth halides, borates and sulphates which are water-soluble and have low melting points. The precise function of fluxes is still a matter of conjecture. Prevalent views regarding their role in phosphor synthesis and the mechanism by which they affect luminescence characteristics are:

- (i) They act as mineralizer and catalyst which allows lower firing temperature and shorter firing time by promoting low temperature recrystallization so rapidly that large grains with lattice imperfections are formed [6, 19, 20].
- (ii) They act as an inhibitor of sublimation [6].
- (iii) They promote even distribution and incorporation of activator in the host lattice [6, 19].
- (iv) Flux atoms arrange themselves around activator atoms [21].
- (v) Flux provides charge compensating ions when ionic charge of the activator differs from that of the lattice ion it replaces and facilitates the entry of such activator, probably, because this way of charge compensation is less costly in energy than formation of vacancies and interstitials [22-25].
- (vi) They promote the formation of defects of lattice distortions and thus affect the luminescence efficiency [20].

In many cases the anions and cations of the flux play an important role in the formation of luminescence centres [22]. The nature and quality of the fluxes have also been found to affect the characteristics of a phosphor and infra-red stimulation of ZnS phosphors.

2.2.4 Mixed Lattice Phosphors:

When the composition of a phosphor is altered by the formation of a solid solution with another compound, its emissive properties are likely to be altered. Examples of such a situation are furnished by certain solid solutions formed with zinc silicate and with zinc sulfide; by the tungstates formed from binary mixture combinations of magnesium, calcium, zinc and cadmium; and by the mixed sulfides of calcium and strontium [26], calcium and barium [27].

Leverenz has found that addition of beryllium to zinc silicate activated with manganese serves to shift the color of the emission to longer wavelengths [28]. This is due to the formation of a solid solution of the isomorphous zinc and beryllium silicates. Their solubility, however, is limited, to an extent depending upon the manganese concentration, and this determines the extent of the spectral shift. Diffraction patterns show that the lattice of zinc silicate is contracted as beryllium silicate is added. The degree of the contraction is directly proportional to the beryllium content up to a critical concentration and remains constant as the concentration is further increased. The color of the emitted luminescence likewise shifts toward the red up to this concentration. The solubility limit was found to lie at 30 molar per cent beryllium for 1 percent manganese content, the same as for a mixture free of manganese. At 4 percent it had fallen to 15 molar percent [29].

A similar case is shown by the zinc cadmium sulfides. As the cadmium content is increased, the emission band of both copper and silver activated phosphors is shifted continuously to longer wavelength [30]. Cadmium sulfide forms mixed crystals with zinc sulfide over the whole composition range. Mutual solution occurs both in coprecipitation and in firing at high temperatures [31]. Cadmium sulfide exists only in the hexagonal form, in contrast to zinc sulfide for which the hexagonal form is stable above 1040°C and the cubic form below. With as small an amount as 10 percent cadmium sulfide, however, the sulfide mixture conforms to the crystalline type of the latter and forms only the hexagonal form at temperatures from 900°C to 1200°C. Just as zinc sulfide alone emits a weak fluorescence, so do also the unactivated mixed sulfides. Again, the fluorescence is shifted from the blue toward the red as the cadmium content rises [28].

A further example of the same shift in fluorescence color is exhibited by the tungstates. Diffraction patterns show that solid solutions are formed and that the tungstate lower in concentration adapts itself to the structure of the predominant tungstate, with appropriate alterations in lattice size, depending on the relative ionic sizes of the metallic elements

involved. The fluorescence color of calcium tungstate is blue and that of the other individual tungstates is bluish white. Formation of a mixed tungstate, however, shifts the fluorescence toward the yellow. This shift is most pronounced in the 50 percent mixtures of magnesium-cadmium tungstate and of zinc-cadmium tungstate. The emission spectra are somewhat ambiguous. It appears from them, however, that the broad emission band characteristic of the individual tungstates of cadmium, magnesium and zinc may be a composite of two bands and that the formation of a mixed tungstate leads primarily to an alternation in the relative intensity of these bands, favoring the one of longer wave length.

Fired mixtures of calcium and strontium sulfides, activated with copper, have been studied by Yamashita [26]. The position of corresponding lines in their diffracton patterns showed a linear change in lattice size within the range of 30 to 100 atomic percent strontium, denoting the formation of solid solutions. The position of the copper lines in the fluorescence spectrum showed likewise a continuous shift within this range.

2.3 Synthesis of Phosphors:

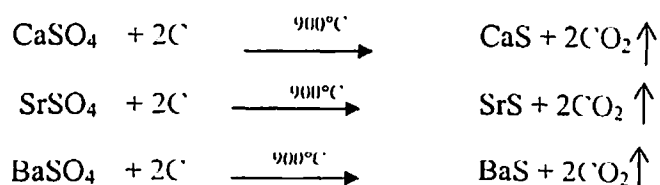
2.3.1 General Considerations:

The luminescent properties of phosphors are known to be affected by a number of preparative parameters, e.g. purity of ingredients [6], particle size of the ingredients, firing time, temperature and atmosphere during firing [32], rate of cooling [6,33,34], grinding [35] and the grain size of the phosphor [36].

2.3.2 Present method of synthesizing phosphors:

Alkaline earth sulphide phosphors can be synthesized by several methods. Theoretically it is possible to start with carbonates, nitrates or sulphates of alkaline earths and reduce them in the form of sulphides. It is also possible to start directly with the sulphides. When the starting materials are carbonates (CaCO_3 , SrCO_3 or BaCO_3) or nitrates (e.g. $\text{Ca}(\text{NO}_3)_2$), they are heated at elevated temperature in the presence of H_2S gas to obtain respective sulphides [26, 37]; and when the starting materials are sulphates, carbon is used as a reducing agent [26, 38]. It is also possible to grow a single crystal of the sulphide [39] or start directly with the poly-crystalline sulphides[40-42].

In the present investigation, the starting materials were extra pure grade (99.99%) CaSO_4 , SrSO_4 , and BaSO_4 (supplied by Reidel (India) Chemicals Pvt Ltd). They were reduced to respective sulphides by heating with the reducing agent, Carbon, (in the form of activated charcoal, AR Grade (99.9 %), supplied by Central Chemical Drug House (P) Ltd.) as per the following reactions.



The activating impurity, copper, was taken in the form of CuSO_4 [AR Grade (99.9%) supplied by Central Chemical Drug House (P) Ltd.]; the solution of the latter (in double distilled water) was used for this purpose. It was not found necessary to use flux in these phosphors.

The charge consisting of constituent (single or double) alkaline earth sulphates, reducing agent, carbon, and desired amount of activator compound was thoroughly grinded using pistol and mortar and dried in the oven and then kept in fused silica crucibles with lids closed. The charge was then fired in the muffle furnace at $900^\circ\text{C} \pm 10^\circ\text{C}$ for one hour. The fired mass was removed from the furnace and immediately crushed to the fine powdered form and transferred to sample tubes and then sealed to protect it from moisture. Six series of phosphors have been synthesized. They are (i) SrS:Cu, (ii) BaS:Cu; (iii)CaS:Cu; (iv) (Ca,Sr)S:Cu, (v) (Sr,Ba)S:Cu and (vi) (Ca,Ba)S:Cu.

The compositions of samples of the above series are given in Tables 2.1 to 2.6.

Table 2.1 Composition of SrS:Cu phosphors

Sample No.	Label on the sample	Weight of SrSO_4 (gm)	Weight of activated charcoal (gm)	Concentration of activator, Cu (mole %)
S ₁	SrS (Cu) .0005M	10	1.4	0.0005
S ₂	SrS (Cu) .001M	10	1.4	0.001
S ₃	SrS (Cu) .002M	10	1.4	0.002
S ₄	SrS (Cu) .003M	10	1.4	0.003
S ₅	SrS (Cu) .005M	10	1.4	0.005
S ₆	SrS (Cu) .007M	10	1.4	0.007
S ₇	SrS (Cu) .009M	10	1.4	0.009
S ₈	SrS (Cu) .01M	10	1.4	0.01

Table 2.2 Composition of BaS:Cu phosphors

Sample No.	Label on the sample	Weight of BaSO ₄ (gm)	Weight of activated charcoal (gm)	Concentration of activator, Cu (mole %)
B ₁	BaS (Cu) .0005M	10	1.2	0.0005
B ₂	BaS (Cu) .001M	10	1.2	0.001
B ₃	BaS (Cu) .002M	10	1.2	0.002
B ₄	BaS (Cu) .003M	10	1.2	0.003
B ₅	BaS (Cu) .005M	10	1.2	0.005
B ₆	BaS (Cu) .007M	10	1.2	0.007
B ₇	BaS (Cu) .009M	10	1.2	0.009
B ₈	BaS (Cu) .01M	10	1.2	0.01

Table 2.3 Composition of CaS:Cu phosphors

Sample No.	Label on the sample	Weight of CaSO ₄ (gm)	Weight of activated charcoal (gm)	Concentration of activator, Cu (mole %)
C ₁	CaS (Cu) .0005M	10	1.8	0.0005
C ₂	CaS (Cu) .001M	10	1.8	0.001
C ₃	CaS (Cu) .002M	10	1.8	0.002
C ₄	CaS (Cu) .003M	10	1.8	0.003
C ₅	CaS (Cu) .004M	10	1.8	0.004
C ₆	CaS (Cu) .006M	10	1.8	0.006
C ₇	CaS (Cu) .009M	10	1.8	0.009
C ₈	CaS (Cu) .01M	10	1.8	0.01

Table 2.4 Composition of (Ca,Sr)S:Cu phosphors

Series No	Label on the sample	Weight of CaSO ₄ (gm)	Weight of SrSO ₄ (gm)	Weight of activated charcoal (gm)	Concentration of activator, Cu (mole %)
CS ₁	CaS1/SrS9	1	9	1.44	0.003
CS ₂	CaS2/SrS8	2	8	1.48	0.003
CS ₃	CaS3/SrS7	3	7	1.52	0.003
CS ₄	CaS4/SrS6	4	6	1.56	0.003
CS ₅	CaS5/SrS5	5	5	1.60	0.003
CS ₆	CaS6/SrS4	6	4	1.64	0.003
CS ₇	CaS7/SrS3	7	3	1.68	0.003
CS ₈	CaS8/SrS2	8	2	1.72	0.003
CS ₉	CaS9/SrS1	9	1	1.76	0.003

Table 2.5 Composition of (Sr,Ba)S:Cu phosphors

Sample No.	Label on the sample	Weight of SrSO ₄ (gm)	Weight of BaSO ₄ (gm)	Weight of activated charcoal (gm)	Concentration of activator, Cu (mole %)
SB ₁	SrS9/BaS1	9	1	1.38	0.003
SB ₂	SrS8/BaS2	8	2	1.36	0.003
SB ₃	SrS7/BaS3	7	3	1.34	0.003
SB ₄	SrS6/BaS4	6	4	1.32	0.003
SB ₅	SrS5/BaS5	5	5	1.30	0.003
SB ₆	SrS4/BaS6	4	6	1.28	0.003
SB ₇	SrS3/BaS7	3	7	1.26	0.003
SB ₈	SrS2/BaS8	2	8	1.24	0.003
SB ₉	SrS1/BaS9	1	9	1.22	0.003

Table 2.6 Composition of (Ca,Ba)S:Cu phosphors

Sample No.	Label on the sample	Weight of CaSO ₄ (gm)	Weight of BaSO ₄ (gm)	Weight of activated charcoal (gm)	Concentration of activator, Cu (mole %)
CB ₁	CaS1/BaS9	1	9	1.26	0.001
CB ₂	CaS2/BaS8	2	8	1.32	0.001
CB ₃	CaS3/BaS7	3	7	1.38	0.001
CB ₄	CaS4/BaS6	4	6	1.44	0.001
CB ₅	CaS5/BaS5	5	5	1.50	0.001
CB ₆	CaS6/BaS4	6	4	1.56	0.001
CB ₇	CaS7/BaS3	7	3	1.62	0.001
CB ₈	CaS8/BaS2	8	2	1.68	0.001
CB ₉	CaS9/BaS1	9	1	1.74	0.001

In order to confirm the composition of the synthesized materials, to verify the formation of mixed lattices and to determine the lattice parameters of the latter, x-ray diffraction spectra of all the samples were recorded. The findings of these investigations have been given in the next chapter.

References

1. G.F. Alfrey, M.A.S. Sweet, Proc. Int. Conf. Lumin, 1, 1022, (1966).
2. D. Poelman, R.L. Van Melrhaeghe, B.A. Vermeersch and F Cardon, J. Phys.D: Appl. Phys., 30, 465, (1997).
3. Y.S. Kim, S.J. Yun, J. Phys: Condens. Matter, 16, 569 (2004).
4. N. Yamashita, Japn. J. Appl. Phys., 30, 3335 (1991).
5. J.Wu, D. Newman and I. V.F. Viney, J. Phys. D : Appl. Phys. 35, 968, (2002).
6. H.W.Leverenz, "An introduction to luminescence of solids", John Wiley & Sons (1950).
7. N.F. Mott and R.W. Gurney, "Electronic processes in ionic crystals", Clarendon Press.
8. W. Lehman, J. Lumin. 6, 455 (1973).
9. J. H. Schulman, L.W. Evans, R. J. Ginther and K. J. Murata, J. Appl. Phys., 18, 732 (1947).
10. J. H. Schulman, R. J. Ginther and C. C. Klick, J. Electronchem, Soc., 97, 123 (1950).
11. T. P. J. Botden and F.A. Kroger, Physica, 14, 553 (1948).
12. G. F. J. Garlick, "Preparation and characteristics of solid luminescent materials", Wiley (1948).
13. G. F. J. Garlick and D. E. Mason, J. Electrochem. Soc., 96, 91 (1949).
14. R. H. Bube, S. Larach and F. E. Shrader, Phys. Rev., 92, 435 (1953).
15. M. Schon, Naturforsch, 69, 251 (1951).
16. S. Larach, J. Chem. Phys, 18, 896 (1950).
17. M. Avinor, J. Chem. Phys., 32, 621 (1960).
18. A. I. Blozhevich, A. G. Zavrahin and A.V. Lavrov, Opt. & Spec., 7, 290 (1959).
19. R. Ward, "Preparation and characteristics of solid luminescent materials", Wiley (1948).
20. A. L. Smith, J. Electrochem, Soc. 96, 75 (1949).

21. N.V. Zhukova, Dokl, Acad. Nauk. SSSR, **85**, 981 (1952).
22. F. A. Kroger and J. E. Hellingman, J. Electrochem. Soc., **93**, 156 (1948); **95**, 68 (1949).
23. R. H. Bube, J. Chem, Phys., **20**, 708 (1952).
24. H. A. Klasens, J. Electrochem, Soc. **100**, 72 (1953).
25. R. H. Bube and S. Laranch, J. Chem. Phys. **21**, 5 (1953).
26. N. Yamashita, K. Ebisumori, K. Nakamura, J. Lumin.**62**, 25 (1994).
27. U. K. Mishra, S. L. Mor and J. D. Ranade; Indian J. Pure & Appl. Phys., **18**, 6(1980).
28. H. W. Leverenz and F. Seitz, J. Appl. Phys., **10**, 479 (1939)
29. G. R Fonda, J. Phys.Chem., **45**, 282 (1941)
30. A. A. Gunz, Compt. Rend., **77**, 479 (1923)
31. F. A Kroger, Zeit. Krist., **102**,132 (1939)
32. F. A. Kroger, Brit. J. Appl. Phys. suppl. 4, **5**, 58 (1955).
33. F. A. Kroger, Some aspects of the luminescence of solids, Elsevier, Amsterdam, (1948).
34. W. E. Ishler, E. F. Apple and H. C. Froelich, Acta Phys. Hungar, **14**, 295 (1962).
35. G. R. Fonda, J. Phys. Chem. **43**, 561 (1939).
36. G. F. J. Garlick, Cornell Symposium, 57 (1948).
37. J. W. Brightwell, B. Ray, P. Sephton and I. V. F. Viney, J. Cryst. Growth, **86**, 634 (1988).
38. B. Ray, J. W. Brightwell, D. Allsop and A.G. J. Green, J. Cryst. Growth, **86**, 644, (1988).
39. J. W. Brightwell, B. Ray and C. N. Buckley, J. Cryst. Growth, **59**, 210 (1982).
40. W. Lehmann, J. Lumin. **5**, 87 (1972).
41. P. K. Ghosh, V. Shanker and T. R. S. Reddy, Indian J. Phys. **50**, 438 (1976).
42. S. Asano, N. Yamashita, Y. Nakao and Y. Matsushima, Phys. Status Solidi (b), **108**, 229 (1981).

Chapter 3

X- ray Diffraction Spectra

3.1 Introduction:

The phenomenon of x ray diffraction by crystals results from a scattering process in which x- rays are scattered by the electrons of the atoms without change in wavelength. A diffraction beam is produced by such scattering only when certain geometrical conditions are satisfied, which may be expressed in either of two forms, the Bragg's law or the Laue equations. The resulting diffraction pattern of a crystal, comprising both the position and intensities of the diffraction effects, is a fundamental physical property of the substance, serving not only for its speedy identification but also for the complete elucidation of its structure.

In single crystals, analysis of the position of diffraction lines leads immediately to a knowledge of the size, shape and orientation of unit cell. In the case of single lattice powder phosphors synthesized by reducing techniques, it gives information about the phase (s) present in the final product, the grain size of the micro-(nano) crystallites as well as the material structure [1-4]. In the case of mixed lattice phosphors, the x-ray diffraction spectra gives the valuable information about the formation of mixed lattice and/or the presence of different phase(s) [5, 6]. Considering all these aspects, x-ray diffraction spectra of synthesized samples were recorded and analyzed. We begin with the relevant theory, in brief, of the powder diffraction method that was employed in our investigation.

3.2 Powder Method of X-Ray Diffraction:

The x- ray powder diffractometer is an outgrowth of the Bragg ionization spectrometer [7, 8], which was applied as early as 1931 to the measurement of reflection from single crystals. Unlike the ionization spectrometer, which disperses a spectrum of x-ray wavelength by means of a crystal grating of some fixed spacing d_{hkl} , the diffractometer is designed to disperse x-rays of a single wavelength by diffracting them from planes of different spacings. Furthermore, an x-ray powder diffractometer is characterized by the use of a local intensity measuring receiver (quantum counter) rather than a photographic film, and a parafocusing arrangement is usually employed to increase the intensity and resolution. The first counter diffractometer for powder studies was developed at the United States Naval Research Laboratory by Friedman [9]. The

subsequent development of the diffractometer into the precision instrument of today may largely be credited to Parrish and coworkers [10].

The parafocusing arrangement utilized in a standard powder diffractometer is shown in Fig 3.1. The flat sample S is tangent to the focusing circle of radius r . The sample (S) – to – source(F) distance FS and sample – to – receiver distance SG are the same and equal to R , the radius of the goniometer circle.

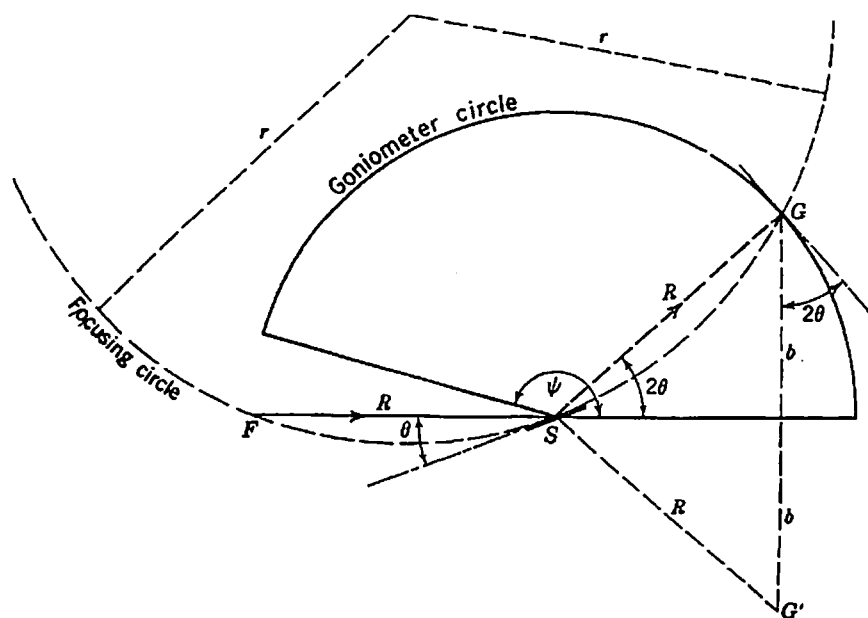


Fig 3.1: Parafocusing arrangement

The triangle SGG' is an axial section through a diffraction cone of semiapex angle 2θ diverging from S; evidently, this triangle represents the intersection of this cone with the plane of the goniometer circle. The diffracted rays come to an approximate focus at G, the position of the receiving slit, and diverge again as they enter the counter window. An inspection of Fig 3.1 shows r to possess the angular dependence

$$r = \frac{R}{2 \sin \theta} \quad (3.1)$$

The base of the diffracted cone intercepted by the receiving slit is a circle of radius

$$b = R \sin 2\theta \quad (3.2)$$

The angle ψ represent the limiting range of the goniometer arc, which is about 165° in most instruments.

3.2.1 Optical Arrangement:

Fig 3.2 shows the optical properties of a typical present day diffractometer. The focal spot is viewed laterally so that the apparent source width is only $\omega \sin\alpha$ where α , is normally 3 to 6° .

An X-ray source of such narrow projected width is often referred to as a line source. The equatorial divergence is limited by the dimension x of the aperture X . Whereas the axial divergence, instead of being prescribed by the height of the divergence slit is more drastically limited by employing two Soller slit collimator [11] s_1 and s_2 for the incident and diffracted beams respectively.

In all the common x ray diffraction methods, it is necessary to limit the x-radiation to a small pencil. It is accomplished with a "collimator" which may take form of pinhole system, or a slit system. The radiation emanating from the focal spot on the target of the x-ray tube is limited by a pair of holes, 1 and 2, of the collimator.

These holes are small apertures, made of lead. Since lead has its own x ray powder diffraction pattern, diffraction by the aperture 2 will interfere with the diffraction by the crystal planes. In order to reduce the diffraction from this aperture diaphragm 3 is added to the sequence. This hole is designed in such a way that it is large enough to pass the desired x ray beam emanating from apertures 1 and 2, without touching by it, but small enough so that it intercepts the smallest cone of the diffracted radiation arising from aperture 2.

As the beam travels through the powdered sample, it meets thousands of powder grains and each grain is like a tiny crystal with different orientation. The orientations of large number of these grains are such that a particular set of plane (hkl) make appropriate glancing angle θ (for that plane) with the x-ray beam. Such grains reflect x rays in the direction making an angle 2θ with the direction of a cone of half angle 2θ . For each solution of Bragg equation given below, there exists a particular case

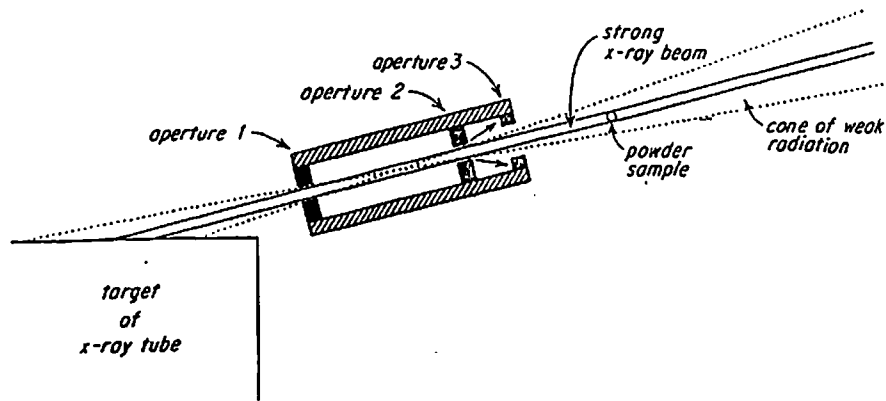


Fig 3.3: Schematic diagram of collimator for x- ray powder method

$$\theta = \text{Sin}^{-1}\left(\frac{\lambda n}{2d_{hkl}}\right) \quad (3.3)$$

where λ is the wavelength of reflected X-ray, n is the order of diffraction, d_{hkl} is the interspacing between reflecting planes, hkl are the Miller indices for that plane.

Considering a particular cone, separate reflections from all crystals which satisfy equation (3.3) for particular value of n/d_{hkl} lie along the vertices of a particular cone of half angle 2θ . If the experimental arrangement is appropriate, these diffracted rays are so numerous that the cone is densely outlined by rays [12].

3.2.2 Choice of Radiation:

The radiation emitted by the x- ray tube is characteristic of the chemical elements, of which the target is composed. In our experiment we have used Copper as target, which emits radiation $K_{\alpha 2}$ (1.54434 Å), $K_{\alpha 1}$ (1.54050 Å) and K_{β} (1.39217 Å). Each element when properly excited emits several characteristic wavelengths. These are named in order of decreasing wavelength, $K_{\alpha 2}$, $K_{\alpha 1}$, K_{β} and so on in order of decreasing wavelength. The first two have wavelengths so close to each other that their reflection constitutes a close doublet which can be ordinarily resolved easily except for large value of θ . Hence when unresolved, these two are lumped together and assigned a combined wavelength, which is intensity- weighted mean of the two wavelengths, namely,

$$K_{\alpha} = \frac{1}{3} (K_{\alpha 2} + 2 K_{\alpha 1}) \quad (3.4)$$

The K_{β} radiation is considerably shorter than the K_{α} and its reflection is always resolved from them under all circumstances. In case of copper the value of K_{α} is 1.5418 Å. This characteristic radiation is superimposed on a background of general radiation, which contains all wavelengths above some minimum value, the minimum value being the function of the voltage across the X-ray tube.

The penetrating power of X-ray radiation increases with decreasing wavelength. Penetrating radiation is sometimes referred to as hard radiation and nonpenetrating one as soft radiations.

3.2.3 Filtered Radiation:

A particular target emits the radiations of different wavelengths, which causes confusion in the diffraction pattern. So we have to design a filter for x-ray radiation, which is quite transparent to a given wavelength, but relatively opaque to somewhat shorter wavelengths. It can be seen from the Fig (3.4) that the filter absorbs K_{β} but K_{α} radiation is passed through it without any attenuation. For the case of Cu as a target, Nickel with the density of 0.019 gm/cm² and optimum thickness of 0.021 mm is used as the filter.

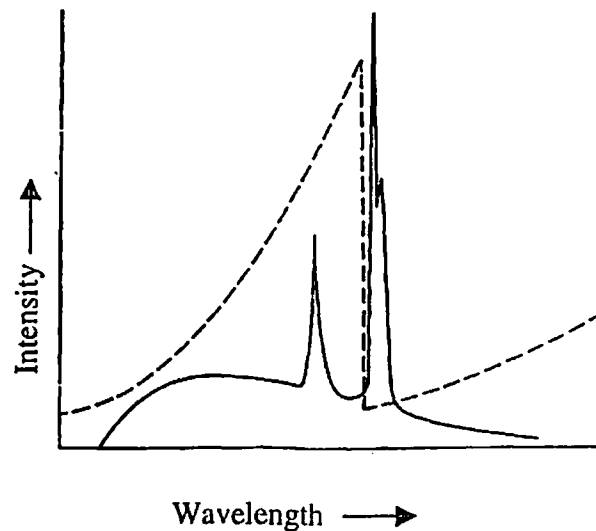


Fig. 3.4 : (a) Emitted radiation (Continuous line) (b) absorption spectrum of filter(broken line)

Since the K_{β} radiation does not add to the information given by the K_{α} radiation it is common practice to use filters to render the x-ray beam approximately monochromatic in this way.

Since the function of a filter is to absorb K_{β} and transmit K_{α} it is immaterial whether the filter is placed between the x-ray tube and the powder specimen or between the specimen and the film. If the first arrangement is used, the filter can be attached either to the window of the x-ray tube or to the collimator of the camera. Since only the direct beam is intercepted by the filter in this arrangement, pieces of foil about $\frac{1}{2}$ cm width are large enough for this purpose.

A much larger filter is required to intercept the diffracted beam if it is to be placed between the specimen and the film. In this case, the filter is usually placed in front of the entire film or detector slit and is kept about $\frac{1}{8}$ in. ahead of it. In addition to absorption of K_{β} , the filter, in this arrangement, also absorbs some of the incoherently scattered radiation, thus decreasing the intensity of the background radiation. So instead of covering the entire film by the filter, only half portion may be covered.

3.2.4 Effect of Specific Absorption:

The absorption of the radiation by an element increases as the wavelength is increased up to a point at which a discontinuity occurs. This wavelength is called absorption edge. At the shorter wavelength side of the discontinuity the absorption is very high and on the longer wavelength side it is very low. If the incident radiation has a wavelength lying on the short wavelength side of the absorption edge of an element, it means that element absorbs that wavelength strongly.

3.2.5 Effect of Sample Size:

As the specimen thickness increases, absorption cuts down to the amount of radiation transmitted through the sample. At the same time, the total amount of radiation deviated towards the diffraction line on the film increases with the volume of sample, and hence with its thickness. It is possible to compute the optimum thickness which a specimen should have, but this is rarely done in practice since means other than decreasing the size of the sample can be used to decrease the amount of radiation being absorbed. By using shorter wavelength radiation, for instance, the absorption may be decreased.

The amount by which a substance decreases the intensity of the transmitted beam can be determined from elementary absorption theory. The relationship between of the intensity of the transmitted beam I to the intensity of the incident beam I_0 is given as

$$I = I_0 e^{-\mu x} \quad (3.5)$$

Since the function of a filter is to absorb K_{β} and transmit K_{α} it is immaterial whether the filter is placed between the x-ray tube and the powder specimen or between the specimen and the film. If the first arrangement is used, the filter can be attached either to the window of the x-ray tube or to the collimator of the camera. Since only the direct beam is intercepted by the filter in this arrangement, pieces of foil about $\frac{1}{2}$ cm width are large enough for this purpose.

A much larger filter is required to intercept the diffracted beam if it is to be placed between the specimen and the film. In this case, the filter is usually placed in front of the entire film or detector slit and is kept about $\frac{1}{8}$ in. ahead of it. In addition to absorption of K_{β} , the filter, in this arrangement, also absorbs some of the incoherently scattered radiation, thus decreasing the intensity of the background radiation. So instead of covering the entire film by the filter, only half portion may be covered.

3.2.4 Effect of Specific Absorption:

The absorption of the radiation by an element increases as the wavelength is increased up to a point at which a discontinuity occurs. This wavelength is called absorption edge. At the shorter wavelength side of the discontinuity the absorption is very high and on the longer wavelength side it is very low. If the incident radiation has a wavelength lying on the short wavelength side of the absorption edge of an element, it means that element absorbs that wavelength strongly.

3.2.5 Effect of Sample Size:

As the specimen thickness increases, absorption cuts down to the amount of radiation transmitted through the sample. At the same time, the total amount of radiation deviated towards the diffraction line on the film increases with the volume of sample, and hence with its thickness. It is possible to compute the optimum thickness which a specimen should have, but this is rarely done in practice since means other than decreasing the size of the sample can be used to decrease the amount of radiation being absorbed. By using shorter wavelength radiation, for instance, the absorption may be decreased.

The amount by which a substance decreases the intensity of the transmitted beam can be determined from elementary absorption theory. The relationship between of the intensity of the transmitted beam I to the intensity of the incident beam I_0 is given as

$$I = I_0 e^{-\mu x} \quad (3.5)$$

where μ is the linear absorption coefficient (in cm^{-1}), and t is the thickness of the substance.

3.3 Indexing of cubic Crystal [13]:

We know that the interplanar spacing, d_{hkl} , can be related to the Miller indices (h, k, l). Thus for cubic crystals,

$$d_{hkl} = \left\{ \frac{1}{\sqrt{h^2 + k^2 + l^2}} \right\} a \quad (3.6)$$

where a is the edge of the cubic lattice (or the unit cell parameter).

Now, consider some families of planes (h, k, l) and note the corresponding values of $h^2 + k^2 + l^2$ (as given in Table 3.1 below).

A close examination of this table reveals that the number 7 is missing. Whatever be the values of h, k, l , the sum of their squares will never be equal to 7. This is known as a forbidden number.

Next two such numbers are 15 and 23.

Table 3.1: Planes (h, k, l) and corresponding values of $h^2 + k^2 + l^2$

Plane represented by (hkl)	$h^2 + k^2 + l^2$
100	1
110	2
111	3
200	4
210	5
211	6
220	8
221	9
300	9
310	10
etc	etc

Another point of interest is that the sum of the squares of the indices 221 and 300 both equal 9. This simply means that the reflections from these planes overlap.

Now combining the expression for d_{hkl} for cubic crystals with the Bragg's equation $n\lambda = 2d_{hkl} \sin\theta_{hkl}$ and putting $n=1$, we get

$$\sin^2\theta_{hkl} = \frac{\lambda^2}{4a^2} (h^2 + k^2 + l^2) \quad (3.7)$$

For a particular powder pattern, λ and a are constant and hence $\sin^2\theta_{hkl}$ is proportional to $(h^2 + k^2 + l^2)$.

Thus, the above relationship may be used to recognize the powder pattern of the cubic lattice. The procedure is as follows. Measure the position of the diffraction lines on the photographic film. Calculate the values of θ and write them in the increasing order and then calculate $\sin^2\theta$ values. If these ratios are approximately 1, 2, 3, 4, 5, 6, 8, etc; then the diffraction pattern is that of a cubic crystal. Once the sequence of numbers is established, the Miller indices (hkl) can be assigned. This is called indexing of cubic crystals.

In order to determine the lattice constant, it is necessary only to determine $\sin\theta$ from one diffraction line with known indices (hkl) of the powder pattern. If this is done for a solid solution of cubic compounds say A and B, and the lattice constants of their end members are known, the molar composition of the solid solution would be $[A_xB_{(1-x)}]$, where

$$x = \frac{a_s - a_B}{a_A - a_B} \quad (3.8)$$

Herein a_s , a_A and a_B are the lattice constant of solid solution end members A and B respectively [14].

3.4 Experimental Setup for Present Investigation:

The schematic diagram of the automatic x-ray powder diffractometer used in the present investigation is shown in Fig. (3.5). This diagram is self-explanatory. The operation of the instrument is as follows [15]:

1. In order to record x-ray diffraction (XRD) patterns, a small amount of sample powder is put on to the glue pasted on the slit. It is then pressed with another slit to make a thin film. The slit is then mounted on the sample mount.
2. Open the water supply for cooling of the generator and the X-ray tube. Switch on the mains by pressing the mains switch on the generator. Be sure that the KV and mA controls are in their minimum positions.
3. Assuming the goniometer is fully aligned, it slews to its calibration point at zero degree 2θ and await its further instructions. Select the desired power with the kV and mA

controls as soon as the minimum setting of kV and mV are reached. At this stage one should not open the window of X-ray tube as long as the goniometer is in zero position because the direct beam from x-ray tube may damage the detector.

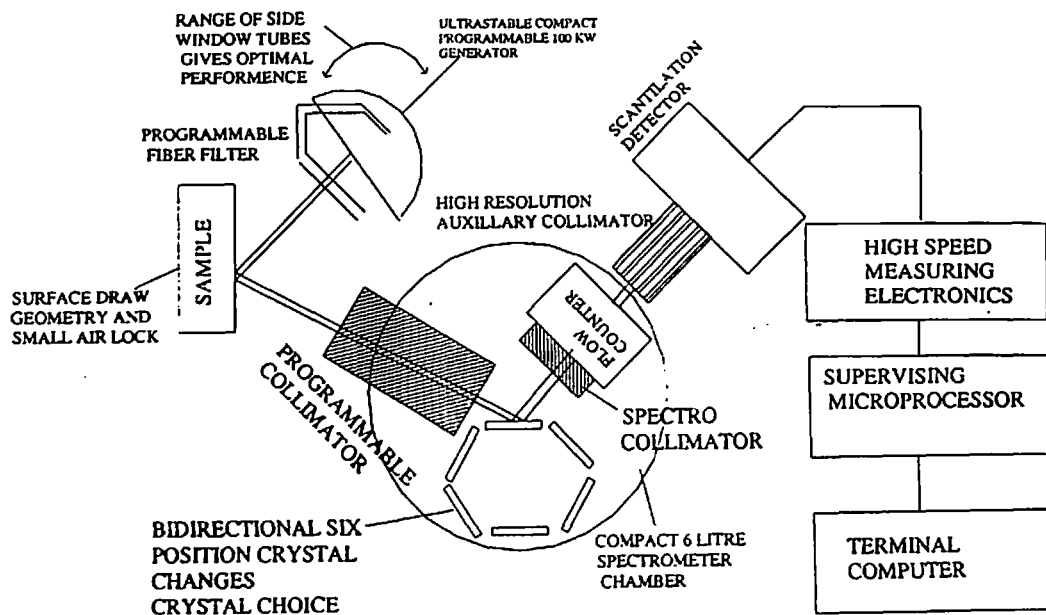


Fig 3.5: Schematic diagram of the automatic X-Ray diffractometer

4 Select the scanning range in 2θ with thumbwheel switch "LOWER ANGLE" & "UPPER ANGLE". Then select the scanning mode, the desired scanning speed, range, desired paper speed on the recorder. The measurement is then started by pressing start button on motor control. When the goniometer reaches its final position the counting unit and recorder are stopped and the printer prints the final angle, the number of count and the time. The goniometer slews back to starting angle.

3.5 Results:

The X-ray diffraction (XRD) spectra of individual alkaline earth sulphide, e.g., SrS, BaS and CaS are shown in Fig 3.6, 3.7 and 3.8 respectively. Sharp lines of XRD demonstrate that the sulphates which are used as starting materials have been converted into respective sulphides. A few extra minor peaks appearing in XRD of some samples seem to be due to Cu_2S . The diffraction lines and the related d_{hkl} values match very well with the standard values reported by National Bureau of Standards [16] and approved by Joint Committee for Powder Diffraction Standards (JCPDS) [17]. Following the procedure given below we have obtained the data from XRD of the three sulphides.

1. The value of θ obtained from the recorded curves were compared with JCPDS values [16] and tentative values of (hkl) were obtained.
2. d_{hkl} corresponding to each θ was calculated using equation (3.3).
3. Using the tentative values of (hkl) and the actual values of d_{hkl} , the value of 'a' was calculating using equation (3.6).
4. Average value 'a' was found from all the experimental values. That average was taken to be equal to d_{100} .
5. From this value of d_{100} , θ was calculated using equation

$$2d\sin\theta = n\lambda, \text{ where } n=1 \text{ and } \lambda=1.544 \text{ \AA}$$

6. From this value of θ_{100} ($=\theta_1$) we found the ratio of $\sin^2\theta/\sin^2\theta_1$ and then following the procedure of section 3.3, we confirmed the values of (hkl) corresponding to all θ .

The same are tabulated in Tables 3.2 to 3.4. This data clearly establishes that all the three sulphides crystallize in cubic lattice form.

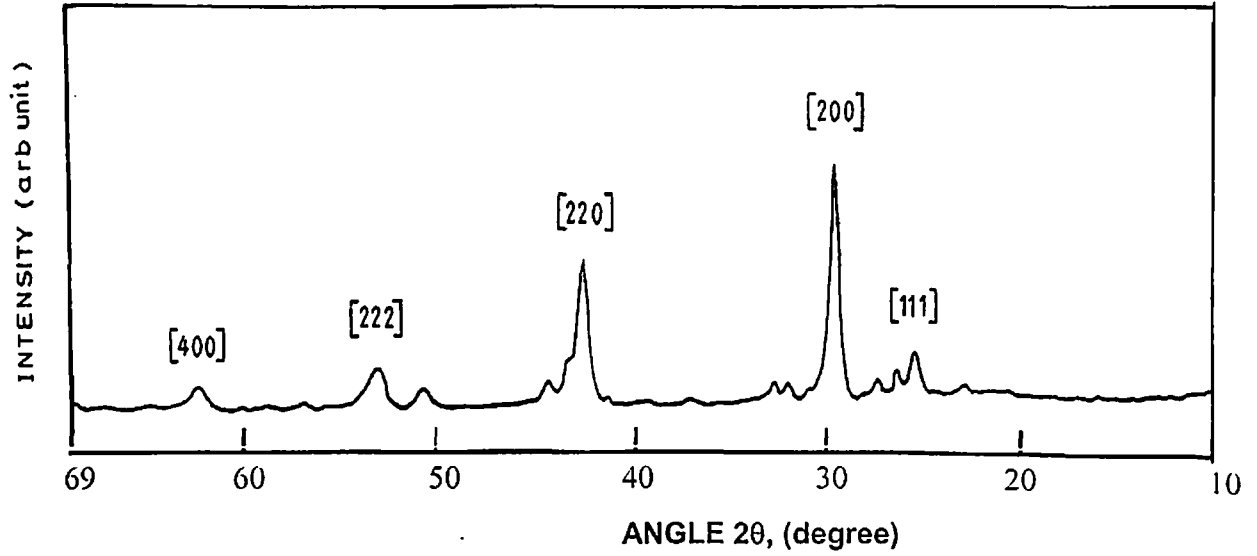


Fig. 3.6: XRD of SrS:Cu (.003 M)

Table 3.2: d_{hkl} and 'a' values for SrS: Cu

Measured value of angle of diffraction (θ)	JCPDS Value of (θ)	$\sin \theta$	$\sin^2 \theta$	$\frac{\sin^2 \theta}{\sin^2 \theta_1}$	(hkl)	d_{hkl}	Lattice constant (a in Å)
7.38 *	-	0.128	0.016	≈ 1	100	5.987	5.987 □
12.8	12.79	0.221	0.048	≈ 3	111	3.475	6.018
14.9	14.84	0.257	0.066	≈ 4	200	2.994	5.988
21.5	21.21	0.366	0.134	≈ 8	220	2.100	5.939
26.5	26.31	0.446	0.199	≈ 12	222	1.725	5.975
31.3	30.79	0.516	0.266	≈ 16	400	1.504	6.016

□ standard value of $a=6.020\text{Å}$

* extrapolated value of diffraction angle

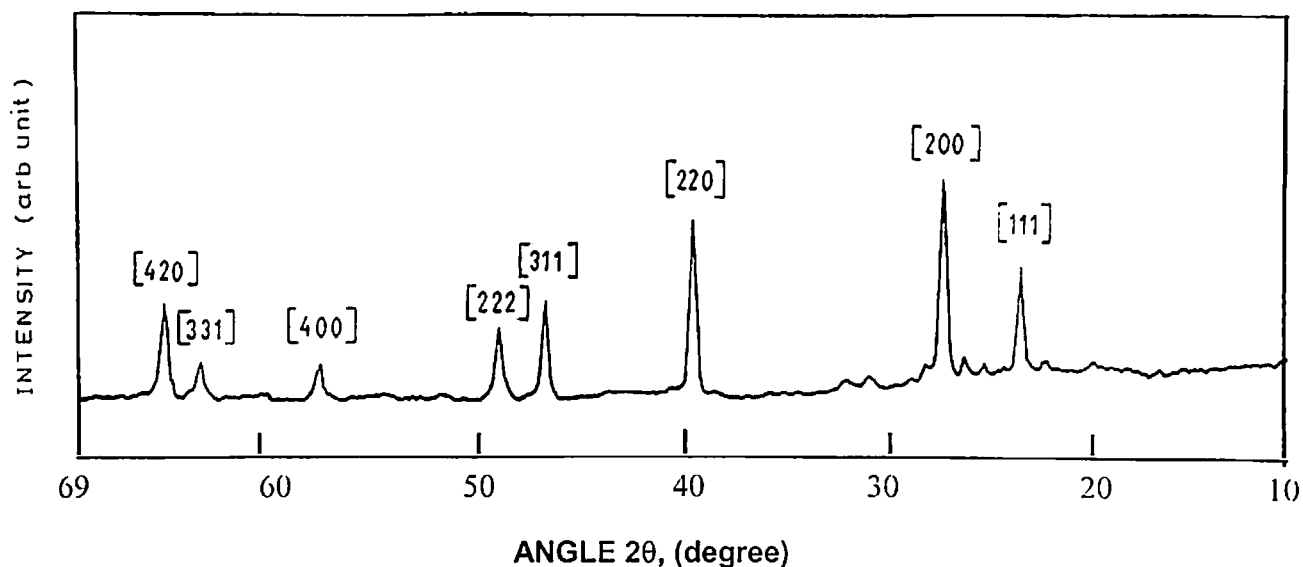


Fig 3.7: XRD of BaS:Cu (.001M)

Table 3.3: d_{hkl} and 'a' values for BaS: Cu

Measured value of angle of diffraction (θ)	JCPDS Value of (θ)	$\sin \theta$	$\sin^2 \theta$	$\frac{\sin^2 \theta}{\sin^2 \theta_1}$	(hkl)	d_{hkl}	Lattice constant (a in Å)
6.89*	-	0.120	0.014	≈ 1	100	6.367	6.367
12.06	12.05	0.208	0.043	≈ 3	111	3.6853	6.383
13.96	13.95	0.241	0.058	≈ 4	200	3.1917	6.383
19.96	19.94	0.341	0.116	≈ 8	220	2.2556	6.379
23.56	23.57	0.399	0.159	≈ 11	311	1.9264	6.389
24.71	24.70	0.418	0.174	≈ 12	222	1.8419	6.380
29.20	28.83	0.487	0.238	≈ 16	400	1.578	6.312
32.0	31.71	0.529	0.280	≈ 9	331	1.453	6.333
32.66	32.62	0.5396	0.291	≈ 20	420	1.4268	6.381

* standard value of $a=6.386\text{Å}$

* extrapolated value of diffraction angle

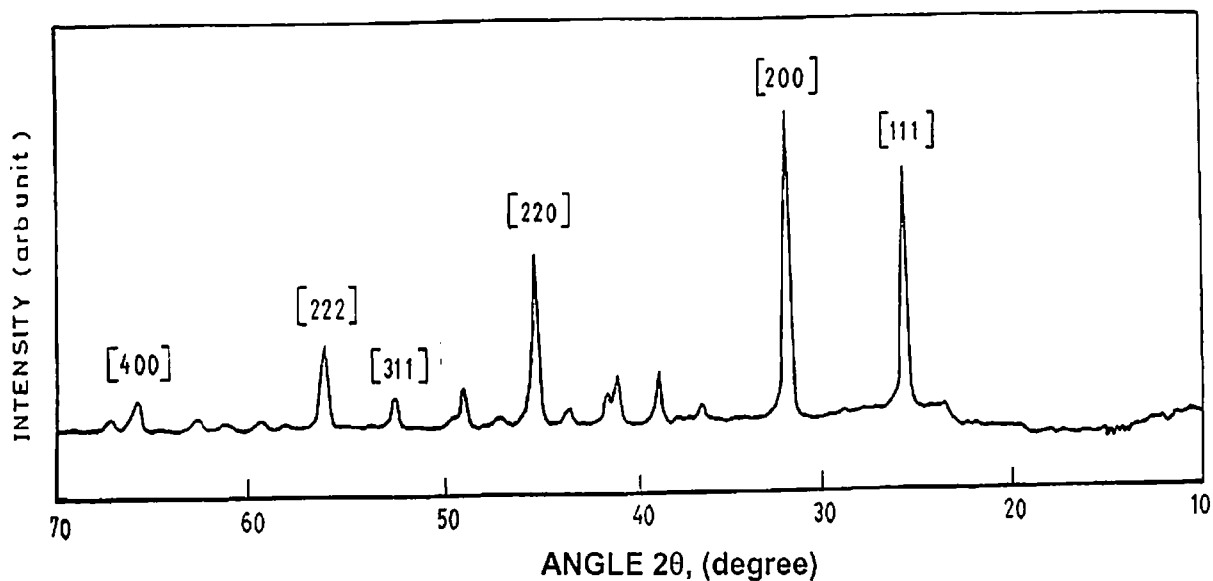


Fig 3.8: XRD CuS:Cu (.003M)

Table 3.4: d_{hkl} and 'a' values for CuS: Cu

Angle of diffraction (θ)	JCPDS Values of (θ)	$\sin \theta$	$\sin^2 \theta$	$\frac{\sin^2 \theta}{\sin^2 \theta_1}$	(hkl)	d_{hkl}	Lattice constant (a in Å)
7.74*	-	0.134	0.018	≈ 1	100	5.745	5.745
12.9	13.58	0.223	0.049	≈ 3	111	3.449	5.973
15.64	15.704	0.269	0.072	≈ 4	200	2.8544	5.6791
22.54	22.49	0.380	0.146	≈ 8	220	2.0079	5.6791
26.3	26.65	0.443	0.196	≈ 11	311	1.7378	5.760
27.94	27.94	0.468	0.219	≈ 12	222	1.6428	5.6910
32.74	32.75	0.540	0.290	≈ 16	400	1.4233	5.6935

[*] standard value of $a=5.6948\text{\AA}$

* extrapolated value of diffraction angle

The XRD of the representative samples of the CS and BS series of mixed sulphide phosphors are shown in Fig 3.9 and 3.10 respectively. The sharp diffraction lines indicate that the mixed lattice in both these cases has been formed and that they crystallize in cubic lattice form. As the XRD is exhibiting only one phase in all the ratios of Ca/Sr and Ba/Sr, it is clear that the solid solution is formed in the complete range of 0 to 100 mole % for these two series of phosphors. The data regarding the variation of lattice constant with the weight fraction of the end members are tabulated in tables 3.5 and 3.6.

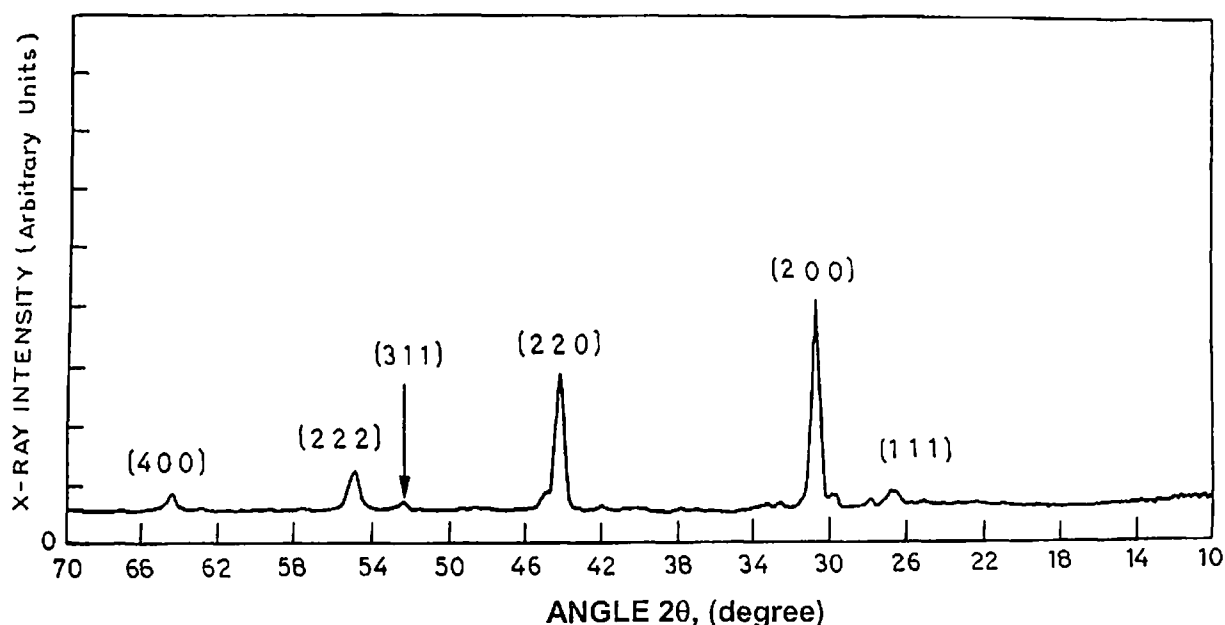


Fig. 3.9: XRD of $(Sr_{0.5}, Ca_{0.5})S:Cu$

Table 3.5: d_{hkl} and a values for $(Sr, Ca)S:Cu$

Sample	Angle of Diffraction (θ)	Miller indices of reflecting plane, (hkl)	Interplanar Spacing, d_{hkl}	Lattice constant (a in Å)
$(Sr_{1.0}, Ca_{0.0})S:Cu$	26.5	222	1.725	5.975
$(Sr_{0.9}, Ca_{0.1})S:Cu$	27.4	222	1.673	5.795
$(Sr_{0.7}, Ca_{0.3})S:Cu$	27.45	222	1.670	5.785
$(Sr_{0.5}, Ca_{0.5})S:Cu$	27.5	222	1.667	5.774
$(Sr_{0.3}, Ca_{0.7})S:Cu$	27.7	222	1.656	5.736
$(Sr_{0.0}, Ca_{1.0})S:Cu$	27.94	222	1.643	5.692

The XRD of the representative samples of the CS and BS series of mixed sulphide phosphors are shown in Fig 3.9 and 3.10 respectively. The sharp diffraction lines indicate that the mixed lattice in both these cases has been formed and that they crystallize in cubic lattice form. As the XRD is exhibiting only one phase in all the ratios of Ca/Sr and Ba/Sr, it is clear that the solid solution is formed in the complete range of 0 to 100 mole % for these two series of phosphors. The data regarding the variation of lattice constant with the weight fraction of the end members are tabulated in tables 3.5 and 3.6.

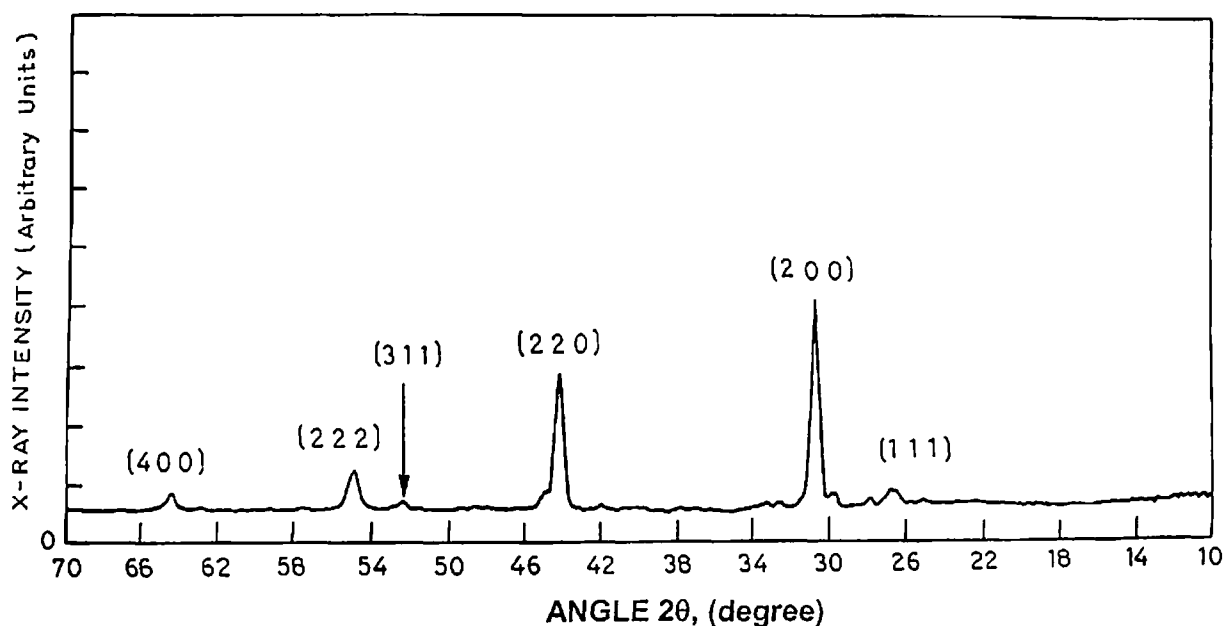


Fig. 3.9: XRD of $(Sr_{0.5},Ca_{0.5})S:Cu$

Table 3.5: d_{hkl} and a values for $(Sr,Cu)S:Cu$

Sample	Angle of Diffraction (θ)	Miller indices of reflecting plane, (hkl)	Interplanar Spacing, d_{hkl}	Lattice constant (a in Å)
$(Sr_{1.0},Ca_{0.0})S:Cu$	26.5	222	1.725	5.975
$(Sr_{0.9},Ca_{0.1})S:Cu$	27.4	222	1.673	5.795
$(Sr_{0.7},Ca_{0.3})S:Cu$	27.45	222	1.670	5.785
$(Sr_{0.5},Ca_{0.5})S:Cu$	27.5	222	1.667	5.774
$(Sr_{0.3},Ca_{0.7})S:Cu$	27.7	222	1.656	5.736
$(Sr_{0.0},Ca_{1.0})S:Cu$	27.94	222	1.643	5.692

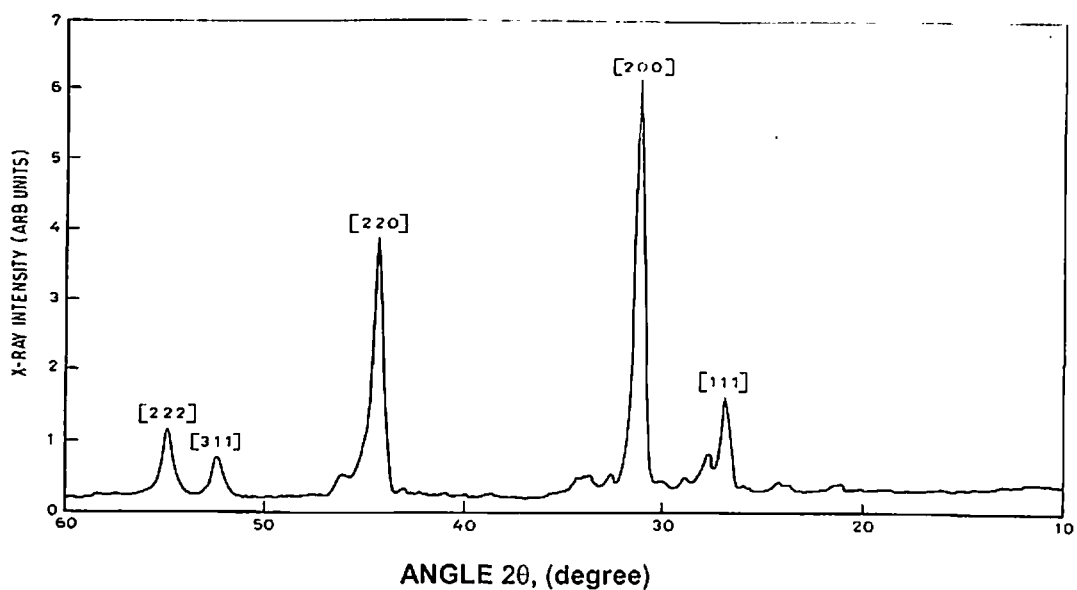


Fig. 3.10: XRD of $(Sr_{0.9},Ba_{0.1})S:Cu$

Table 3.6: d_{hkl} and a values for $(Sr,Ba)S:Cu$

Sample	Angle of diffraction (θ)	Miller indices of reflecting plane (hkl)	Interpalnar Spacing, d_{hkl}	Lattice constant (a in Å)
$(Sr_{0.0},Ba_{1.0})S:Cu$	24.71	222	1.8419	6.3808
$(Sr_{0.1},Ba_{0.9})S:Cu$	24.90	222	1.8288	6.3352
$(Sr_{0.3},Ba_{0.7})S:Cu$	25.00	222	1.8219	6.3115
$(Sr_{0.5},Ba_{0.5})S:Cu$	25.40	222	1.7951	6.2185
$(Sr_{0.9},Ba_{0.1})S:Cu$	26.03	222	1.7540	6.0734
$(Sr_{1.0},Ba_{0.0})S:Cu$	26.50	222	1.7250	5.975

From this data, mole fraction, x of each constituent member was calculated using eq. (3.8). The plot of variation of lattice constant with x for these two series of phosphors are given in Fig 3.11 and 3.12. It is clear from these figures that the lattice constant varies with x linearly, i.e., obeys Vegard's law. This is a further confirmation of the formation of a solid solution in these two cases.

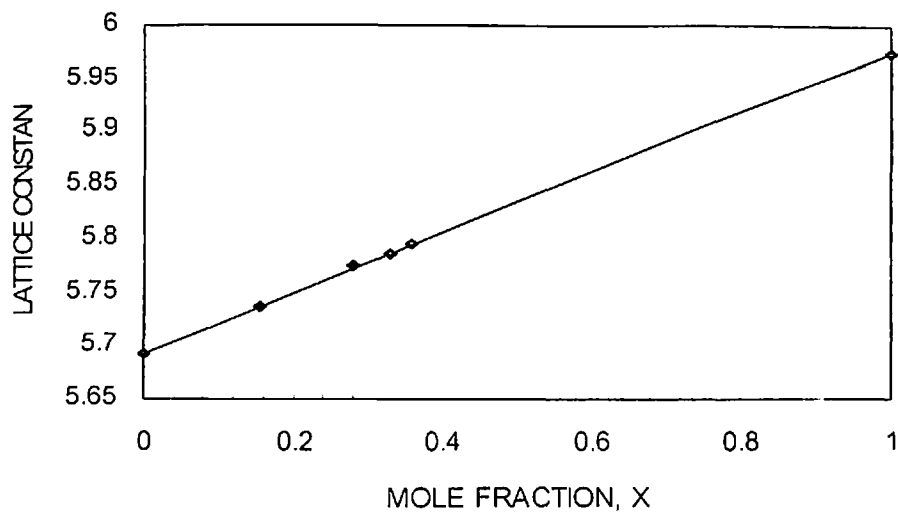


Fig 3.11: Variation of lattice parameter 'a' as a function of x for $(Cu_{(1-x)}Sr_x)S:Cu$

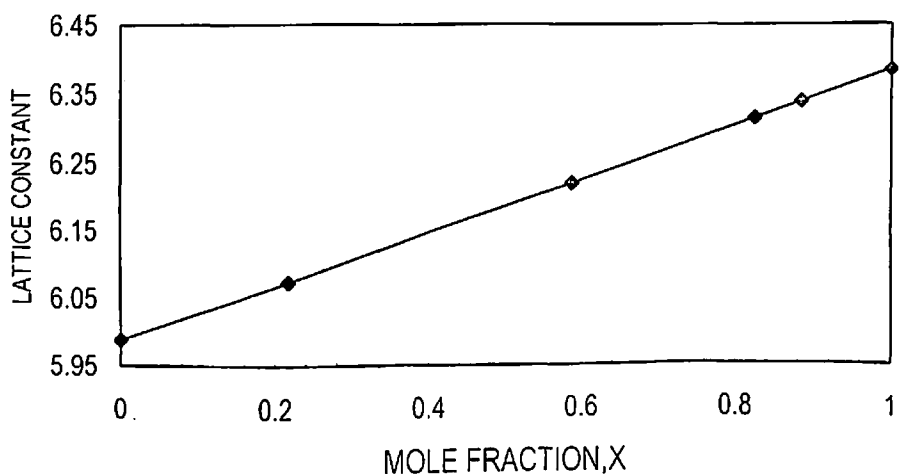


Fig 3.12: Variation of lattice parameter 'a' as a function of x for $(Sr_{(1-x)}Ba_x)S:Cu$

The XRD of representative samples of CB series are shown in Fig 3.13. It is clear from this figure that, the XRD shows the presence of both the phases i.e., CaS as well as BaS.

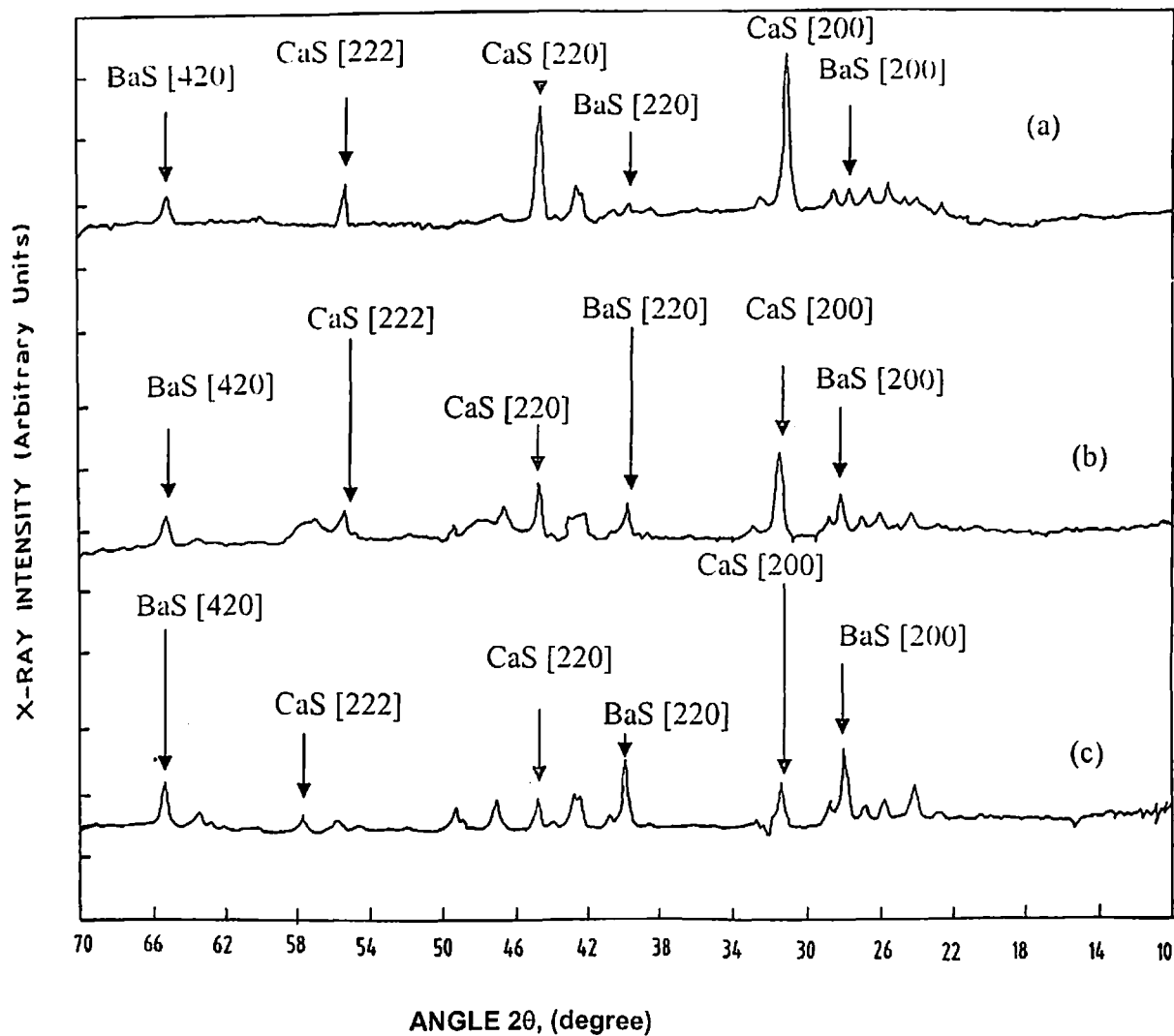


Fig. 3.13: XRD of (a) $(\text{CuS}_7/\text{BaS}_3):\text{Cu}$ (b) $(\text{CuS}_5/\text{BaS}_5):\text{Cu}$ (c) $(\text{CuS}_3/\text{BaS}_7):\text{Cu}$

However, the intensities of the diffraction lines vary with increase in the content of the respective phases. For example the intensities of lines corresponding to planes [200], [220] and [420] of BaS- phase increase with increase in BaS content. Similarly, the intensities of lines corresponding to planes [200], [220] and [222] of CaS-phase increase with increase in the CaS content. This means that the solid solution of CaS and BaS is not formed. Therefore, the lattice parameters of this series have not been calculated as such parameters for individual phases have already been calculated earlier.

References:

1. S. J. Lee, J. E. Jang, Y. W. Jin, G. S. Park, S. H. Park, N. H. Kwon, Y. J. Park, J. E. Jung, N. S. Lee, J. B. Yoo, J. H. You and J. M. Kim, *J. Electrochem. Soc.*, **148**, 4139 (2001).
2. Q. Zhai, J. Li, J. S. Lewis, K. A. Waldrip, K. Jones, P. H. Holloway, *Thin Solid Films*, **414**, 105, (2002).
3. V. G. Kravets, A. A. Kryuchin, V. A. Ataev, V. M. Shershukov, *Optic. Mater.*, **19**, 421, (2002).
4. J. Ihanus, M. Ritala, M. Leskela, E. Soininen, W. Park, A. E. Kaloyeros, W. Harris, K. W. Barth, A. W. Topol, T. Sajavaara and J. Keinonen, *J. Appl. Phys.*, **94**, 3862 (2003).
5. M. A. Santana-Aranda, M. M. Lira, *Sociedad Mexicanade Ciencia de Superficies y de Vacio*, **10**, 36 (2000).
6. N. Yamashita, K. Ebisumori, K. Nakamura, *J. Lumin.***62**, 25 (1994).
7. W.Parrish (ed), *Advances in X- ray Diffractometry and X-ray Spectrography*, Centrex Publ. Company Eindhoven, The Netherland,(1962)
8. W.H. Bragg and W.L. Bragg, *Proc. Roy Soc.(London)* **88A**, 428 (1913)
9. H.Geiger aand W.Muller, *Phys.Z.*,**29**,839 (1928)
10. A.R.Lang, *Rev. Sci.Instrum*, **27**, 17 (1956)
11. W.Soller, *Phys Rev.*, **24**, 158 (1924)
12. L. V.Azaroff and M.J Buerger, *The Powder Method in X-Ray crystallography*, Mcgraw Hill Book Company Inc (1958)
13. R. P. Kharc, "Analysis Instrumentation: An Introduction, (CBS, New Delhi), 135 (1993).
14. F W Harrison and B J Curtis, *Brit. J. Appl. Phys.*,**13**,247(1962)
15. *Manual of Automatic X-Ray Powder diffractometer Model PW 1390.*
16. *National Bureau of Standards (USA), Circ 539,7, 8 & 52 (1957).*
17. *JCPDS- International centre for Diffraction Data (1999).*

Chapter 4

Excitation and Emission Spectra

4.1 Introduction:

Luminescence is a general term applied to emission of light but is different from incandescence. Wiedemann [1], defines luminescence as a phenomenon that involves the absorption of energy by matter and its re-emission as visible or near-visible radiation. Luminescence is subclassified into fluorescence and phosphorescence on the basis of the mechanism by which the atom or molecule undergoes the reverse transition from the excited state to the ground state. Garlick [2] defines fluorescence as the luminescence emitted during excitation while phosphorescence as that emitted after the cessation of excitation. On the basis of physical processes, Perrin [3] defines fluorescence as the emission that takes place by one or more spontaneous transitions and phosphorescence as that which occurs with the intervention of a metastable state followed by return to the excited state due to addition of energy [4].

One often sees in literature, terms such as photoluminescence, radioluminescence, electroluminescence, cathodoluminescence etc; the classification being based on the type of exciting source employed. Excellent reviews of the subject may be found in the work of Curie [5], Butler [6], Ropp [7] and Grattan and Zhang [8].

4.2 Theories of Luminescence:

To explain the phenomenon of luminescence, different models have been proposed, a brief description of which is given below:

4.2.1 Configurational Coordinate Model:

Originally proposed by Von Hippel [9], Seitz [10] applied this model to explain the characteristic luminescence processes. Fig. 4.1 shows the curves representing potential energies of the normal and the excited states of the luminescence centre in relation to the variation of its configuration coordinates. Absorption of radiation raises the centre from the ground state A to the excited state B. The energy absorbed corresponds to the vertical distance AB ($h\nu$) according to Frank - Condon principle.

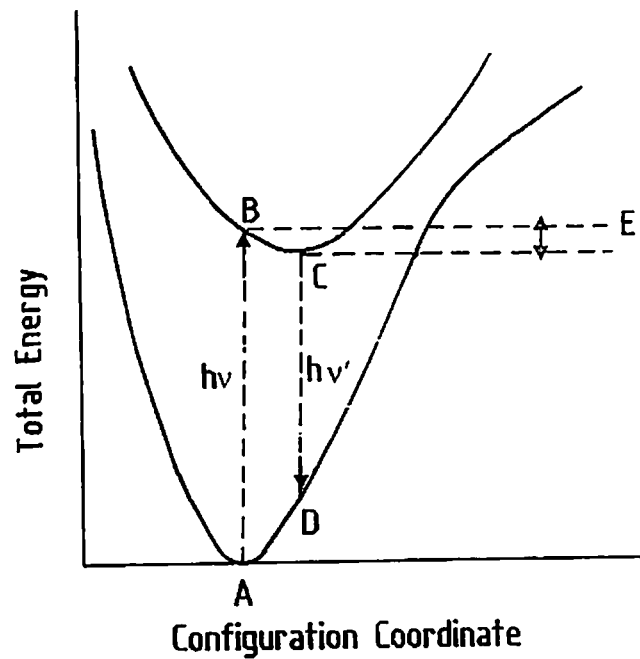


Fig 4.1: Configuration coordinate model

At B, the system is not in equilibrium and hence tries to adjust itself so as to reach C, giving off the energy difference BC as lattice vibrations or phonons. Finally, the centre returns to the ground state by the emission of luminescence CD ($h\nu'$) and then relaxes to A by giving up energy to the lattice. The energy of absorbed photon ($h\nu$) is greater than the energy of emitted photon ($h\nu'$). This corresponds to a shift which is known as Stoke's shift.

Modification to this model helps to explain the radiationless transition. Fig. (4.2) gives the Seitz[10] model for exciton. In this model the system after excitation relaxes to such an extent that its minimum (A) lies outside the ground state curve and this increases the probability of non-radiative transition.

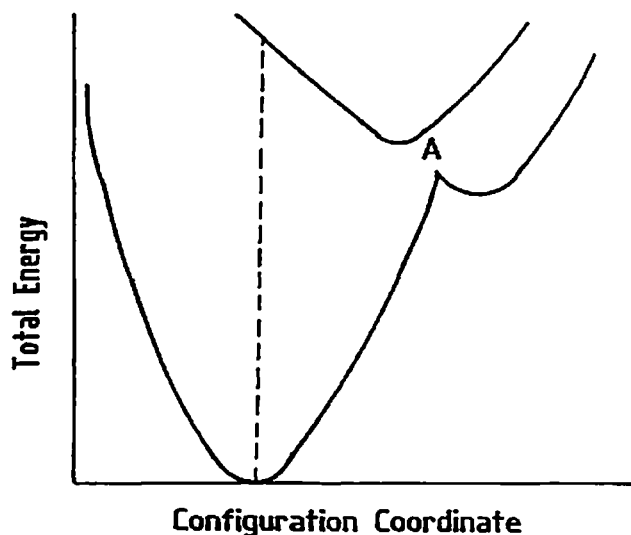


Fig 4.2: Seitz model

The other model (Fig. 4.3) was proposed by Dexter et al [11]. In this model the energy dissipated during relaxation is less than that dissipated according to Seitz model and the system comes quite close to the ground state from where the radiative return is not possible.

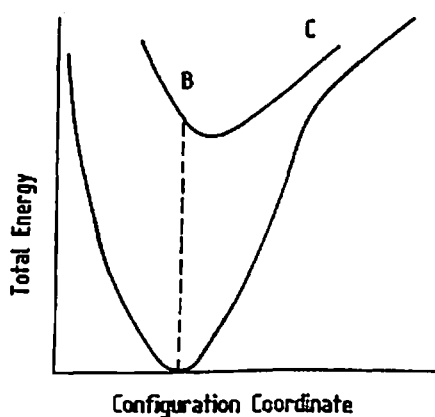


Fig 4.3: Model of Dexter, Klick & Russel

In fact, this model along with its few quantum – mechanical modifications successfully explains (i) Stoke's shift, (ii) width of absorption and emission bands at low temperatures (iii) thermal quenching of luminescence and other temperature effects [12, 13], (iv) monomolecular decay , (v) F- centre luminescence and (vi) sensitization processes in doubly activated solids [14]. Its

limitations are (i) it can not be applied to the process occurring between absorption and emission, e.g. photoconductivity and (ii) because of the configurational difficulties, it is difficult to have precise configuration coordinate diagrams on theoretical considerations only.

4.2.2 Continuous Dielectric Model:

This model removes the defects of the above model by considering the interactions between the centre and the lattice as of a short range type. Huang and Rhys [15] have proposed a theory where they treated the lattice as continuous dielectric in which the centre is embedded and considered long range interactions, electrical in nature. In absorption the centre experiences a difference in charge distribution resulting in a change in lattice polarization which is accompanied by the creation of lattice phonons. This model has been treated very elegantly by Lax & Burstein [16].

4.2.3 Energy Band Model:

An energy band model based on the "collective electron theory" of Bloch [17] has been developed and has been used by many workers [18-24]. According to this theory, qualitatively, when atoms are arranged in an orderly way and in close proximity with each other to form a crystal, the energy states for the electrons in the atoms are distributed by mutual interaction. As a result, the discrete electronic states are broadened into bands of allowed energy separated by bands of forbidden energy. Thus, instead of the discrete energy states there are discrete energy bands for the electrons inside the crystal. The uppermost completely filled band is called the valence band and the next higher allowed band is called the conduction band. The energy levels in an allowed band are so closely spaced that effectively they form a continuum.

The incorporation of an activator atom in a crystalline solid will, in general, give rise to localized energy levels in the normally forbidden energy gap, which produces emission centres for luminescence. (L) represents the ground state of the centre above the filled band called valence band (V) and (L') is its excited state. Other impurities, lattice perturbation due to activator or defects and the presence of vacant lattice sites produce unoccupied levels (T) at various depths in the forbidden gap below the conduction band (C), in which excited electrons can be trapped. These levels are known as electron traps. Absorption and emission processes in phosphors may be explained on the basis of this model. The excitation of luminescence by photon absorption in the matrix lattice or luminescence centre involves rising of an electron from valence band or

from the ground state of the luminescence centre to the conduction band or from a filled activator ground level to some higher activator level as shown in Fig. (4.4) by transitions (A), (B) and (D) respectively. The absorption of energy may also result in transition (E) of the electron from the filled band directly into trapping states, the positive hole left behind migrating to the luminescence centres and emptying them. The luminescence emission occurs when an excited electron returns to an empty ground state of the luminescence centre.

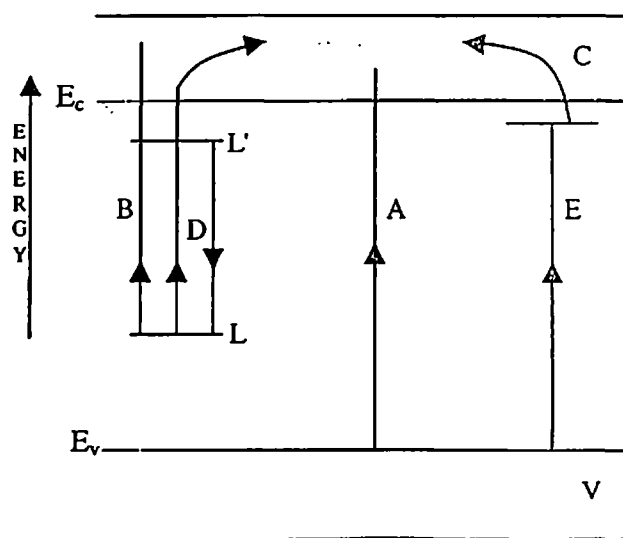


Fig. 4.4: Energy band model

Electrons in the conduction band can return to luminescence centre or may be captured by the traps (T) and phosphorescence is then determined by their activation (thermal, optical or electrical) from traps and subsequent return to the empty luminescence centre.

4.3 Processes in Crystalline Phosphors:

Luminescence systems have been divided into three categories, which are discussed below.

4.3.1 System in Which the Absorption and Emission of Energy Take Place in the Same Centre

The luminescence process involves three stages viz., (a) absorption and excitation (b) transfer and storage of energy and (c) conversion of stored energy as light i.e. emission.

(a) Absorption and Excitation:

The absorption and excitation characteristics of phosphors are primarily functions of the nature of the host lattice and the activator [5]. Some of the possible modes of excitation [25, 26] are shown in Fig. (4.5) and may be described as follows:

- (i) Excitation by fundamental lattice absorption produces a free electron in the conduction band (C) and a free hole in the valence band (V) on absorption of each photon.
- (ii) Excitation of the normal valence electrons produces a bound electron – hole pair called exciton. In this case, no free electrons or holes are produced and energy transferred by the diffusion of the exciton as one unit.
- (iii) Excitation of the luminescence centre produces a free electron in the conduction band and a free hole in the neighbourhood of the centre.
- (iv) Excitation of valence electrons raises an electron to an unoccupied centre and a free hole in the valence band.
- (v) Excitation of the valence electron creates a mobile hole in the valence band and the electron is trapped at 'T'.
- (vi) Excitation within a luminescence centre raises an electron to the excited state of the centre. In this case, no free electrons or holes are produced and the luminescence is highly localized, determined only by the centre configuration.

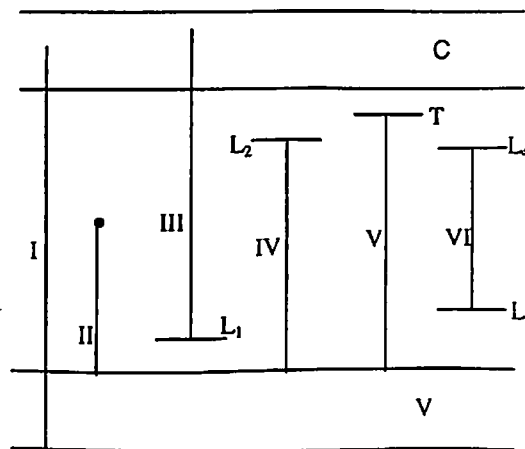


Fig. 4.5: Modes of excitation and physical picture of absorption processes

L₁ – Occupied state of luminescence centre L₂ – Unoccupied state of luminescence centre

L₃ – Ground state of luminescence centre L₄ – Excited state of luminescence centre

T – Trapping state

Corresponding to these transitions the absorption characteristics may be described as follows:

(i) Any radiation of energy greater than the separation between conduction band and valence band raises electrons from the valence band to the conduction band and the absorption due to this is known as a fundamental absorption band. The wavelength corresponding to minimum energy required for the above transition is known as the fundamental absorption edge. For light of energy greater than minimum required, the absorption is continuous and fairly constant up to a certain minimum energy (transition I).

(ii) In the processes of excitation (marked II) where the energy is lower than the band gap energy, the absorption by the lattice creates excitons, which are thermally dissociated at room temperature. These electron - hole pairs move in each other's field in the crystal with no net charge. The absorption is manifested by a series of narrow absorption lines on the low energy side of the absorption edge.

(iii) Other absorption bands at longer wavelength than the absorption edge will be present corresponding to the electronic transitions III, IV and V which are dependent on the matrix and activator or both [27]. These transitions give some structure in the tail of the absorption spectrum lying outside the absorption edge.

(iv) Corresponding to the electronic transition VI the absorption band occurs at still longer wavelength and is due to the electronic transition confined to the luminescent centre or impurity centres [28].

(v) The trapped electrons may be raised by optical stimulation into the conduction band giving rise to a further set of absorption bands in the long wavelength region. These have been observed in materials in the powder form.

In addition, electron in excited phosphors may be raised into emptied centres, thus giving long wavelength absorption band similar to trapped electrons. Defects and impurities present also give new absorption bands usually on the long wavelength side of the characteristic absorption [29].

In general, the absorption spectrum of a crystalline phosphor may be divided into a short wavelength absorption region associated with the matrix crystal lattice, culminating in the fundamental absorption edge and a longer wavelength region associated with the activators and other impurities.

(b) Transfer and Storage of Energy:

When a luminescence centre absorbs energy, it becomes ionized. This energy is not immediately converted into phonons or photons and may be stored in localized metastable states, first proposed by Jablonski [30] and later adopted by Johnson [31] to explain long decay phosphorescence. As shown in Fig. (4.6) absorption of exciting radiation by a luminescence centre raises an electron into the excited state (F). It may then directly return to the ground state (G) with the emission of fluorescence or it may fall into the metastable state (M) lying just below (F). The transition (M \leftrightarrow G) is usually forbidden. The electron in the metastable state requires some activation energy to return to the ground state via (F). The energy is supplied by thermal activation. The resulting delayed emission is phosphorescence.

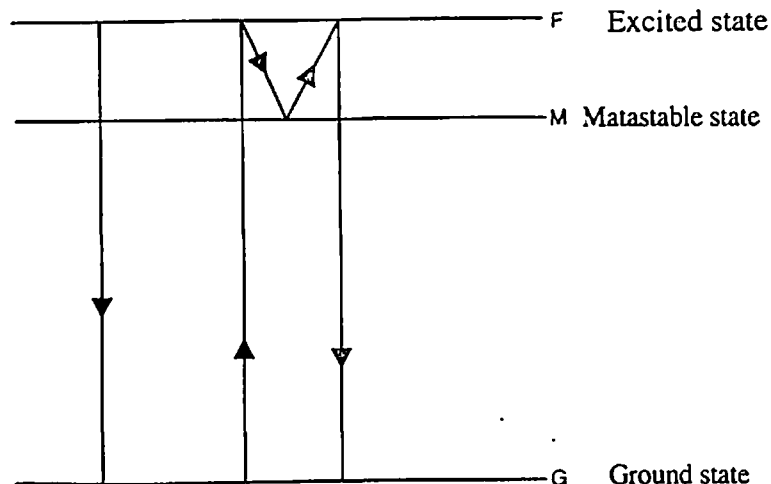


Fig 4.6 : Jablonski model

(c) Emission

Luminescence emission takes place when an excited electron in the conduction band or in the excited state of a centre, returns to the ground state of the luminescence centre. The probability of direct transition from the conduction band to the valence band is low and generally not observable [32]. The temporary storage of energy, by trapping of excited quasi or free electrons, positive holes or excitons in metastable state makes the luminescence emission complicated. The excited electrons may fall into these levels releasing energy as lattice

(b) Transfer and Storage of Energy:

When a luminescence centre absorbs energy, it becomes ionized. This energy is not immediately converted into phonons or photons and may be stored in localized metastable states, first proposed by Jablonski [30] and later adopted by Johnson [31] to explain long decay phosphorescence. As shown in Fig. (4.6) absorption of exciting radiation by a luminescence centre raises an electron into the excited state (F). It may then directly return to the ground state (G) with the emission of fluorescence or it may fall into the metastable state (M) lying just below (F). The transition (M \leftrightarrow G) is usually forbidden. The electron in the metastable state requires some activation energy to return to the ground state via (F). The energy is supplied by thermal activation. The resulting delayed emission is phosphorescence.

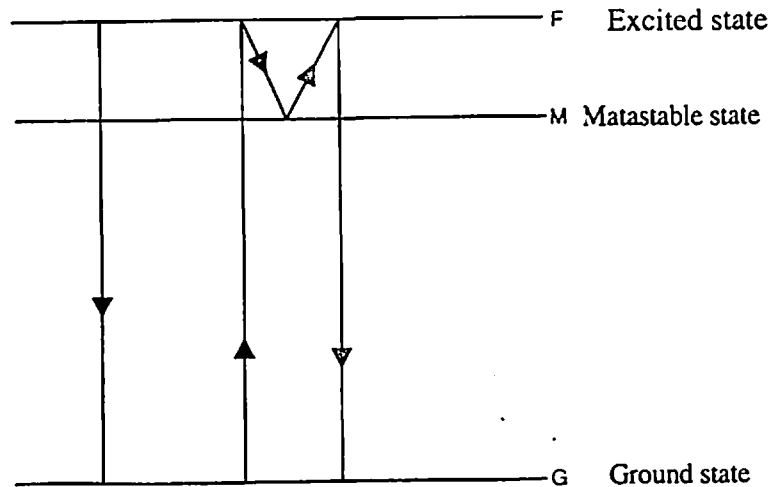


Fig 4.6 : Jablonski model

(c) Emission

Luminescence emission takes place when an excited electron in the conduction band or in the excited state of a centre, returns to the ground state of the luminescence centre. The probability of direct transition from the conduction band to the valence band is low and generally not observable [32]. The temporary storage of energy, by trapping of excited quasi or free electrons, positive holes or excitons in metastable state makes the luminescence emission complicated. The excited electrons may fall into these levels releasing energy as lattice

vibrations or phonons. The nature of trapping centres is a major factor in determining the nature of phosphorescence [33].

The 'anti-stokes' luminescence, the emission of shorter wavelength than the exciting one, has been observed some phosphors [34, 35]. This has been explained on the basis of a two stage excitation process. The first infrared photon ionizes the impurity level into the conduction band and a second one raises a valence electron into the empty level, thus creating an electron –hole pair followed by luminescence emission of shorter wavelength.

4.3.2 Systems in Which Absorption Occurs in One Centre and the Luminescence is Emitted by Another Centre and the Transfer of Energy Takes Place without Movement of Charge Carriers.

There are three different mechanisms of such transfer:

(a) Cascade or Radiative Mechanism:

It occurs when the phosphor contains two activators (i. e. two luminescence centres). One centre after absorbing excitation energy partially emits radiation and partially transfers to the second centre which on being excited emits radiation. This mechanism involving radiative transfer of energy between two centres is known as cascade mechanism. In inorganic phosphors, very often activator transitions involved are forbidden [36] and as a result, this mechanism becomes of trivial importance.

(b) Exciton Migration:

According to this mechanism, the energy transfer takes place by metastable excitons of the base lattice. Broser [37] and Balkanski [38] have shown experimentally the possibility of the action of exciton at large distances from their point of creation. However, exciton migration over large distances is only possible in very pure defect free crystals. It is particularly sensitive to the presence of surface states.

(c) Resonance or Non- Radiative Transfer:

There is third mechanism, which is based on electromagnetic interaction between the sensitizer (S), which transmits the energy and the fluorescer (F) which receives the energy and then radiates. This is often termed resonance transfer mechanism. It was developed quantum – mechanically by Forster [39] in the dipole approximation for energy transfer between organic

molecules. Dexter [40] generalized the theory to higher order interactions and applied it to energy transfer between point defects in inorganic solids.

The life time of the excited sensitizer is reduced by resonance transfer but not by radiative energy transfer. However, both depend upon overlap of the emission spectrum of the sensitizer and the absorption spectra of the absorber. Sensitization by resonance transfer has been reported several workers [28, 41- 44].

4.3.3 Systems in which the transport of energy by charge carriers is the dominant feature.

Energy can also be transferred from one point to another by the movement of excited electrons and holes. Many characteristics of photoconducting phosphors have been explained by the storage action of electron traps [31, 45].

Three different models have been proposed for such systems they are Schon –Klasen's model (47) Lambe-Klick's model [18] and Williams and Prener model [47,48].

4.4 Experimental Setup for Recording Excitation Spectra:

The experimental setup for the recording excitation spectra is shown in Fig 4.7. The excitation source is Xenon lamp. This lamp is powered by high voltage source. The radiation emerging out from the lamp are allowed to fall on to the monochromator. The monochromator allows single wavelength radiation to pass through its exit slit. The slit is adjusted before starting the experiment. The phosphor sample is kept in the sample holder. The radiation of specific wavelength is made to fall onto the sample. The holder is aligned in such a way that whole sample is exposed. The material is excited and emits the characteristic fluorescence. The emitted radiation is focused on to the detector through an optical filter. The filter can be changed for different maximum emission wavelengths.

The detector produces photocurrent corresponding to the light intensity which falls on it. This photocurrent is measured with the help of a sensitive digital readout. The description and working of major components of this setup are given as follows.

4.4.1 Xenon Lamp:

Xenon lamp provides a continuum from 200 nm well into infrared. The output for this source is maximum around 465 nm, with a lower output in the far UV region. One important issue in the use of xenon lamp is the method of maximizing the amount of light that is focused

on the entrance slit of the excitation monochromator (since if more light impinges on the sample, more fluorescence takes place and hence it increases the sensitivity).

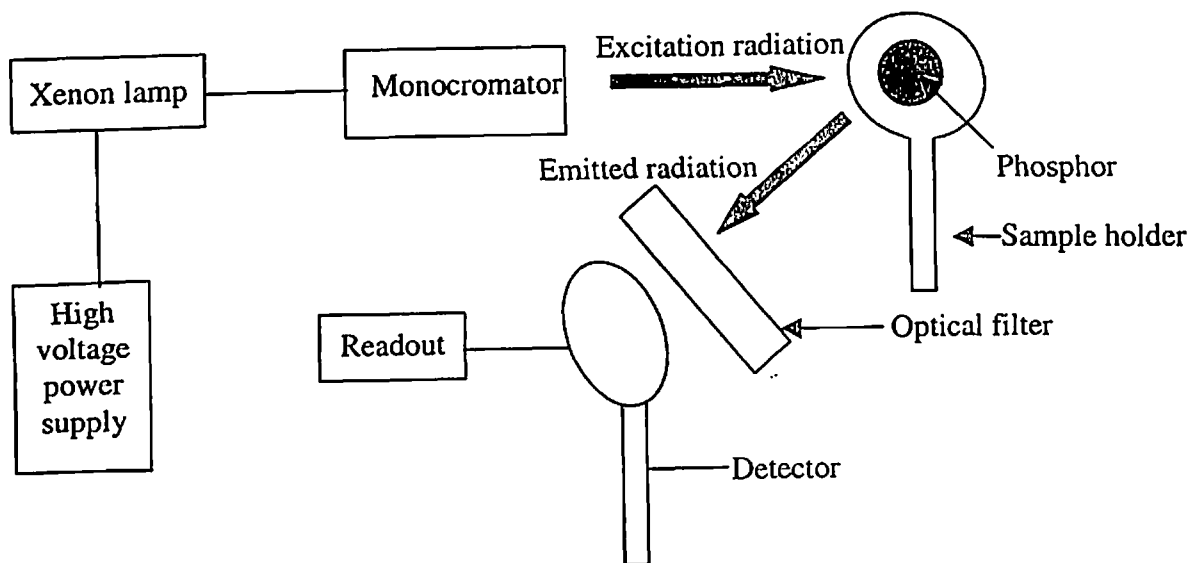


Fig. 4.7: Block diagram of experimental setup for recording excitation spectra at RT

4.4.2 Optical Filters:

We used interference filters which consist of evaporated coatings of a transparent dielectric spacer sandwiched between semitransparent films. Light incident on the face of the filter (usually right angle) is reflected back and forth between the films. Constructive interference between different pairs of superimposed light rays occurs only when the path difference is exactly one wavelength or some multiple thereof.

The important parameters which should be considered while selecting an interference filter are (i) the wavelength of maximum transmission (ii) band pass (The band pass, or peak width at half maximum (PWHM), can range from 5 nm to 20 nm) and (iii) percentage transmission.

4.4.3 Monochromator :

Monochromator is a device which includes a wavelength dispersing component, as opposed to an optical filter, which serves to block certain wavelengths. The present monochromator employs a diffraction grating. When a beam of polychromatic light is focused on a diffraction grating, each groove acts as a source of radiation. On the opposite side of the grating, constructive interference will occur at certain points and other points destructive

interference will occur for certain wavelength. Constructive interference will result in bright line and destructive interference will result in a dark line. The upshot of this is a series of bright lines with dark region between them. The wavelength of the light that is transmitted depends upon the angle of the exciting radiation with respect to the grating. The grating is rotated to transmit light of various wavelengths onto the reflective optics that pass the light out of the monochromator. The two critical factors which define the utility of a grating are the blaze angle or blaze wavelength and the number of lines. The basic equation defining a diffraction grating is indicated in eq. (4.1), where n is diffraction order (which must be an integer), λ is the wavelength, d is the distance between adjacent grooves, and θ is angle of diffraction. As the grating is rotated, the value of θ gets changed, thus presents different wavelengths for analytical work.

$$n\lambda = 2d \sin\theta \quad (4.1)$$

Blaze angle of the grating is fixed by manufacturer for obtaining specific range of maximum efficiency.

In addition to transmitting light of desired wavelengths, a diffraction grating will also pass light of higher orders. In equation (4.1) n can be equal 1, 2, 3,..... Thus a grating that is normally set to transmit 500nm light ($n=1$) will also transmit the wavelength of 250nm ($n=2$), 166.7nm ($n=3$), etc. from the practical point of view. Only the 250nm radiation could be a problem, since the 166.7nm radiation would be absorbed by the oxygen atmosphere. Where necessary, the second order radiation was separated using an appropriate filter.

The second critical issue in describing a grating is its resolving power. The resolving power (R) of a grating is defined by Eq. (4.2), where $\Delta\lambda$ is the wavelength difference between two lines that are barely distinguishable, λ is their average wavelength; N is the number of lines in the grating. While the resolving power is entirely determined by the optical design of the monochromator, the observed resolution depend on the resolving power, the source intensity, monochromator transmittance, detector sensitivity and the degree of perfection of other optical electronic component.

$$R = \frac{\lambda}{\Delta\lambda} = nN \quad (4.2)$$

where n is order of diffraction.

Typical data of the grating monochromator is given as follows:

Blaze wavelength	300 nm
Lines/mm	1200
Reciprocal dispersion	4.65
Useful working range	200-650 nm
Resolution (R)	64800 for n=1

4.4.4 Detector and Readout:

The detector used in the present, setup was a wide area silicon diode. This has fairly uniform response over the range of investigation. The output of the detector was amplified and given to digital readout.

4.5 Experimental Setup for Recording Fluorescence Spectra and Decay of Fluorescence:

A schematic block diagram of the setup is shown in Fig. 4.8. With this instrument, it is possible to record fluorescence spectra at room temperature and the variation of fluorescence intensity with temperature. It is also possible to record the decay of fluorescence from which the lifetime of fluorescence can be calculated.

The apparatus consists of an excitation source which is a stable Hg- lamp followed by a wood filter (transmitting uv band centred around 3650 Å). Thus 3650 Å radiation forms wavelength of excitation (λ_{exc}). The phosphor is kept in a brass sample holder which is provided with a heating element at its bottom and is connected to a variable voltage power supply. A copper constantan thermocouple is used to measure the temperature of the phosphor. The radiation (λ_{exc}) emitted by the phosphor is focused onto the entrance slit of the Carl Zeiss Prism monochromator (SPM-2) with the help of focusing optics. The details of SPM-2 are briefly discussed as follows.

Mirror monochromator SPM-2 is particularly useful for the spectral dispersion of light in the ultraviolet, visible and infrared regions of the spectrum. Its advantage over the lens-type Monochromator consists in the fact that their utilizable wavelength range is not restricted by the dispersion and absorption properties inherent in the lens material and that the focusing process is independent of the wavelength. Together with these general properties the mirror monochromator SPM-2 combines the following salient features.

- (i) High light intensity and resolving power due to the arrangement of the autocollimator of the dispersion prism and excellent stigmatic depiction of the slit.

- (ii) Large spectral region from 0.2 to 40 microns due to the interchangeability of dispersion prisms.
- (iii) Interchangeability of dispersion prisms for diffraction grating
- (iv) Direct reading of the set wavelength and possibility of ascertaining the spectral bandwidth by projection of the wavelength scale
- (v) Facility of taking into consideration the true prism -angle and the measuring temperature by way of correcting the deviations from the nominal values
- (vi) Coupling possibility of entrance and exit slits and logarithmical adjustment of slit-widths from 0 to 1.5 mm respectively from 0 to 4.5 mm
- (vii) variable attaching facilities of the radiation sources and receivers

Relevant data is given as follows

Focal length of parabolic mirror	400 mm
Effective diameter of parabolic mirror	72mm
Aperture ratio referred to the effective beam limiting prism face	1: 8.4
Surface coating of mirrors	Aluminium
Slit width	logarithmically adjustable from 0mm... 1.5 mm resp. from 0 to 4.5 mm
Slit height	maximum 20mm, continuously adjustable by means of wedge stop
Transmission ranges of slit caps:	
Slit caps with quartz window	0.2-3.2 microns
Slit caps with calcium fluoride window	0.2-9.0 microns
Slit caps with potassium bromide window (hygroscopic)	1-25 microns

Prisms for which wavelength scales are built in:

Material	Height mm	Base mm	Angle	Division of wavelength- scale in microns
Quartz (Si 68)	47-50	76.5 -77.5	67° 33'	0.2-3.2
Flint glass (G 60)	49.5- 50.5	69.5-70.5	60°	0.36-2.8
Lithium fluoride (LiF 82)	45-50	77-80	82°	0.3 – 6.0
Rock- salt (NaCl 56)	45-50	57.5- 61.5	56°	0.2 –16
Potassium bromide (KBr 67)	45-50	70-74	67°	1-25

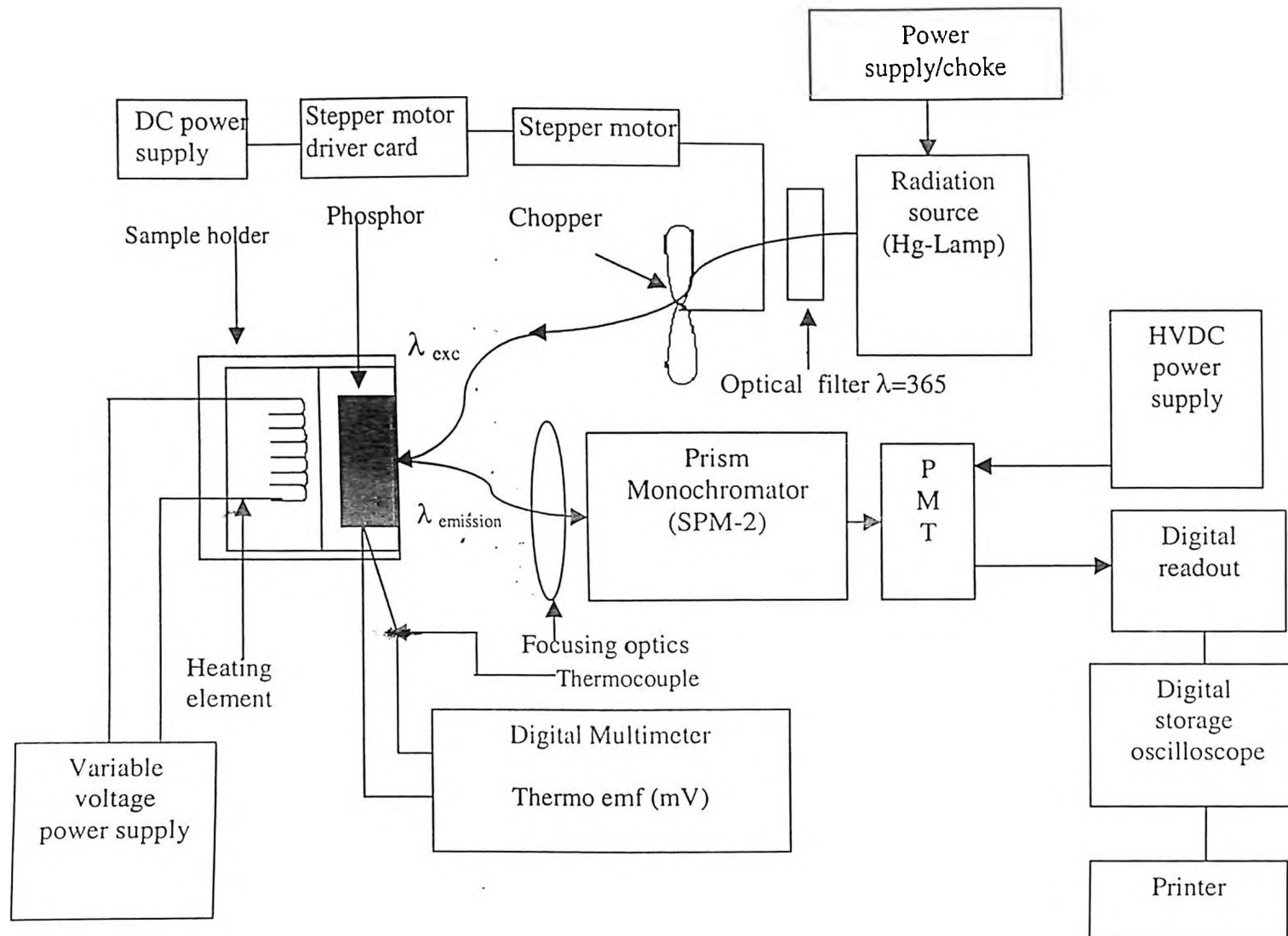


Fig 4.8: Block diagram of experimental setup for recording fluorescence spectra at RT,
Decay time and temperature dependence of fluorescence

The optical path in this monochromator is shown in Fig. 4.9. After reflection from the specular cathetus of the prism (7) the radiation coming through the entrance slit (2) strikes the inclined, extra axial parabolic mirror (1) which acts as a collimator. After spectral dispersion and reflexion from the Wadsworth and autocollimation mirror (4, 5) the prism is traversed a second time. The emerging and spectrally dispersed radiation is then used by the parabolic mirror to produce, via a second specular face of the reflexion prism (7) a spectrum in its focal plane within which the exit slit (8) lies.

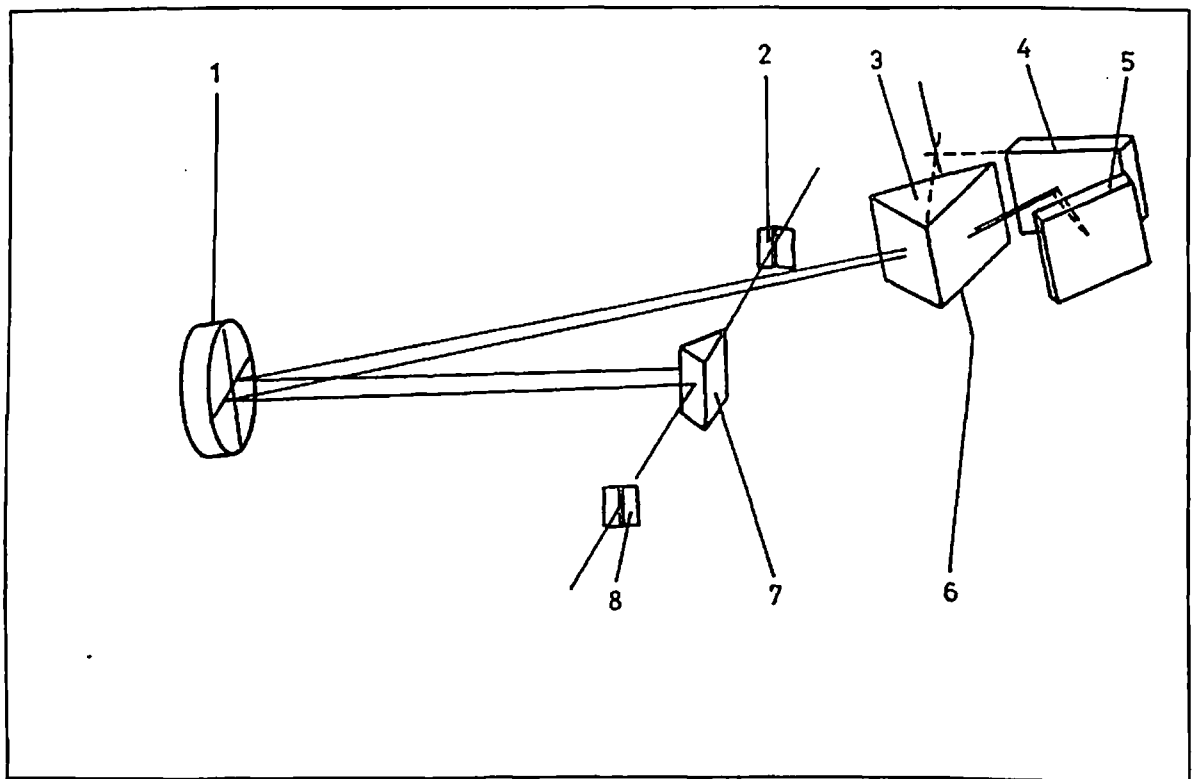


Fig. 4.9: Optical path in mirror monochromator 'SPM2'

1. Extra axial parabolic mirror, 2. Entrance slit, 3. Dispersion prism, 4. Wadsworth mirror,
 5. Autocollimation mirror, 6. Rotational axis for bot wadsworth and autocallimation
 mirrors, 7. Reflection prism, 8. Exit slit

The optical elements of construction are so arranged as to unite on the exit slit that respective radiation whose main beam is inclined at an angle 1° relative to the direction which is marked by minimum of the deflection. In view of the wavelength –dependent curvature of the spectral lines, the mirror monochromator is fitted with a curved exit slit. The curvature of slit jaws has been laid down for average conditions.

The dispersion prism and the Wadsworth mirror are attached on the same stage; by turning this stage about the axis (6) passing through the mirror plane and the bisector of the prism angle the wavelength adjustment is effected.

The wavelength coming on to the exit slit is detected by Oriel photodetection system. The latter consists of a photomultiplier tube (PMT), a high voltage DC power supply for energing PMT and a digital read out that can measure both the voltage supplied to the PMT and the photocurrent generated by the PMT. Specific features of this detection system are given as follows:

The ORIEL Model 7070 detection system is an instrument designed for a wide variety of applications in the measurement of light radiation. This highly sensitive, extremely stable unit, can, with the appropriate external sensor, enable measurements over the ultraviolet, visible and near infrared portions of the spectrum.

The specifications of model 7070 are given follows:

Radiometer readout

Operating temperature range	14-40 °C
Overall accuracy at 27 °C ambient	$\pm 1\%$ (\pm digit)
Linearity	0.05 %
Gain drift vs temperature	0.07%/°C
Zero drift	± 1 digit

BCD output description

The parallel BCD output lines are at +5 V logic level (positive logic), capable of driving two LPTTL loads

The multiplexed BCD output lines are at +5V logic level (negative logic), capable of driving four CMOS loads. The load pulses are at + 5V logic level (positive logic), capable of driving two CMOS loads

Analog recorder output

100 mV full scale, source impedance =200 ohms

High voltage power supply

Output adjustable from -10V to -1000 VDC

Stability at 27 ° ambient - $\pm 0.1 \%$

At room temperature, under uv excitation, the fluorescence spectrum is recorded manually by changing the wavelength (through a wavelength knob) and noting the corresponding reading in the digital readout.

In order to record the lifetime of fluorescence some additional modules have been added. The radiation from the Hg-lamp is modulated using a 90 ° rotating sector (chopper). This chopper is run by a stepper motor and its speed can be controlled by stepper motor driver card. Thus excitation is not continuous but it is in the form of pulses whose frequency can be controlled by the stepper card. Due to the pulse excitation, the fluorescence first rises and then falls. The rise and decay can be recorded by taking the output of the digital readout to the digital storage oscilloscope (DSO). The patterns on the screen can be printed by the printer connected to the DSO. The time constant can be recorded at RT as well as at different temperatures. The special features of DSO are given as follows.

Table 4.1: Special features of oscilloscope

Vertical Systems	Bandwidth Rise time Dynamic range Math functions Input resistance Input capacitance Channel 1 and 2 Range Accuracy Verniers Band width limit Coupling Inversion	Dc to MHz- 3dB ac coupled, 10Hz to 100 MHz -3 dB 3 ns ± 32 V or ± 8 divisions, whichever is less Channel 1 + or – channel 2 1MΩ ≈ 13 pf 2 mV/ div to 5 mV div ±1.9 % Fully calibrated, accuracy about ± 3.5% ≈ 20 MHz Ground , ac, and dc Channel 1 and channel 2
Horizontal system	Sweep speed Accuracy Vernier Horizontal resolution Cursor accuracy Delayed jitter Delayed sweep Operation	5 s/div to 2 ns /div main and delayed ±0.01 % ± 0.2% of full scale ± 200ps Accuracy ± 0.05% 100ps ±0.01% ± 0.2% of full scale ± 200ps 100 ppm Main sweep Delayed sweep 5 s/ div to 10ms/div upto 200 times main 5 ms/div and faster up to 2 ns/div

4.6 Results:

4.6.1 Excitation spectra:

The excitation spectra of SrS:Cu, BaS:Cu and CaS:Cu are shown in Figs. 4.10, 4.11 and 4.12 respectively.

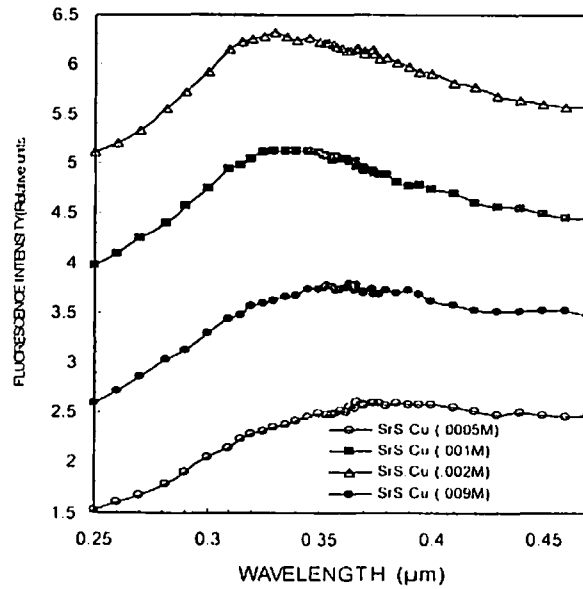


Fig 4.10: Excitation spectra of representative samples of S- series of phosphors (SrS:Cu), $\lambda_{em}=0.52 \mu m$

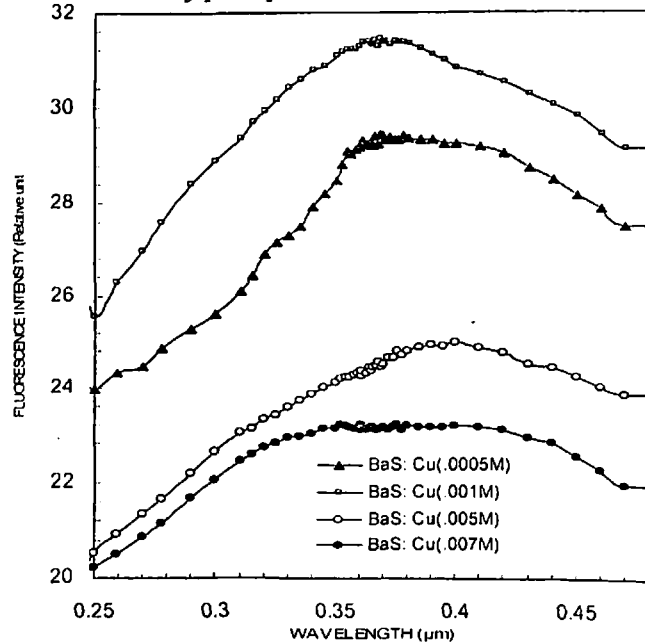


Fig 4.11 Excitation spectra of representative samples of B- series of phosphors (BaS:Cu), $\lambda_{em}=0.61 \mu m$

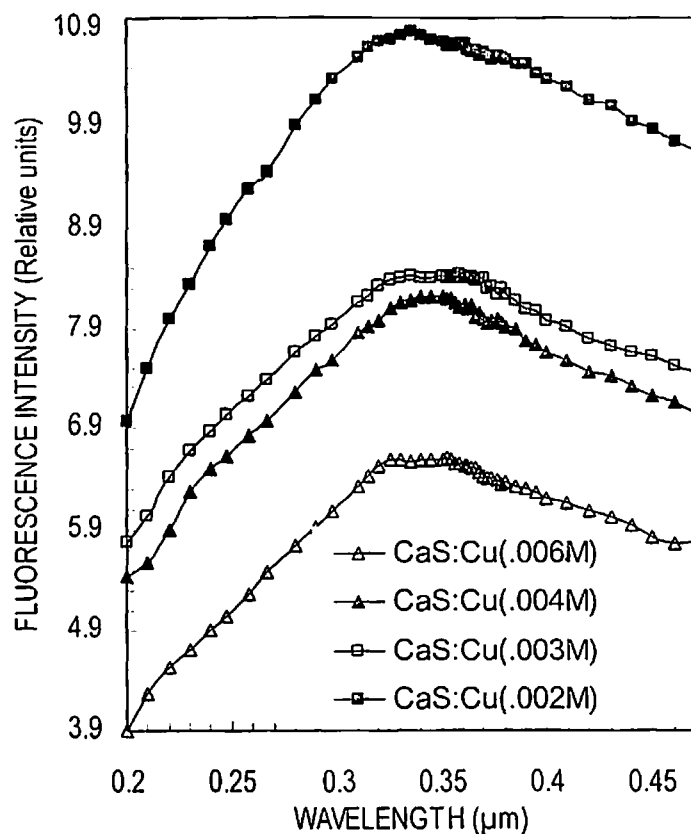


Fig 4.12: Excitation spectra of representative samples of C-series of phosphors (CaS:Cu)

In all the three cases the fluorescence intensity peaks in the range from 0.30 μm to 0.40 μm . It appears that there are two peaks but they are not resolved. There seems to be no systematic change in the peak wavelength with change in concentration of activator. The intensity changes occur due to concentration quenching, as expected.

In the case of mixed sulphides again we observed a broad band peaking in almost the same range. The peak excitation wavelength varies slightly with the variation of ratio of two sulphides in the cases of (Sr,Ca)S:Cu and (Sr,Ba)S:Cu phosphors as shown in Figs. 4.13 and 4.14 respectively. However in the case (Ca,Ba)S:Cu, λ_{exc} peaks at 0.34 μm for CaS dominant phosphor and at 0.4 μm for BaS dominant phosphors as shown in Fig 4.15.

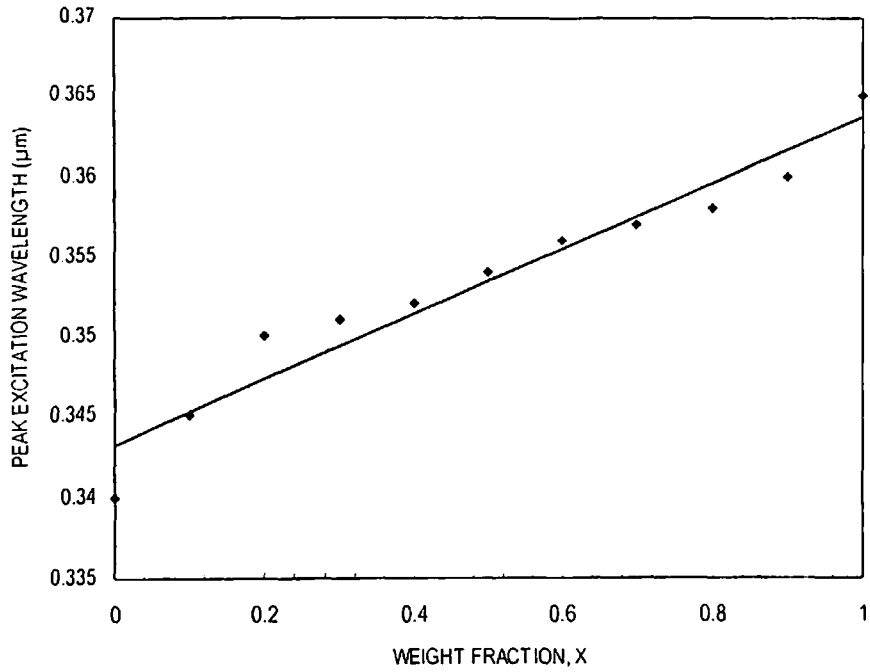


Fig 4.13: Variation of peak λ_{exc} with weight fraction, x for $(\text{Sr}_x\text{Cu}_{1-x})\text{S}:\text{Cu}(0.003\text{M})$

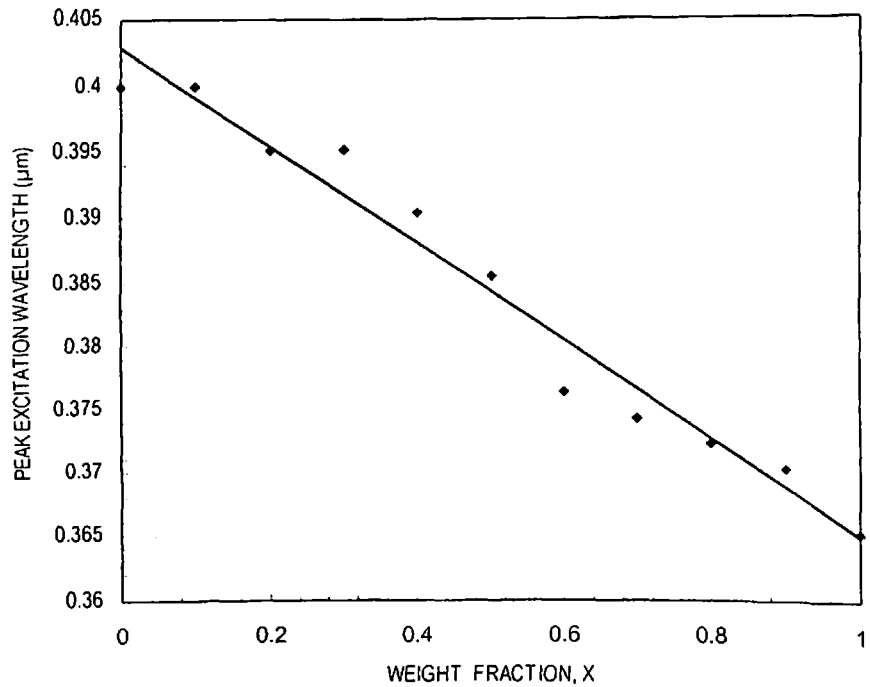


Fig 4.14 Variation of peak λ_{exc} with weight fraction, x for $(\text{Sr}_x\text{Ba}_{1-x})\text{S}:\text{Cu}(0.003\text{M})$

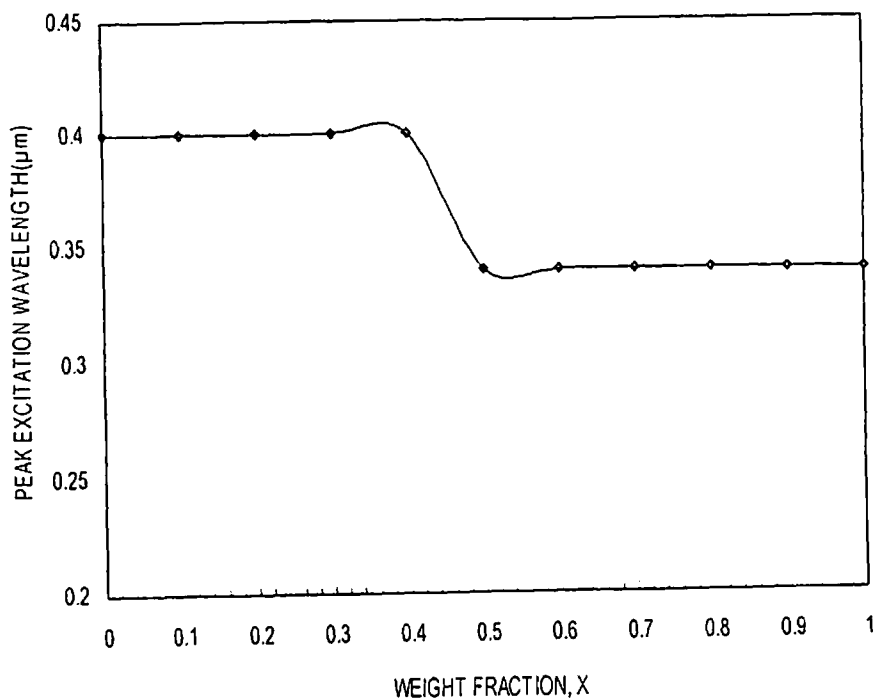


Fig 4.15: Variation of peak λ_{exc} with weight fraction, x for $(Ba,Ca)S:Cu(0.001M)$

Consistent with these results we have chosen 0.365 μm radiation for the excitation of fluorescence in all the samples.

4.6.2 Emission Spectra:

The emission spectra of representative samples of SrS:Cu, BaS:Cu and CaS:Cu are shown in Figs. 4.16, 4.17 and 4.18 respectively. In all the three cases a single broad band has been observed. The wavelength of maximum emission (λ_{max}) for the three cases are given as follows:

Table 4.2: The maximum emission wavelength (λ_{max}) of alkaline earth sulphide phosphors activated with copper

Phosphor	λ_{max} (μm)
SrS:Cu	0.52
BaS:Cu	0.61
CaS:Cu	0.49

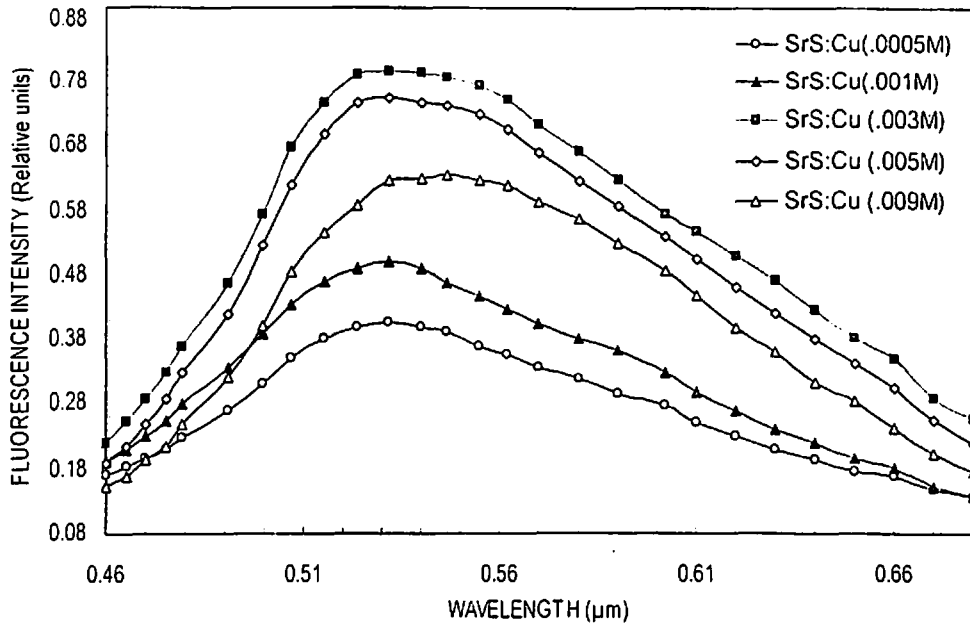


Fig 4.16 Emission spectra of representative samples of S- series of phosphors (SrS:Cu)

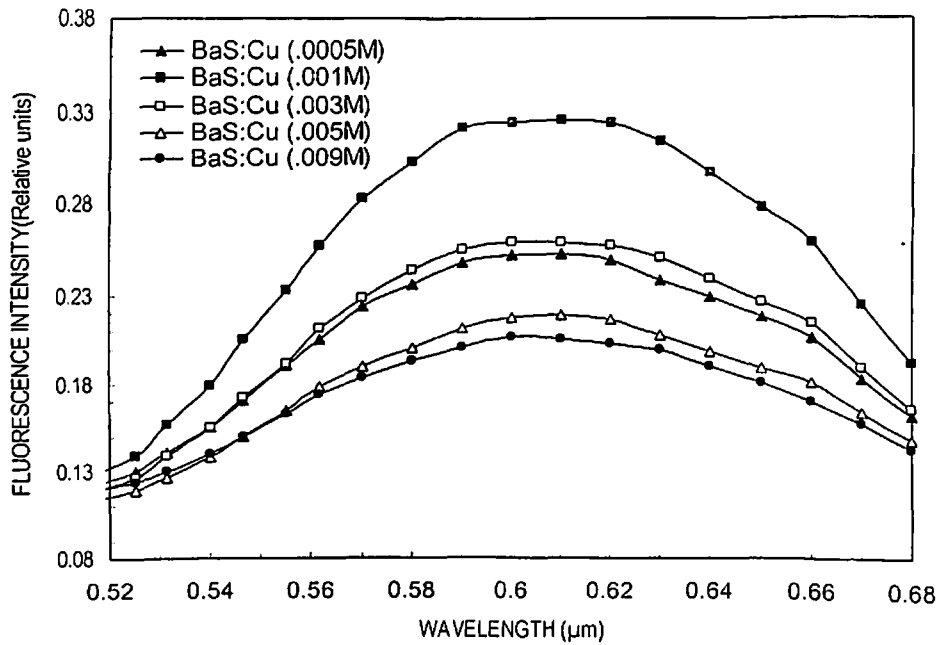


Fig 4.17: Emission spectra of representative samples of B- series of phosphors BaS:Cu

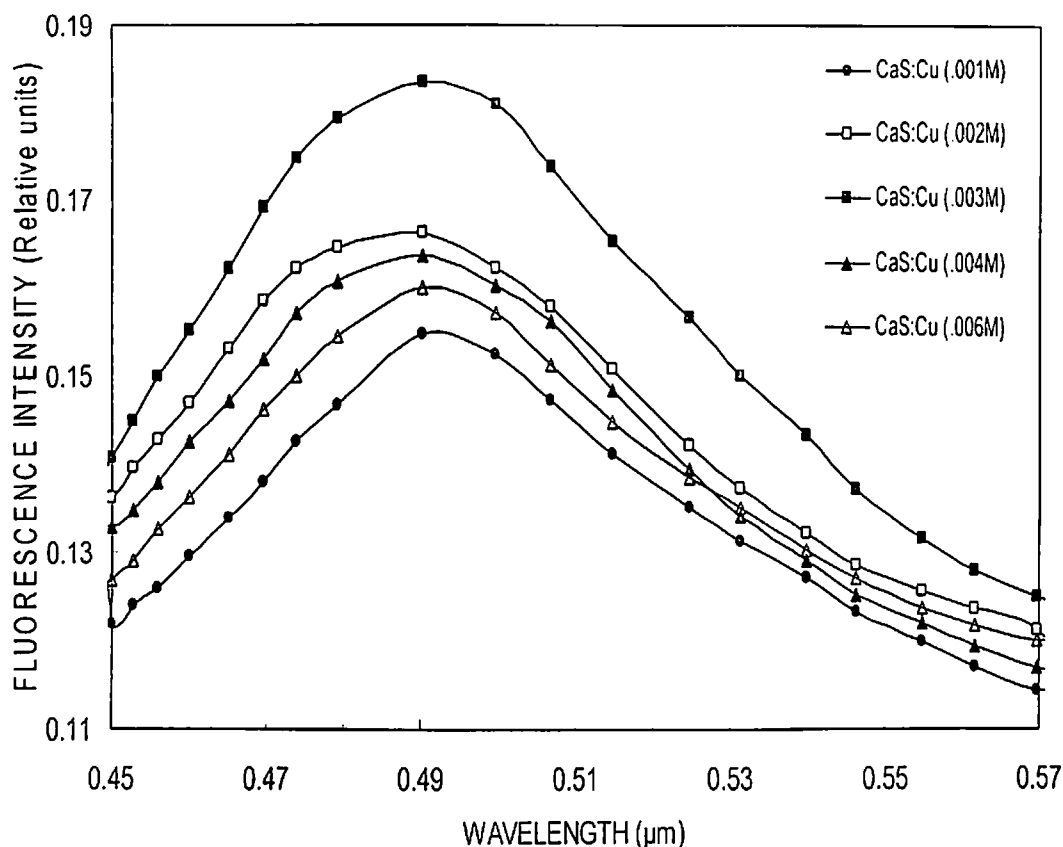


Fig 4.18: Emission spectra of representative samples of C-series of phosphors (CaS:Cu)

The results of the mixed series of phosphor are quite interesting. The emission spectra of (Sr,Ca)S:Cu phosphors are shown in Fig. 4.19(a). It is clear from this figure that as the ratio of Sr increases in the lattice, the emission peak gradually shifts from 0.49 to 0.52 μm . Fig 4.19 (b) shows the plot of variation of λ_{max} with lattice constant 'a' of the mixed lattice. λ_{max} increases with increase in 'a'. Similarly shifting of emission peak has been observed in (Sr,Ba)S:Cu series of phosphors. It can be seen from Fig 4.20 (a) that as the fraction of Ba increases in the lattice from 0 to 1.0 the emission peak shifts from 0.52 to 0.61 μm . The variation of λ_{max} with 'a' is shown in Fig 4.20(b).

The behaviour of emission curves of (Ca,Sr)S:Cu and (Sr,Ba)S:Cu series of phosphors further confirms the formation of mixed lattice in these cases. However the behaviour of (Ca,Ba)S:Cu phosphors is different as shown in Fig 4.21.

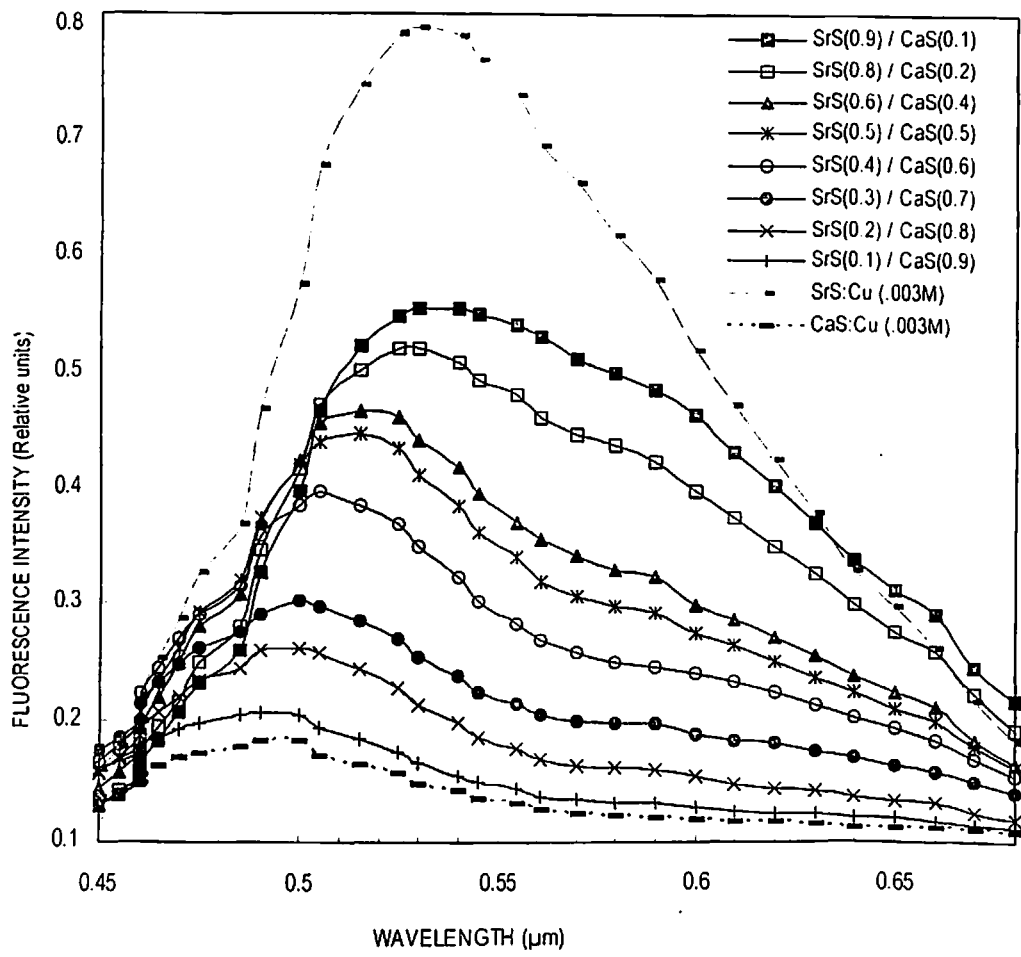


Fig 4.19(a): Emission spectra of representative samples of CS-series of phosphors, (Sr,Ca)S:Cu

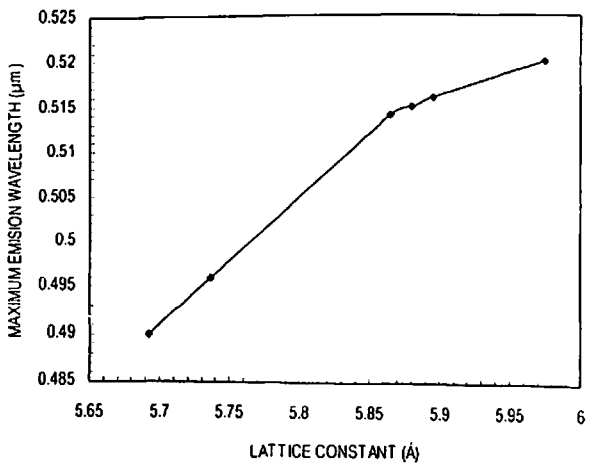


Fig 4.19(b): Plot of λ_{max} as a function of lattice parameter for (Sr,Ca)S:Cu

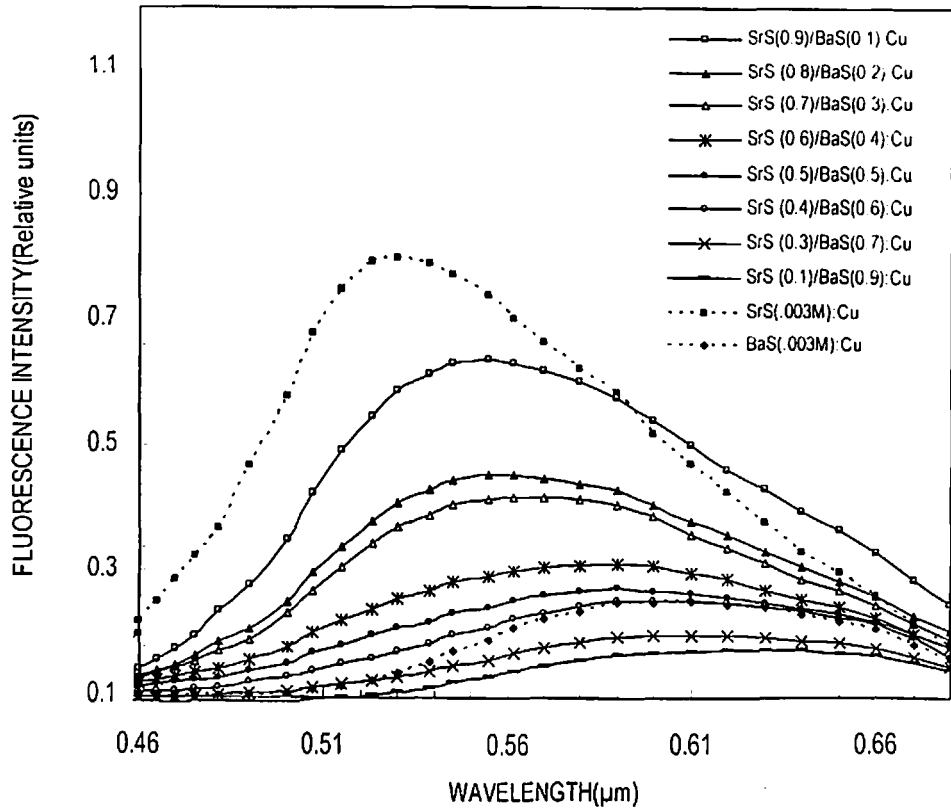


Fig 4.20(a): Emission spectra of representative samples of SB-series of phosphors, (Sr,Ba)S:Cu

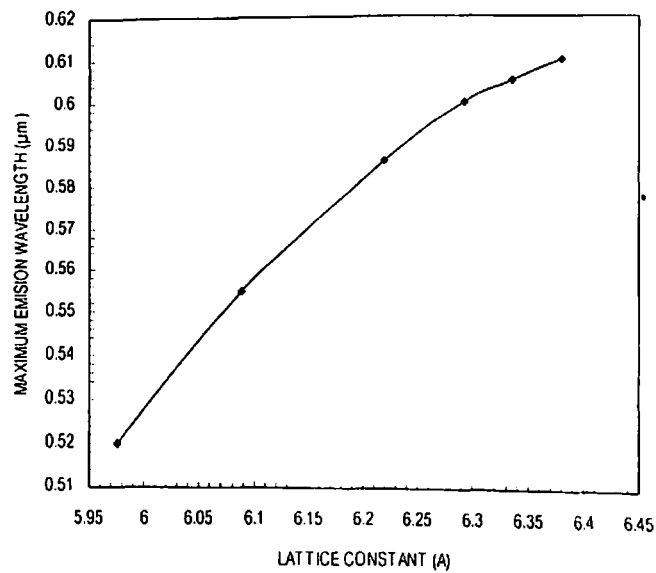


Fig 4.20(b): Plot of λ_{max} as a function of lattice parameter for (Sr,Ba)S:Cu

In this case the fluorescence is characteristic of the dominant phase in the phosphor. Thus for $\text{CaS}(0.8)/\text{BaS}(0.2):\text{Cu}$ and $\text{CaS}(0.7)/\text{BaS}(0.3):\text{Cu}$ phosphors, there is single emission peak at $0.49 \mu\text{m}$ and in the phosphors where BaS phase is dominant e.g; $\text{CaS}(0.2)/\text{BaS}(0.8):\text{Cu}$ and $\text{CaS}(0.3)/\text{BaS}(0.7):\text{Cu}$ the peak is about at $0.61 \mu\text{m}$. Further where the two phase are in equal proportion e.g; $\text{CaS}(0.5)/\text{BaS}(0.5):\text{Cu}$, two peaks have been observed. They are at 0.49 and $0.61 \mu\text{m}$. This shows that mixed lattice has not been formed in this case. We will further discuss these results in chapter 6.

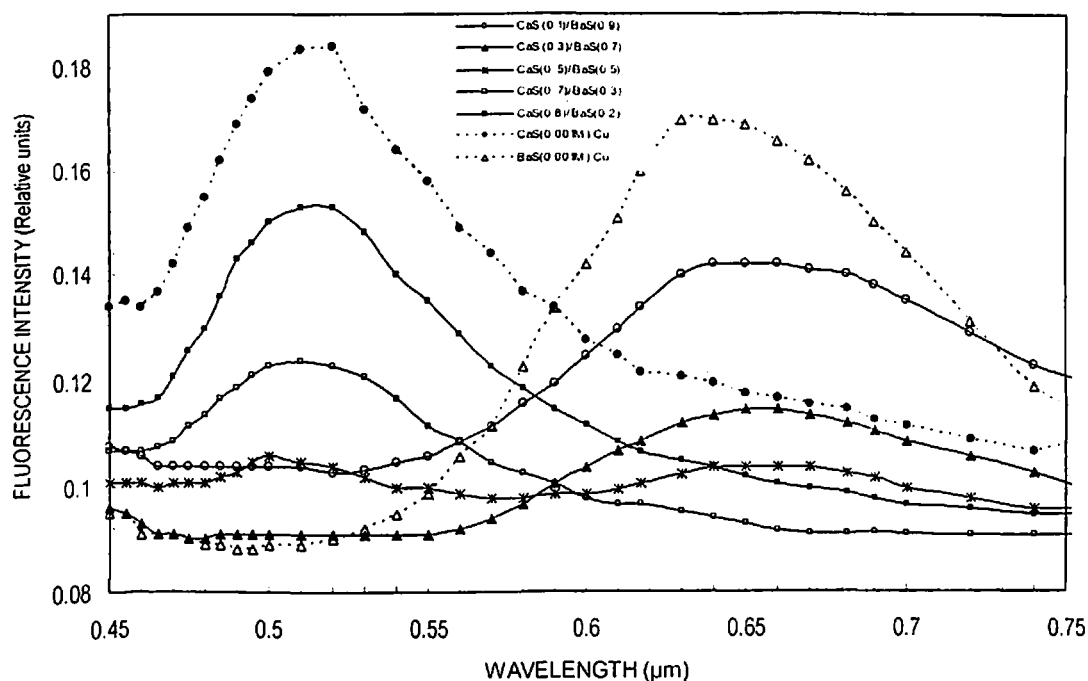


Fig 4.21 Emission spectra of representative samples of CB-series of phosphors, (Ba,Cu)S:Cu

References:

1. E. Wiedemann, *Wied. Ann.* **37**, 177 (1889).
2. G. F. J. Garlick, "Luminescent Materials", Oxford Univ. Press, London (1949).
3. F. Perrin, *Ann. de Phys.*, **12**, 169, (1929).
4. P. Pringsheim, "Fluorescence & Phosphorescence", Interscience Pub. Inc. N.Y. (1949).
5. D. Curie, "Luminescence in Crystals" translated by G.F.J. Garlick, Methuen & Co. Ltd., London (1963).
6. K. H. Butler, "Fluorescent Lamp phosphors", Pennsylvania State University press, University Park, PA, (1980).
7. R. C. Ropp, "Luminescence and the Solid State", *Studies in Inorganic Chemistry* **12**, Elsevier, Amsterdam, (1991).
8. K.T.V Grattan, Z. Y. Zhang, "Fiber Optic Fluorescence Thermometry, Chapman and Hall, London, (1995).
9. A. V. Hippel, *Z. Phys.* **101**, 680 (1936).
10. F. Seitz, *Trans. Faraday Soc.* **35**, 79 (1939).
11. D. L. Dexter, C. C. Klick and G. A. Russel, *Phys. Rev.*, **100**, 603 (1956).
12. W. H. Fonger and C. W. Struck, *J. Chem. Phys.* **52**, 6364 (1970).
13. C. W. Struck and W. H. Fonger, *J. Appl. Phys.* **42**, 4515 (1971).
14. M. Schon, *Ann. de Phys. (6)*, **3**, 343 (1948).
15. K. Huany & A. Rhys, *Proc. Roy. Soc. A-204*, 406 (1950).
16. M. Schon, *Z. Phys.* **119**, 463, (1942).
17. F. Bloch, *Z. Phys.* **52**, 555 (1928).
18. M. Lax and E. Burstein, *Phys. Rev.*, **100**, 592 (1955).
19. H. A. Klasens, E. W. Ramsden & C. Quantie, *J. Opt. Soc., Am.* **38**, 60 (1948).
20. J. Lambe & C.C. Klick, *Phys. Rev.* **98**, 909 (1955). *J. Phys. Rad.* **17**, 663 (1956).
21. H. A. Klasens, *J. Phys. Chem. Solids*, **9**, 185 (1959).
22. K. S. K. Rebane, *Opt. & Spec. (USA)* **13**, 3330 (1962).
23. S. Shionoya, T. Koda, K. Era & H. Fujiwara, *J. Phys., Soc. (Japan)* **19** 1157 (1964)
24. S. Shionoya, K. Era & H. katamaya, *J. Phys. Chem., Solids.* **26**, 697 (1965).
25. R. H. Bube, *Photoconductivity in Solids*", John Wiley, N.Y. (1968).

26. G. F. J. Garlick, "Progress in Semiconductors", Vol. 1 Heywood & Co. . Ltd., London (1956).
27. F. A. Kroger, "Some aspects of Luminescence of Solids", Elsevier Pub. Co., Amsterdam (1948).
28. R. P. Khare and J. D. Ranade, *J. Mater. Sc.* **15**, 1868, (1980).
29. R. Pandey and S. Sivaraman, *J. Phys. Chem. Solids*, **52**, 211(1991).
30. A. Jablonski, *Z. Phys.* **94**, 38 (1935).
31. R. P. Johnson, *J. Opt.Soc. Am.* **29**, 387 (1939).
32. J. J. Hopfield, *J. Phys. Chem. Solids*, **10**, 110 (1959).
33. J.T. Randall and M. H. F. Wilkins, *Proc. Roy. Soc., London*, **A184**, 366 (1945).
34. R. E. Halsted, E. F. Apple & J. S.Prener, *Phys. Rev., Letters* **2**, 420 (1959).
35. George G. Guilbault (Ed): "Practical Fluorescence" 2 nd Edition, Marcel Dekker, NY, 9 (1990)
36. M. Schon, "Semiconductor Physics Conference" Prague, 788 (1960).
37. I. Broser and R. Broser- Warminsky, *J. Phy. Chem. Solids*, **6**, 386 (1958).
38. M. Balkanski, *J. Phy. Chem. Solids*, **6**, 401 (1958).
39. T. Forster, *Naturwiss*, **33**, 166 (1946).
40. D. L. Dexter, *J. Chem. Phys.* **21**,836 (1953).
41. R. P. Khare and J. D. Ranade, *Ind. J. Pure Appl. Phys.*, **13**, 664 (1975).
42. J. M. P. J. Versteegen, J. L. Sommerdijk and J. G. Verriet, *J. Lumin.* **6**, 425 (1973).
43. G. L. Blasse, *J. Lumin.* **14**, 231 (1976).
44. G. L. Blasse and A. Bril, *J. Chem. Phys.* **47**, 1920 (1967).
45. G. F. J. Garlick, *Brit. J. Appl. Phys.* **6**, suppl. 4, 885 (1955)
46. H.A. Klasens, *Nature*, **158**, 306 (1946)
47. F.E. Williams, *J. Phys. Chem. Solids*, **12**, 265 (1960)
48. J. S. Prener and D. J. Weil, *J. Electrochem. Soc.* **106**, 409 (1959)

Chapter 5

Temperature Dependence of Fluorescence

5.1 Introduction:

In past few decades the temperature dependent characteristics of fluorescence of so called "thermographic phosphors" have been used for remote (or noncontact) measurement of temperature of both static and moving surfaces and have performed many other tasks that standard sensors (thermocouple, thermistors, etc) cannot. The range of usefulness of this class of materials extends from cryogenic temperatures to those approaching 2000 °C [1-11]. The study of temperature dependent luminescence is also important from the point of view of its stability and applicability in other devices [12-20]. In addition such systems have also been successfully employed to make contact measurements of temperature. It is from this point of view that the temperature dependence of fluorescence intensity as well as lifetime were studied in detail in our system of phosphors. The instrument for recording temperature dependence and lifetime of fluorescence has already been described in chapter 4. This chapter presents the results of such measurements after briefly reviewing the prevalent theory of temperature dependence of fluorescence.

5.2 Theory of Temperature Dependence of Fluorescence:

The intensity of fluorescence during excitation falls if the temperature is raised sufficiently due to the emission of phonons in competition with photon emission. If P_r is the probability of radiative transitions and P_{nr} the probability of a non-radiative transitions, then the fluorescence is proportional to the ratio

$$\eta = \frac{P_r}{P_r + P_{nr}} \quad (5.1)$$

which is called fluorescence efficiency. It is assumed that P_r is sensibly independent of temperature, while P_{nr} rises rapidly with temperature. The latter is given by

$$P_{nr} = s \exp (-W/kT) \quad (5.2)$$

where s is called the frequency factor (which is of the order of magnitude of 10^9 s^{-1}); W is the thermal activation energy or the energy of the point of intersection of the ground and excited states on the configuration coordinate diagram above the minimum of the excited state; k is Boltzmann constant and T is the temperature (K).

Rearranging eq. (5.1), we get

$$\eta = \frac{1}{1 + \frac{P_{nr}}{P_r}}$$

and substituting for P_{nr} from eq. (5.2) we see that

$$\eta = \frac{1}{1 + \left(\frac{s}{P_r}\right) \exp\left(-\frac{W}{kT}\right)}$$

or $\eta = \frac{1}{1 + C \exp\left(-\frac{W}{kT}\right)}$ (5.3)

where $C(=s/P_r)$ is a constant. In most phosphors, the nature of fluorescence efficiency is adequately described by equation (5.3). In some cases, it may be more complex.

Based on the band theory of solids, Klasens [21] has given a satisfactory model for thermal quenching in sulphide phosphors. When electrons are in the conduction band, the holes in the luminescence centers may be filled up by electrons from the valence band. This process requires a certain activation energy W (energy necessary to remove an electron from the valence band) which can be supplied thermally above a certain temperature. The electron previously removed from the center by optical excitation now cannot return to it and after wandering in the conduction band for a short time may be captured by a non-radiative recombination center. If sufficient numbers of such centers are available, the thermal activation process will determine the probability of non-radiative transitions.

5.3 Some Relevant Parameters Related to Thermal Quenching:

Quenching Range, ΔT

Following Kroger [22] and Mishra and Sharma [23] we define quenching range as the temperature range within which the fluorescence intensity decreases with temperature after non-radiative transitions begin to dominate and is given by

$$\Delta T = T_2 - T_1 = 5W/3k \{ (\ln C - \ln 4)^{-1} - (\ln C + \ln 4)^{-1} \} \quad (5.4)$$

Quenching Temperature, T_Q

It is defined as the point of intersection of the abscissa and a straight line drawn through the points at which the intensity has fallen to 80 and 20% of the maximum value. In Fig.5.1, T_2 is the quenching temperature and is often denoted as T_Q and is given by the expression.

$$T_Q = W/3k \{ 4(\ln C - \ln 4)^{-1} - (\ln C + \ln 4)^{-1} \} \quad (5.5)$$

Breaking Point Temperature, T_B

It is a sharply defined temperature and is the temperature at which non-radiative transitions set in [24] and is approximately given by

$$T_B = \frac{W/k}{\ln C + 0.9} \quad (5.6)$$

Half-Value Temperature, T_H

It is the temperature at which the intensity has decreased to half its maximum value within the quenching range ΔT . It is given by the expression [25]

$$T_H = \frac{W/k}{\ln C} \quad (5.7)$$

When the value of C is very large, T_Q changes into T_H and T_B changes into T_H .

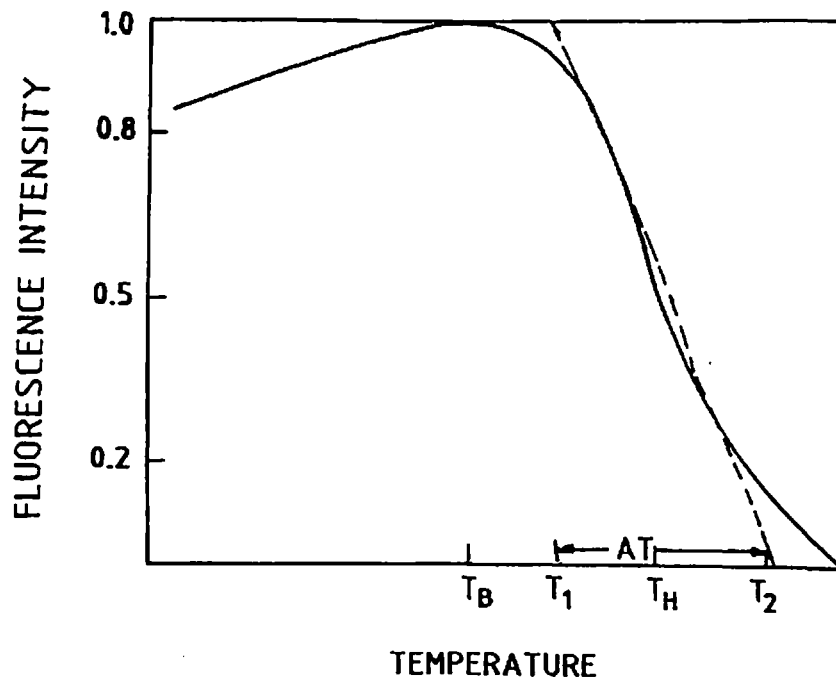


Fig 5.1: Definition of parameters

5.3 Kinetics and Decay of Luminescence:

We usually distinguish two kinds of luminescence process, that with kinetics of the first order (monomolecular mechanism) and that having second-order kinetics (bimolecular mechanism).

It is generally accepted, but not quite correct, to use these terms, taken from chemical kinetics, as synonymous for such processes. A bimolecular reaction is one in which two molecules combine. In photoconducting luminescent solids, there occurs in all cases a 'bimolecular recombination' of electrons and empty centers, but the kinetics may be of first or of second order, depending on the particular conditions. However, if this is generally understood, then the term bimolecular can still be applied to the particular case of a second order kinetics recombination.

In the case of first-order kinetics, the number of excited electrons n decreases according to a constant probability law

$$\frac{dn}{n} = -\alpha dt \quad (5.8)$$

which gives $n = n_0 e^{-\alpha t}$, and since the fluorescence intensity $I = \frac{dn}{dt}$ then

$$I = I_0 \exp(-\alpha t) = I_0 \exp\left(-\frac{t}{\tau}\right) \quad (5.9)$$

where τ is mean life time of fluorescence.

In the case of second order kinetics, the probability of recombination is proportional to the number of available centers

$$\frac{dn}{n} = \alpha n dt \quad (5.10)$$

and so n decreases hyperbolically with time

$$n = \frac{n_0}{(1 + n_0 \alpha t)}$$

The fluorescence decay then is given by

$$I = \left| \frac{dn}{dt} \right| = \alpha n^2$$

$$\text{Thus } I = \frac{I_0}{(1 + at)^2}, \text{ where } a = \sqrt{I_0 \alpha} \quad (5.11)$$

The decay thus becomes more rapid as the excitation intensity is increased.

The above kinetics can only apply to fluorescence since their foundation does not consider the intermediate process of trapping.

If the kinetics is of the first order, the temperature dependence of fluorescence and the mean life time of fluorescence are similar mathematically [26, 27]. Thus the fluorescence life time (τ) at temperature T may be expressed adequately by the following relation;

$$\eta = \frac{\tau}{\tau_0} = \frac{1}{1 + C \exp\left(-\frac{W}{kT}\right)} \quad (5.12)$$

where τ_0 is the life time at zero degree Kelvin.

5.4 Results:

5.4.1 Variation of Fluorescence Intensity with Temperature:

The record of the variation of fluorescence intensity at λ_{\max} (the wavelength of maximum intensity at RT) as a function of temperature for single alkaline earth sulphides activated by copper are shown in Figs. 5.2, 5.3 and 5.4 respectively. As is evident the fluorescence intensity decreases in all the cases. However the brightness of phosphors is in the following order SrS:Cu > BaS:Cu > CaS:Cu. There is no significant variation in the trend with the concentration of dopant i.e copper. As there is no change in the pattern of variation of fluorescence intensity with temperature, we have included only selected samples for clarity on the diagram.

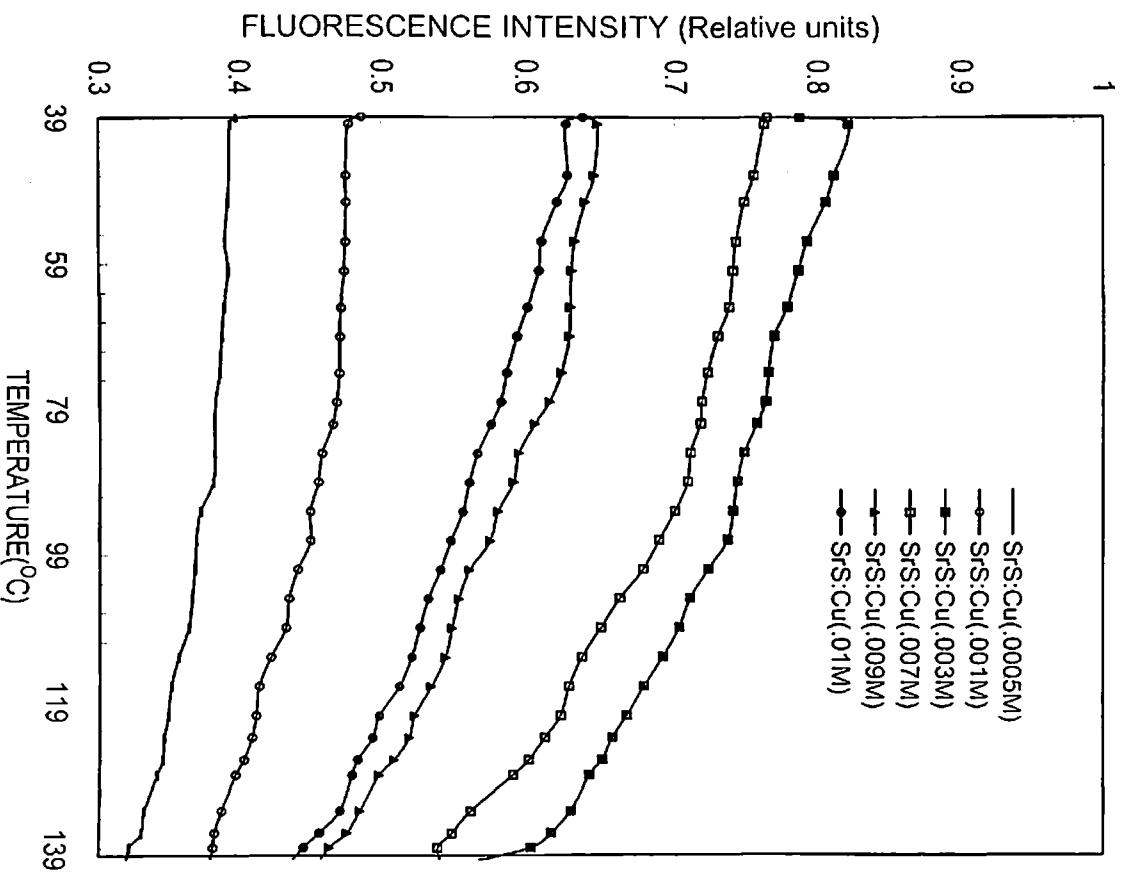


Fig 5.2: Temperature dependence of fluorescence intensity of representative samples of SrS:Cu

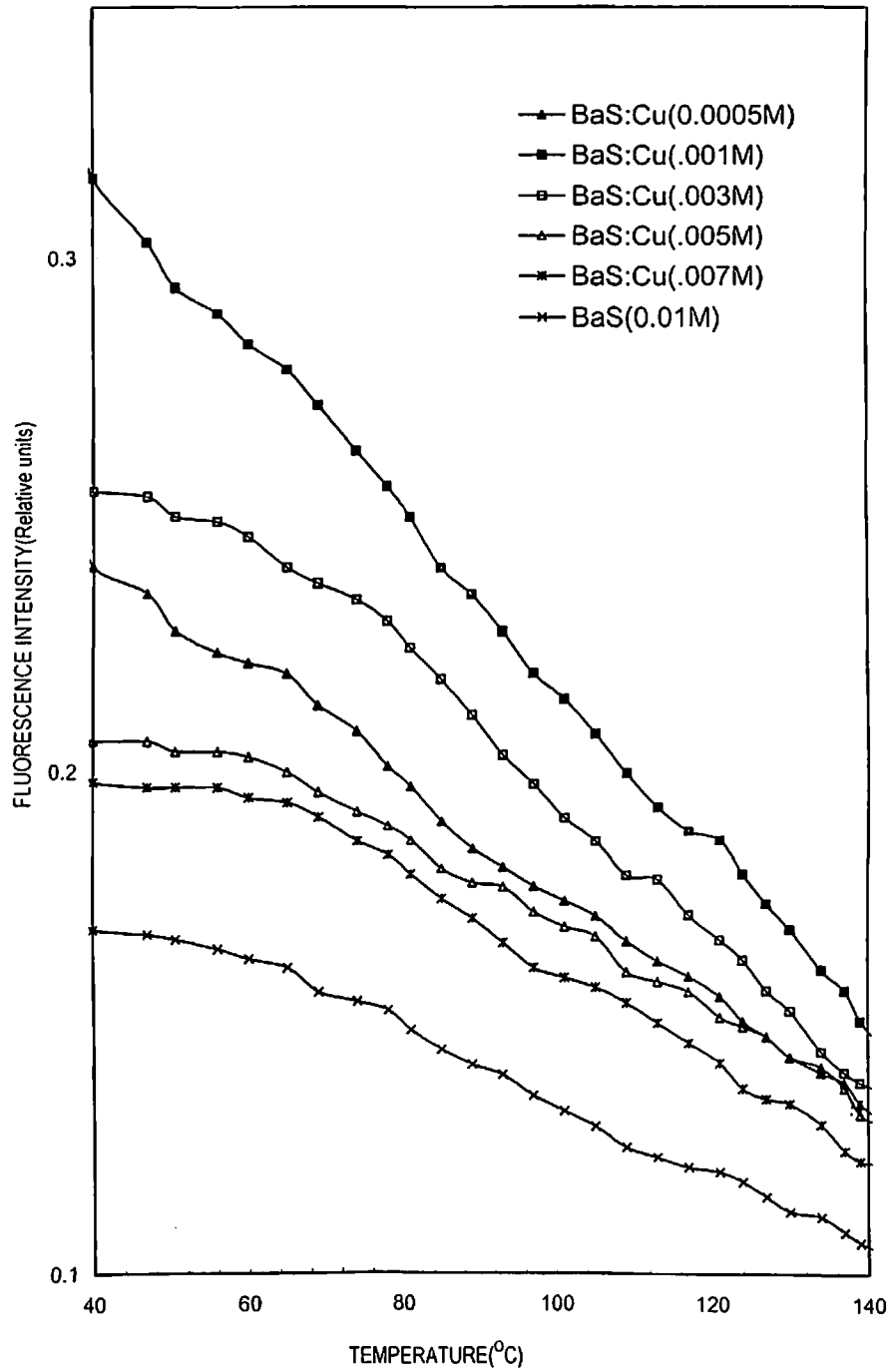


Fig 5.3: Temperature dependence of fluorescence intensity of representative samples of BaS:Cu

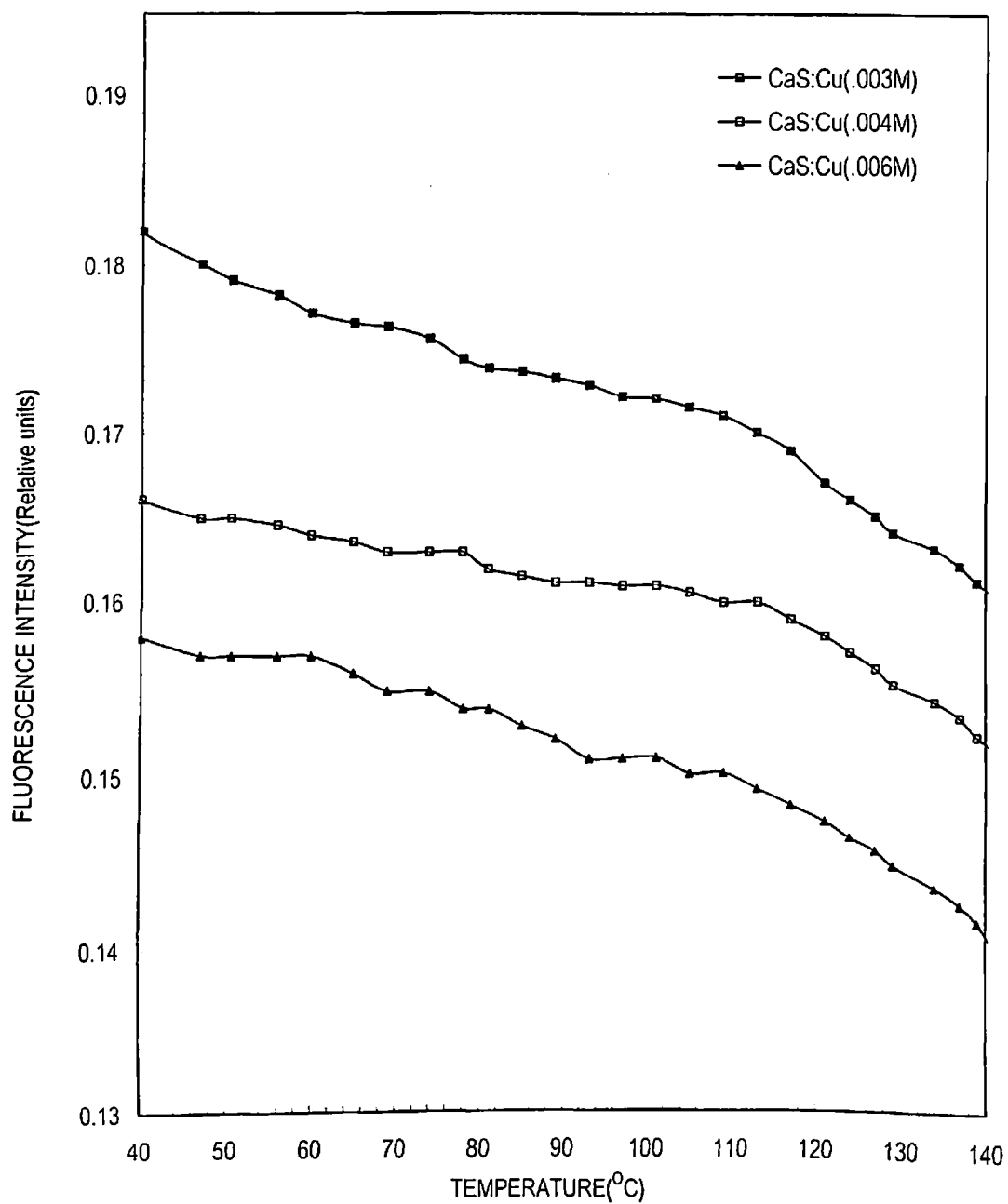


Fig 5.4: Temperature dependence of fluorescence intensity of representative samples of CaS:Cu

In the case of mixed alkaline earth sulphide phosphors this variation has been found to be much more pronounced as shown in Figs 5.5, 5.6, 5.7 for (Sr,Ba)S :Cu, (Sr,Ca)S:Cu, (Ca,Ba)S:Cu phosphors respectively. No shift in λ_{\max} with temperature has been found in any of the phosphors; though all of them exhibited thermal quenching.

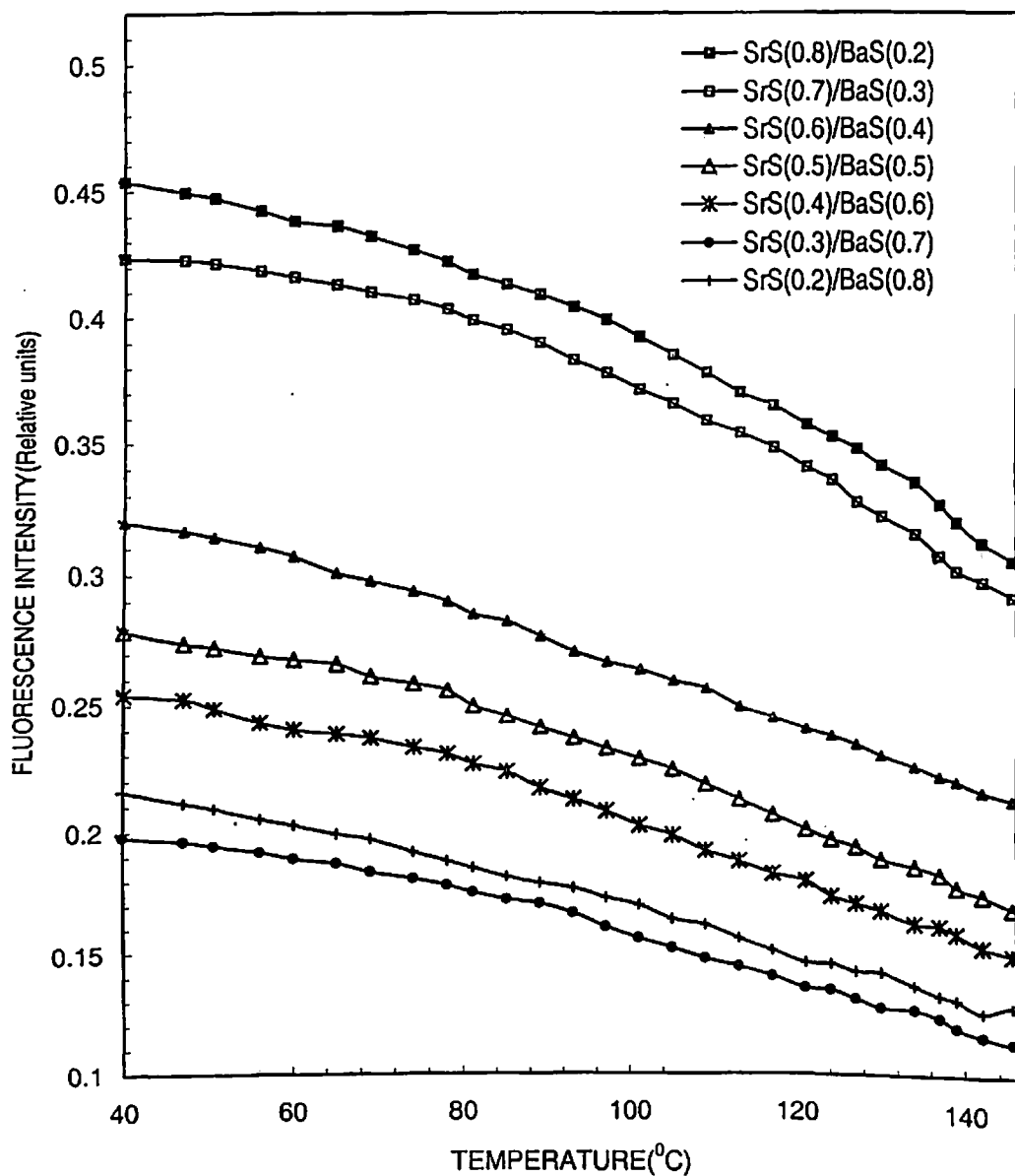


Fig 5.5: Temperature dependence of fluorescence intensity of representative samples of (Sr,Ba)S:Cu

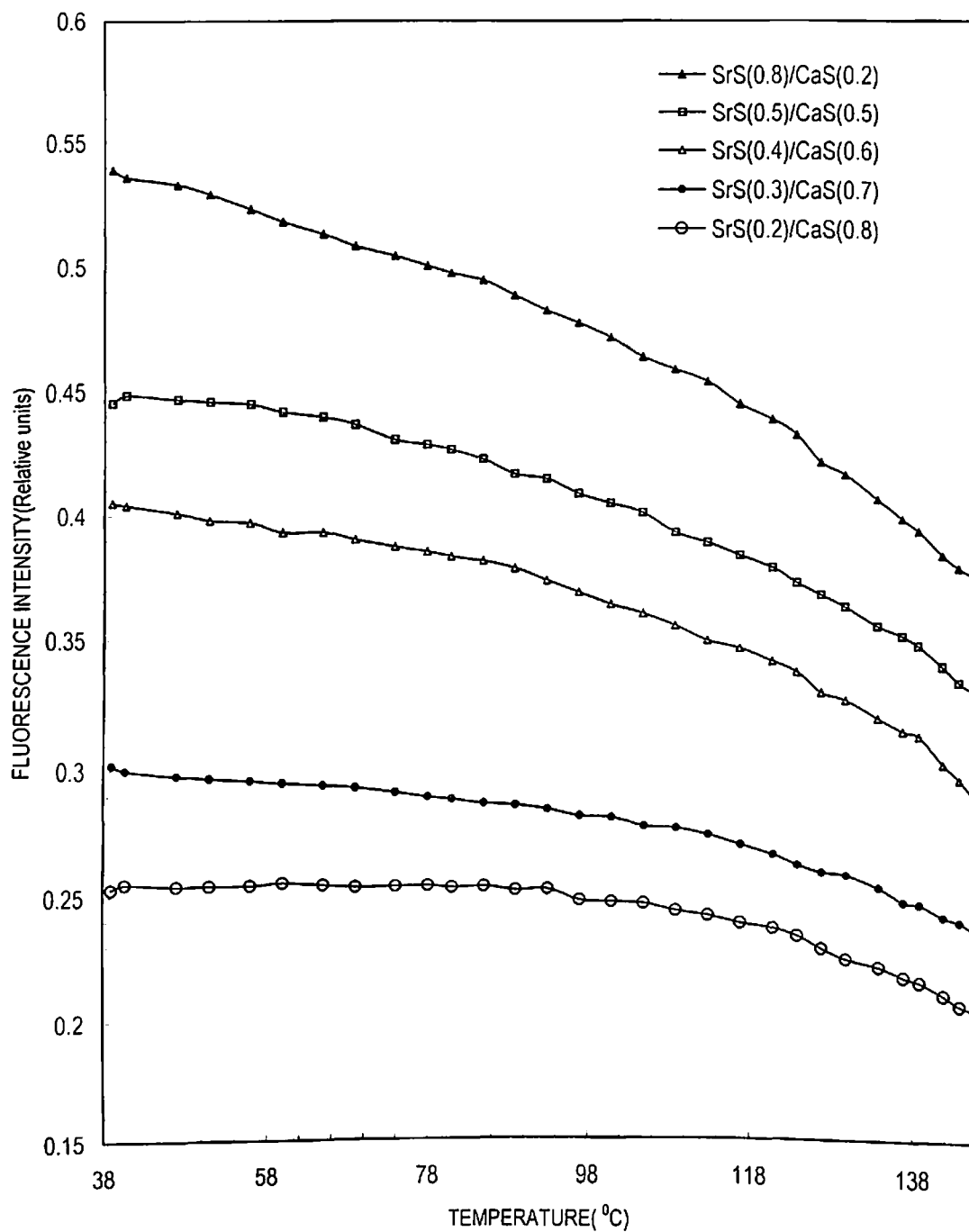


Fig 5.6: Temperature dependence of fluorescence intensity of representative samples of (Sr,Ca)S:Cu

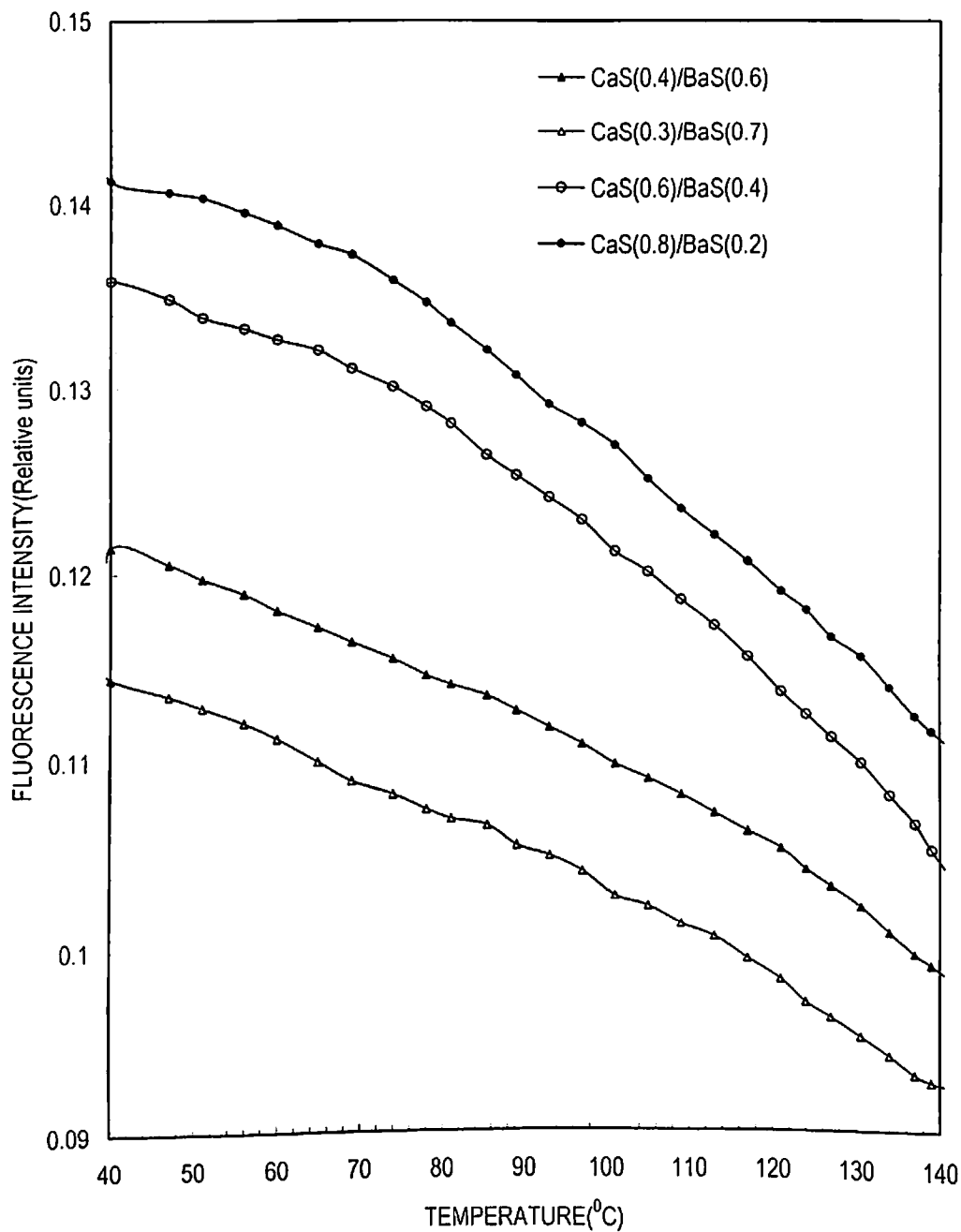


Fig 5.7: Temperature dependence of fluorescence intensity of representative samples of (Ca,Ba)S:Cu

5.4.2 Calculation of Relevant Parameters:

In order to determine the thermal activation energy W and other relevant parameters related to thermal quenching, the plots of logarithm of (I_0/I) as a function of $1/T$ for all the samples have been utilized. Some such representative curves are shown in Fig 5.8. Herein I is fluorescence at temperature $T(K)$ and I_0 is that at RT. The slope of this curve gives the value of W/k . Here the main assumption is that η of eq. (5.3) is analogous to the normalized intensity I/I_0 and that $1/\eta$ is much greater than 1. The results of such calculations are tabulated in table 5.1.

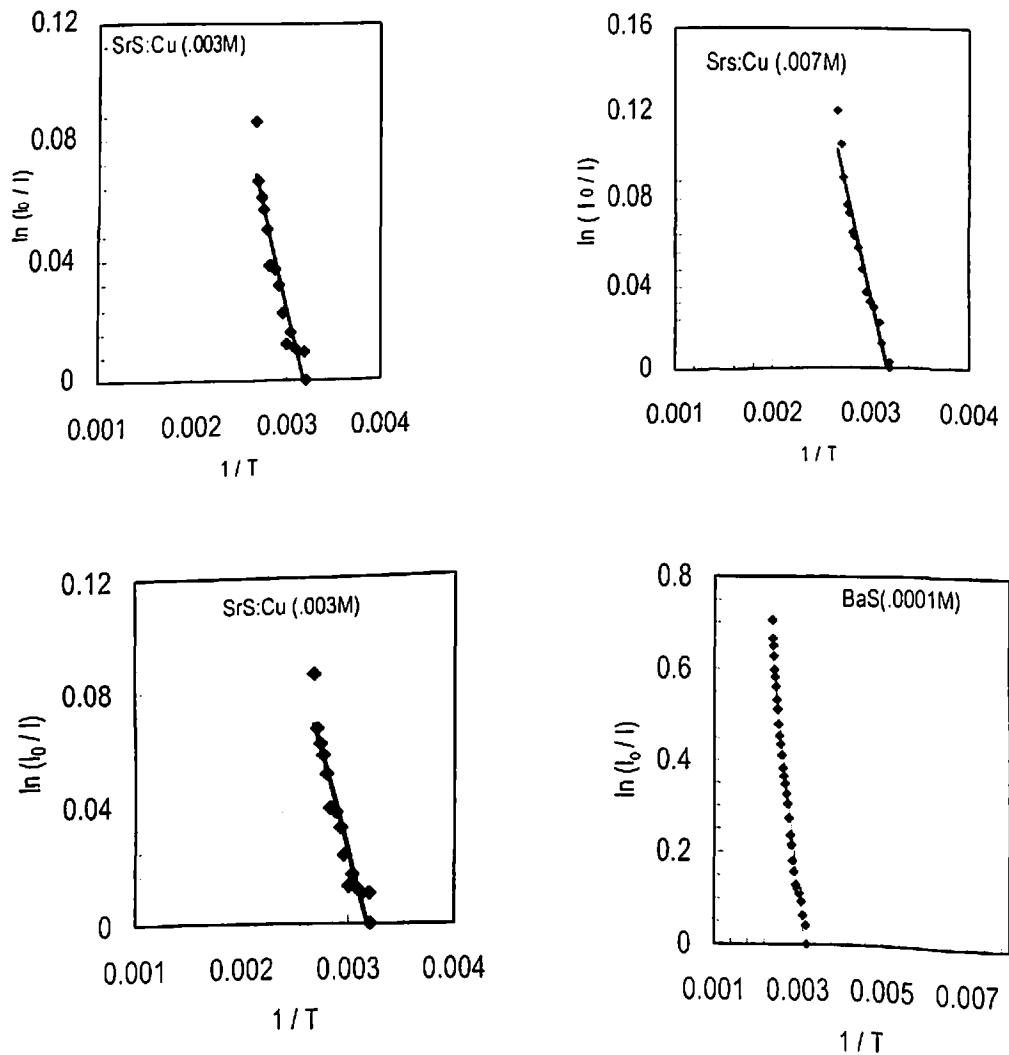


Fig. 5.8 Plots of $\ln(I_0/I)$ versus $1/T$ for representative samples

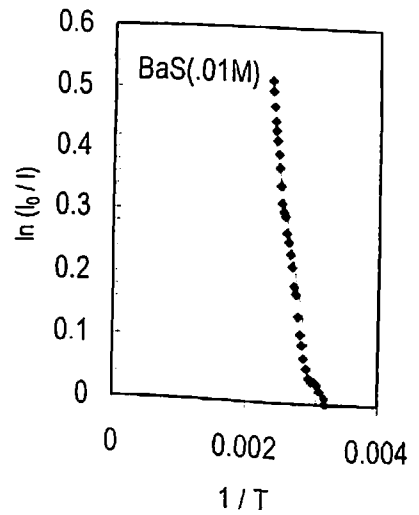
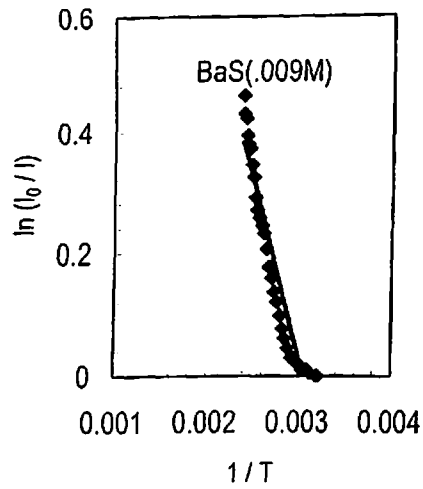
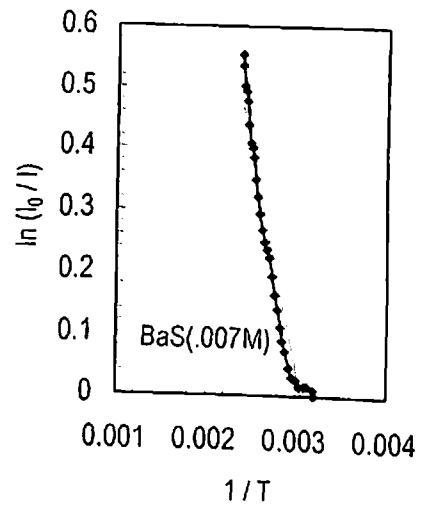
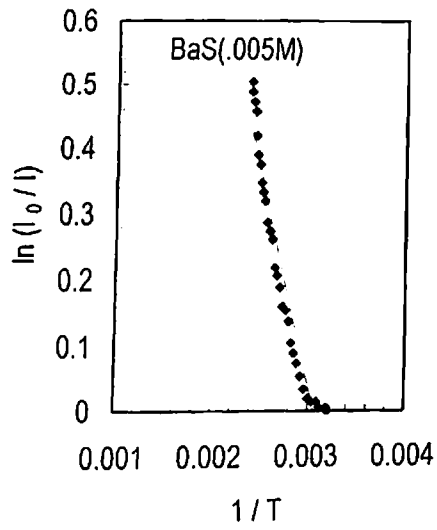
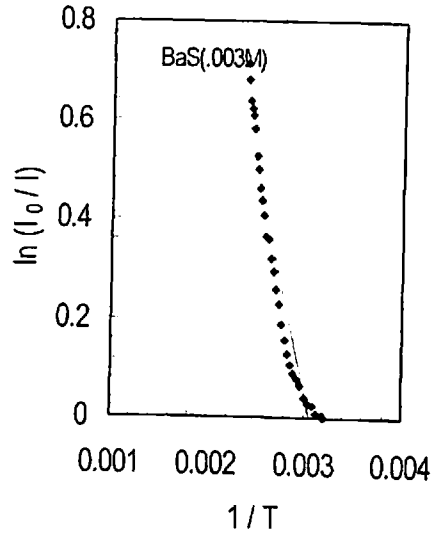
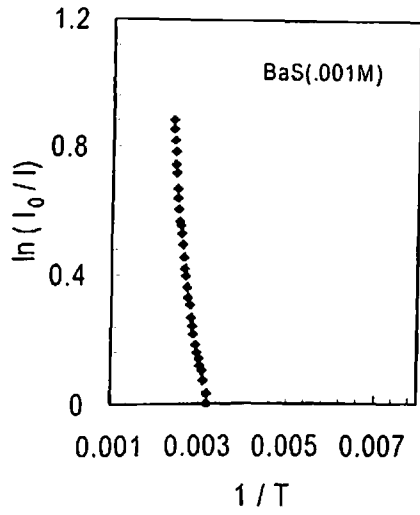


Fig. 5.8 Contd..

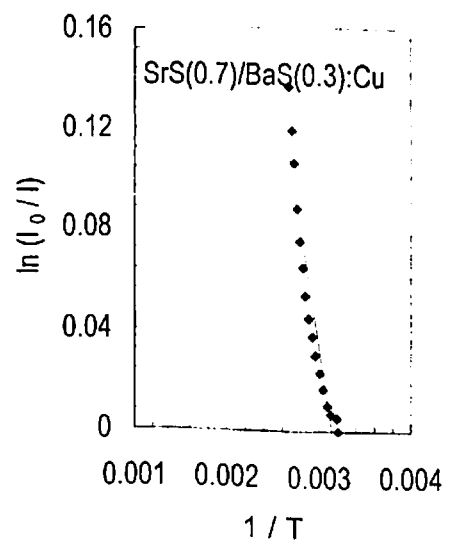
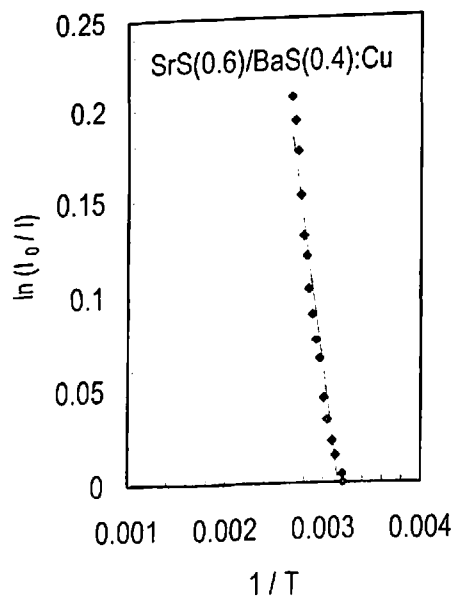
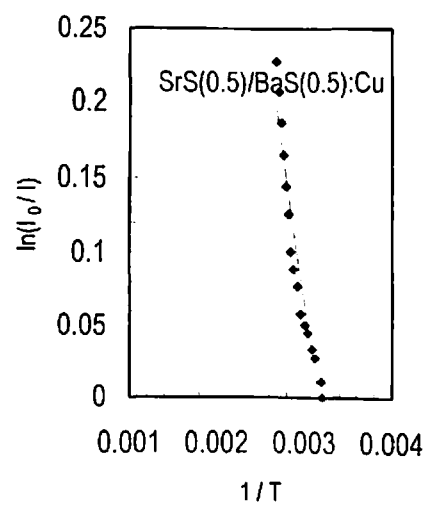
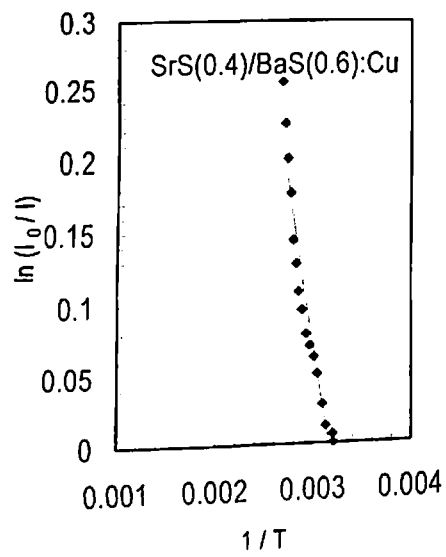
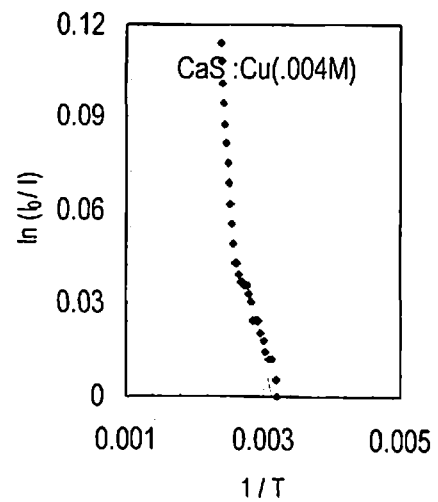
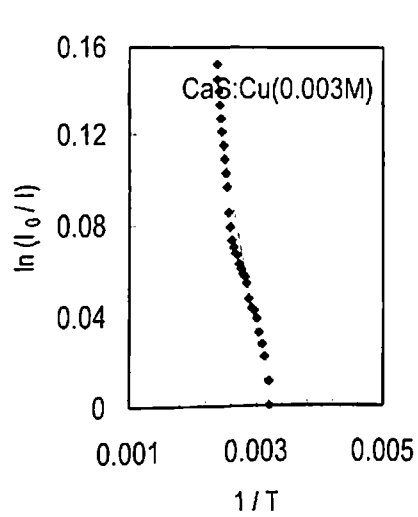


Fig. 5.8 Contd..

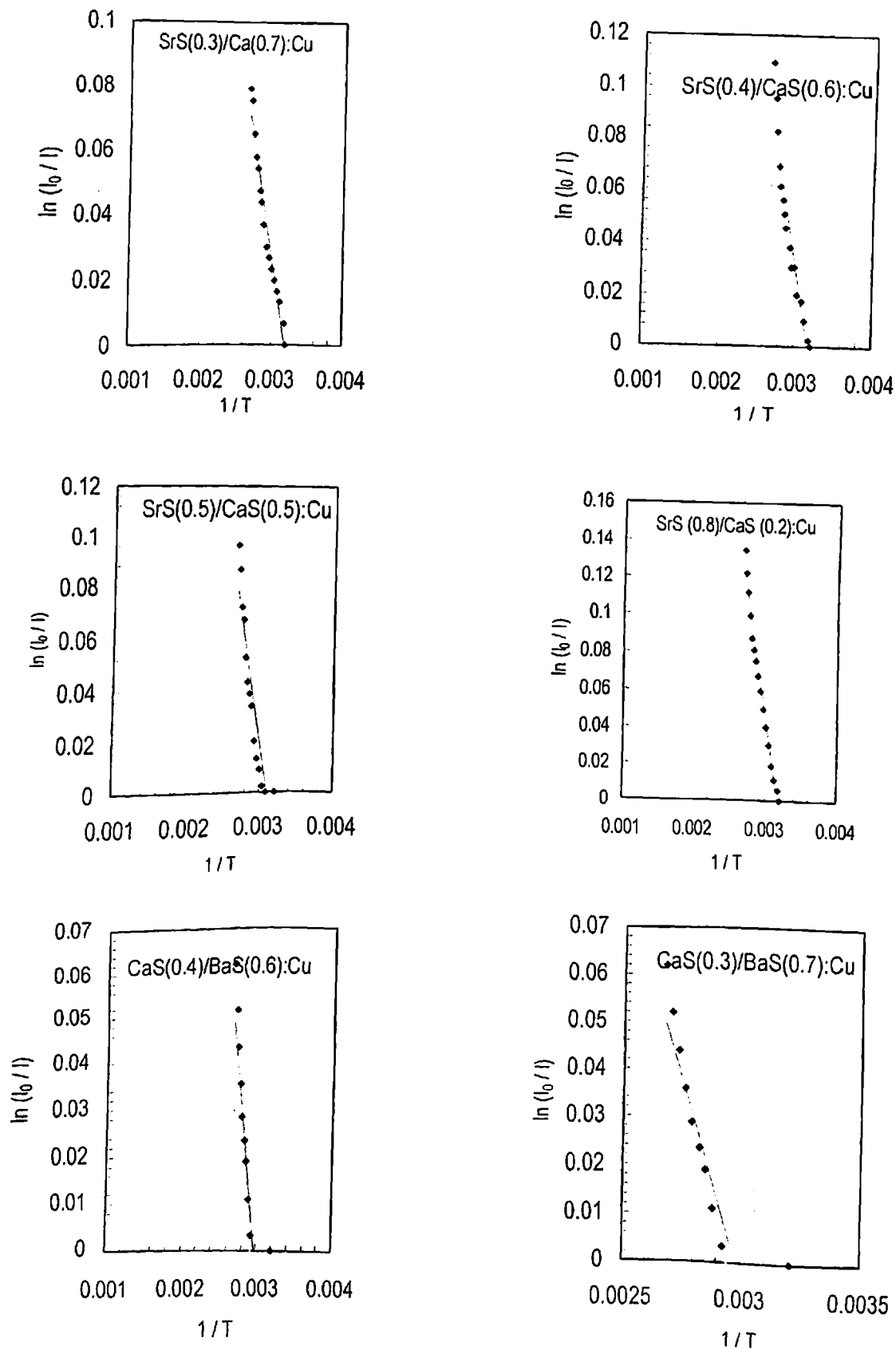


Fig. 5.8 Contd..

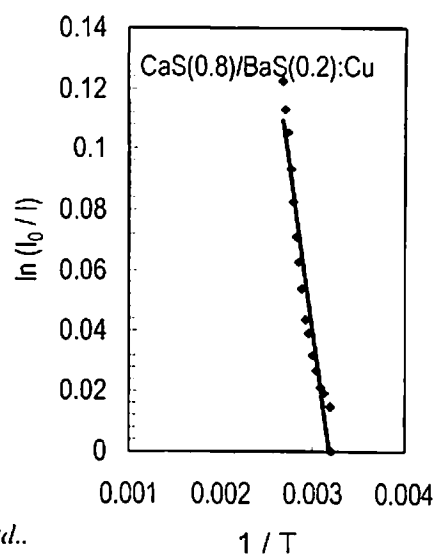
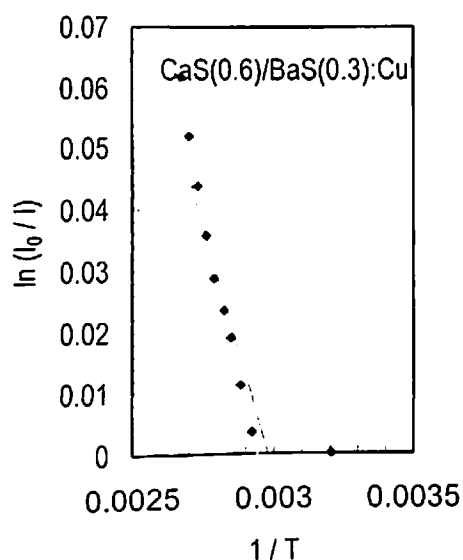


Fig. 5.8 Contd..

Table 5.1: Parameters relevant to thermal quenching for alkaline earth sulphides phosphors

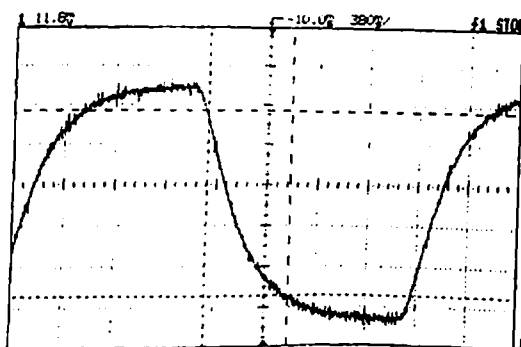
Sample composition	W (eV)	C	T _B	T _H
SrS: Cu (.0005M)	0.235012	24.74589	66.51075	85.16641
SrS: Cu (.003M)	0.350794	24.95964	99.07074	126.7849
SrS: Cu (.005M)	0.392272	25.03652	110.7021	141.6405
SrS: Cu (.007M)	0.382227	25.01789	107.8869	138.0455
SrS: Cu (.01M)	0.425494	25.09822	120.0059	153.5188
BaS:Cu (.003M)	0.444482	25.13353	125.3188	160.3001
BaS:Cu (.005M)	0.341695	24.94279	96.51689	123.5223
BaS:Cu (.007M)	0.373326	25.00138	105.3914	134.8584
BaS:Cu (.009M)	0.278184	24.82544	78.66739	100.7108
BaS:Cu (.01M)	0.361105	24.97874	101.9639	130.4807
CaS:Cu(.003M)	0.134573	24.56149	38.15488	48.88198
CaS:Cu(.004M)	0.098255	24.49504	27.87625	35.7202
CaS:Cu(.006M)	0.134478	24.56131	38.12812	48.84773
(Sr _{0.8} , Ba _{0.2})S: Cu	0.228889	24.73462	64.785	82.95919
(Sr _{0.7} , Ba _{0.3})S: Cu	0.204078	24.68899	57.78844	74.00921
(Sr _{0.6} , Ba _{0.4})S: Cu	0.332158	24.92515	93.83905	120.101
(Sr _{0.5} , Ba _{0.5})S: Cu	0.343888	24.94685	97.1325	124.3088
(Sr _{0.4} , Ba _{0.6})S: Cu	0.383225	25.01974	108.1666	138.4026
(Sr _{0.3} , Ba _{0.7})S: Cu	0.395669	25.04282	111.654	142.8559
(Sr _{0.2} , Ba _{0.8})S: Cu	0.424169	25.09576	119.6352	153.0456
(Sr _{0.8} Ca _{0.2})S:Cu	0.210623	24.70102	59.63459	76.37102
(Sr _{0.5} Ca _{0.5})S:Cu	0.161233	24.61034	45.69154	58.52958
(Sr _{0.4} Ca _{0.6})S:Cu	0.158558	24.60544	44.93577	57.56225
(Sr _{0.3} Ca _{0.7})S:Cu	0.118955	24.5329	33.73646	43.2248
(Ca _{0.8} /Ba _{0.2})S:Cu	0.183249	24.65073	51.90987	66.48763
(Ca _{0.6} /Ba _{0.4})S:Cu	0.140275	24.57193	39.76736	50.94633
(Ca _{0.4} /Ba _{0.6})S:Cu	0.140275	24.57193	39.76736	50.94633
(Ca _{0.3} /Ba _{0.7})S:Cu	0.140275	24.57193	39.76736	50.94633

The calculation clearly shows that the value of constant C is constant for all the samples and is approximately $25 \text{ (s}^{-1}\text{)}$. However the activation energy is different for different phosphors and it has been found to vary from 0.14 to 0.44 eV.

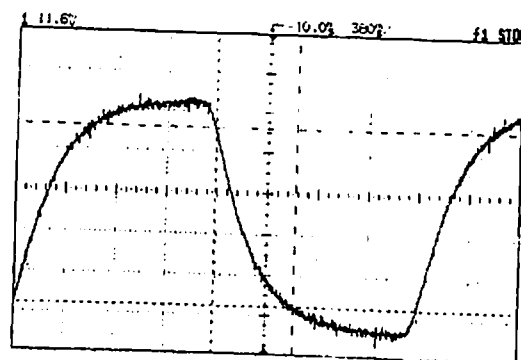
5.4.3 Variation of Lifetime of Fluorescence:

At λ_{MAX} , with pulsed excitation the decay of fluorescence was recorded at different temperatures for all the phosphors. A representative record of rise and decay of fluorescence of typical sample $\frac{1}{2} \text{ (Sr}_{0.7}\text{, Ba}_{0.3}\text{)S:Cu}$ at different temperatures is shown in Fig. 5.9.

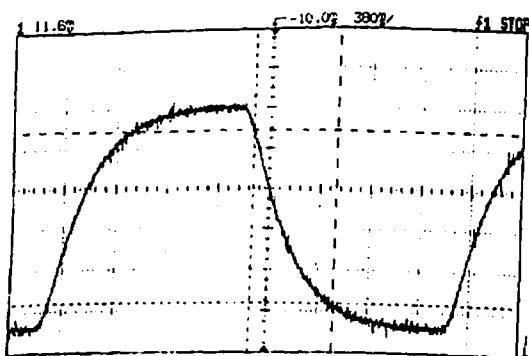
Temperature 36°C



Temperature 44°C



Temperature 55°C



Temperature 67°C

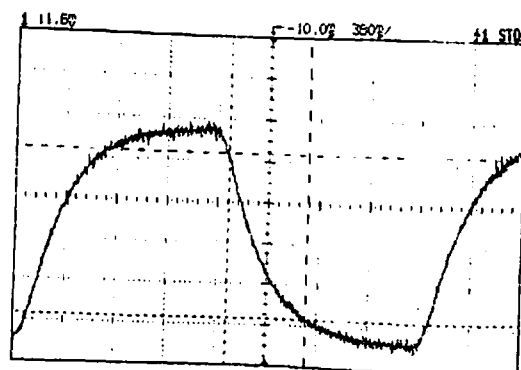
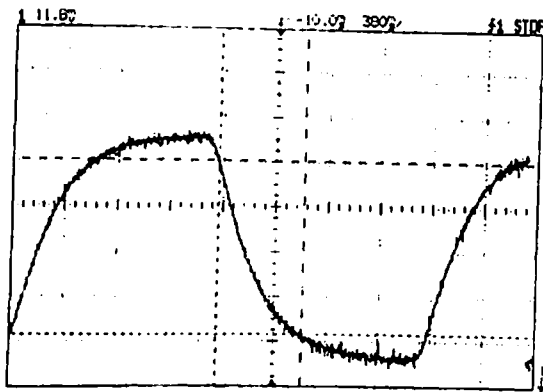
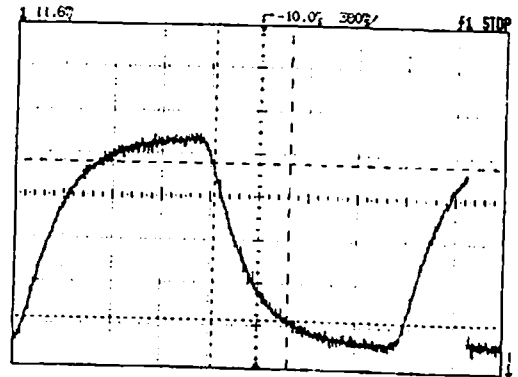


Fig.5.9 Record of Rise and Decay of fluorescence of $\text{(Sr}_{0.7}\text{, Ba}_{0.3}\text{)S:Cu}$ phosphor at different temperatures

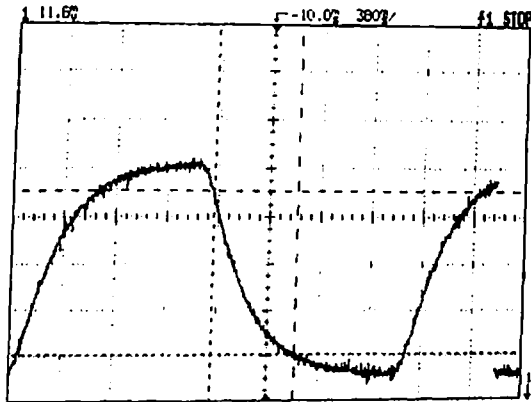
Temperature 77°C



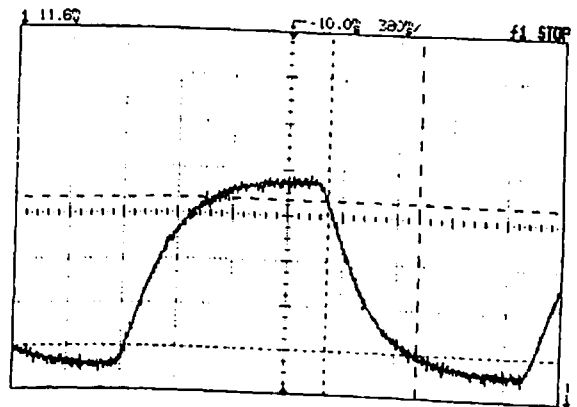
Temperature 87°C



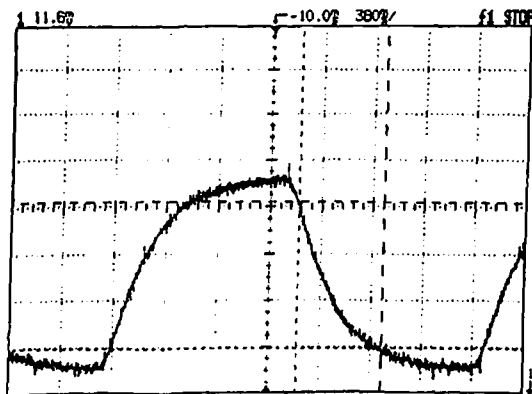
Temperature 97°C



Temperature 107°C



Temperature 117°C



Temperature 125°C

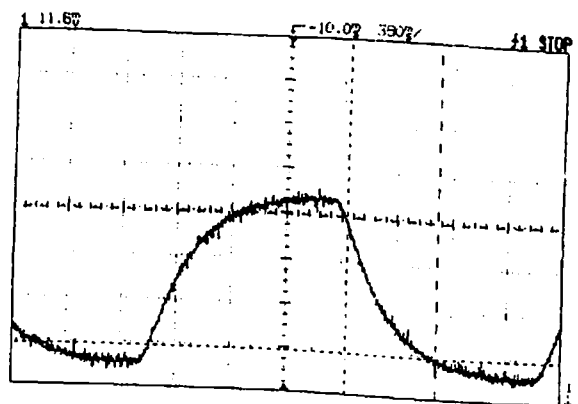
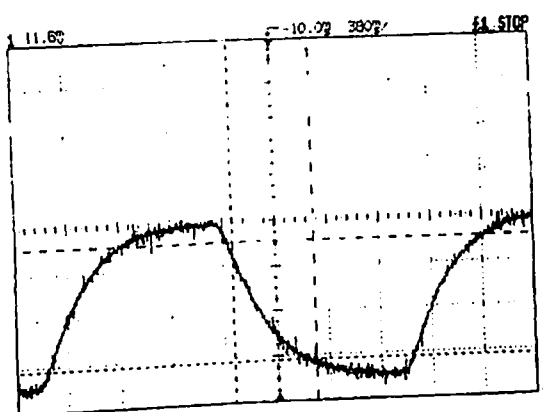
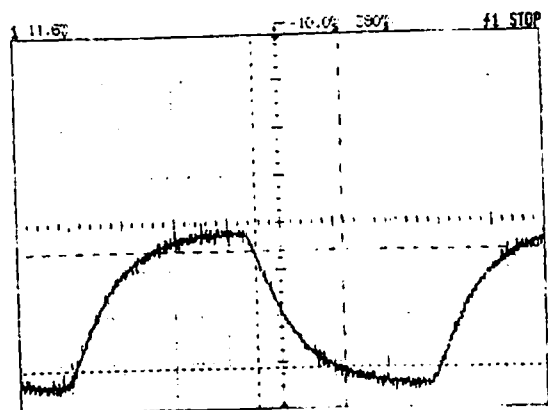


Fig 5.9: Contd...

Temperature 133°C



Temperature 140°C



Temperature 146°C

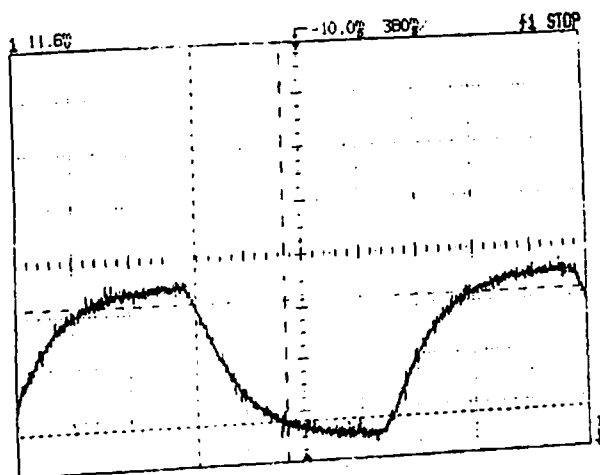


Fig. 5.9: Contd..

From these records, the lifetime of fluorescence at different temperature was determined using eq. 5.9. We utilized these values of τ to calculate the activation energy W involved. For this purpose the plots of $\ln(\tau_0/\tau)$ vs $1/T$ were plotted (where τ_0 is the extrapolated value of lifetime at absolute zero). The slope of this curve gives the value of W/k . These plots of representative samples are shown in Fig. 5.10. The values of W so obtained are listed in Table 5.2.

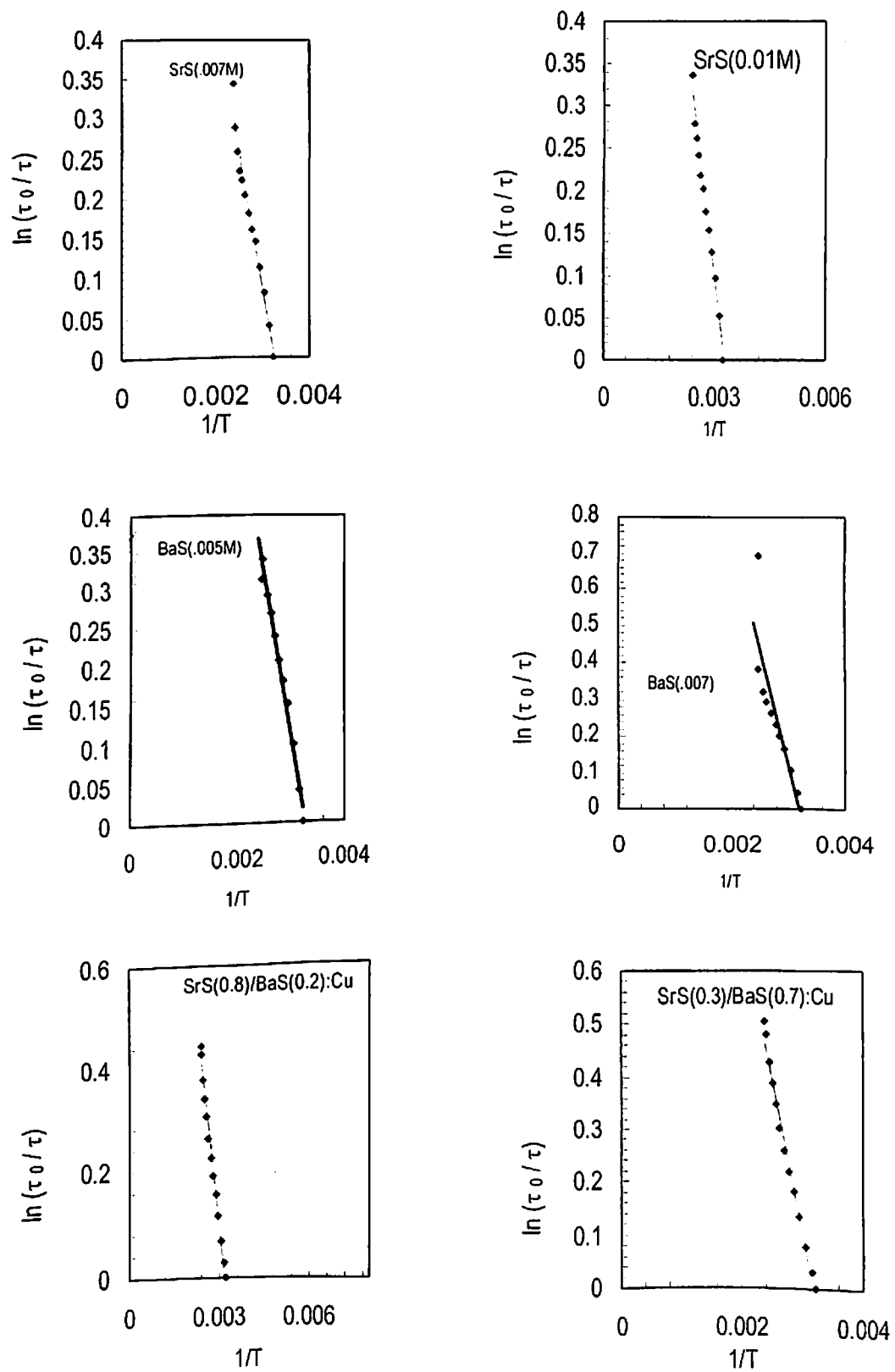


Fig. 5.10 Plots of $\ln(\tau_0/\tau)$ vs. $1/T$ for representative phosphors

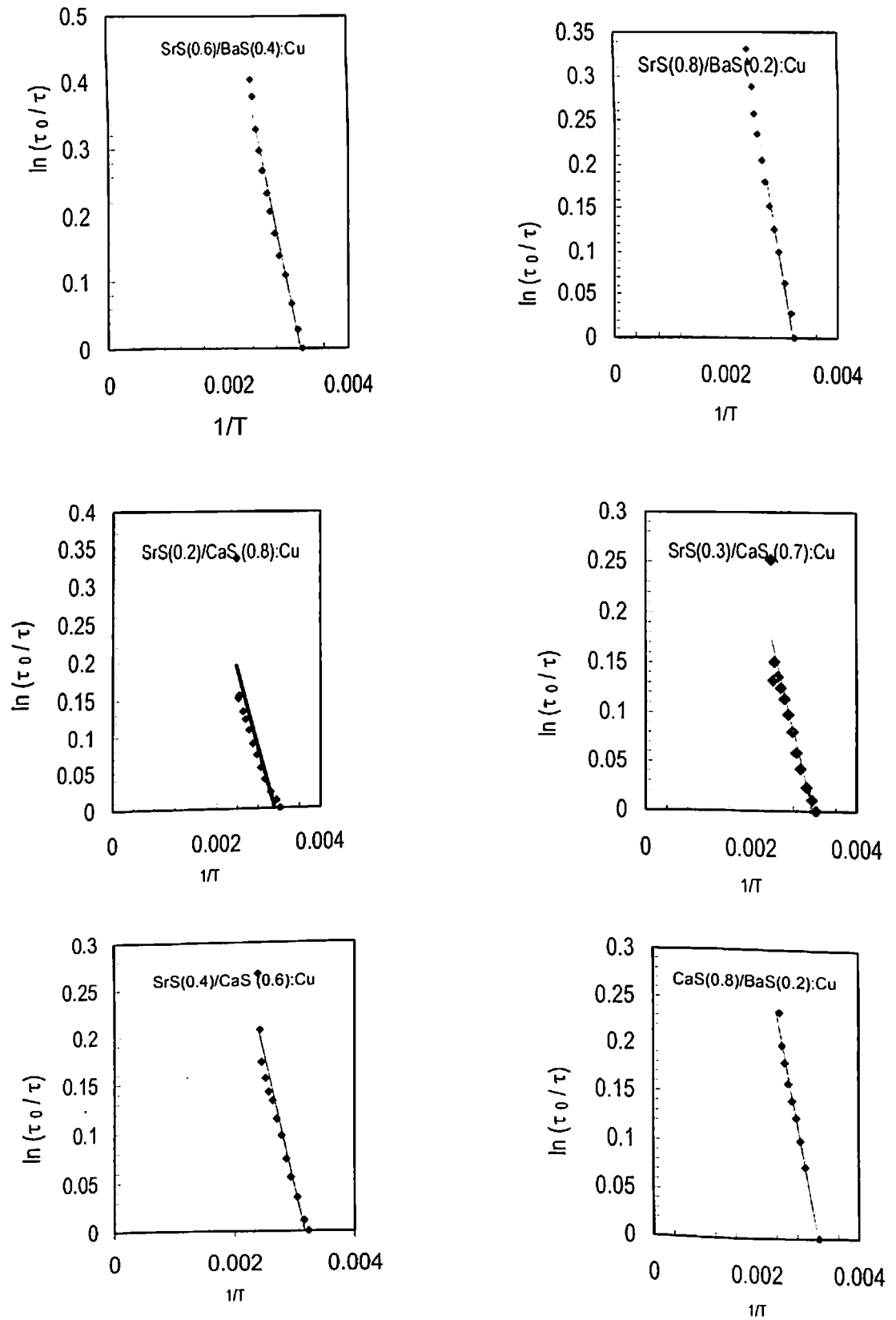


Fig. 5.10: Contd..

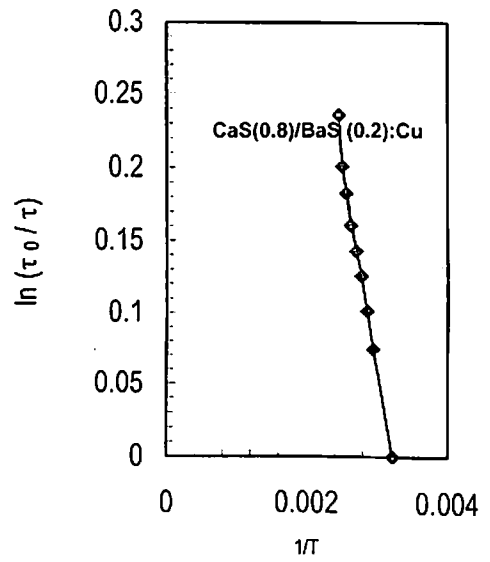
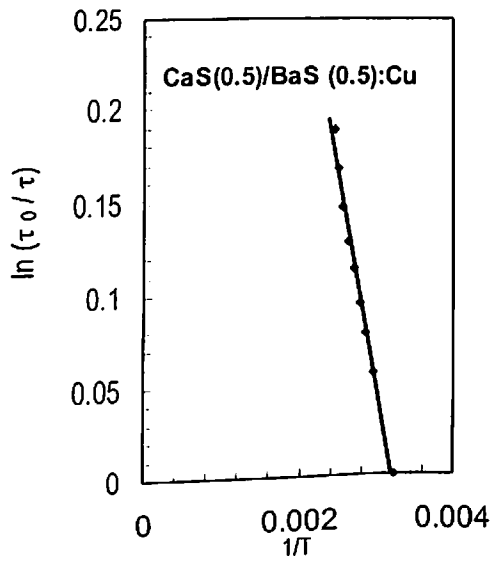
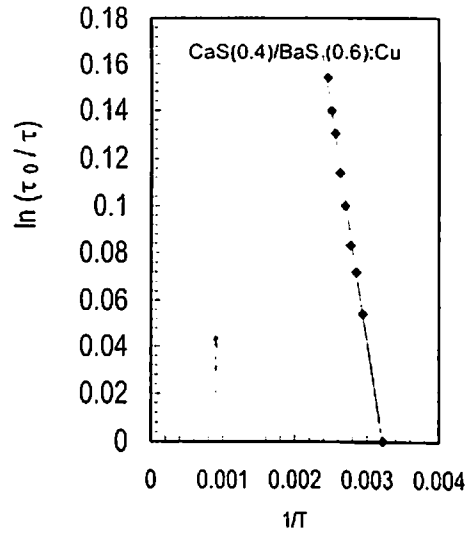
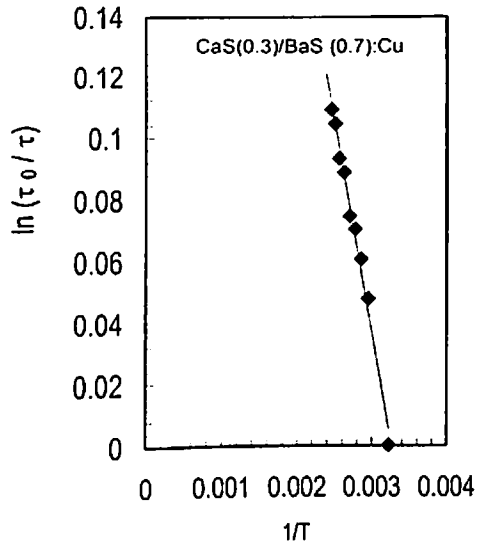


Fig. 5.10 Contd..

Table 5.2: Calculation of W

Sample composition	τ (ms) at room temperature	W (eV)
SrS :Cu (.007M)	380	0.20
SrS :Cu (.009M)	375	0.496
SrS :Cu (.01M)	370	0.312
BaS:Cu (.003M)	467	0.54
BaS:Cu (.005M)	442	0.35
BaS:Cu (.007M)	390	0.54
CaS:Cu(.001M)	385	0.352
CaS:Cu(.002M)	370	0.320
CaS:Cu(.003M)	350	0.310
(Sr _{0.8} , Ba _{0.2})S: Cu	380	0.327
(Sr _{0.6} , Ba _{0.4})S: Cu	304	0.392
(Sr _{0.3} , Ba _{0.7})S: Cu	311	0.504
(Sr _{0.2} , Ba _{0.8})S: Cu	304	0.447
(Ca _{0.8} , Sr _{0.2})S:Cu	360	0.229
(Ca _{0.7} , Sr _{0.3})S:Cu	357	0.195
(Ca _{0.6} , Sr _{0.4})S:Cu	342	0.229
(Ca _{0.5} , Sr _{0.5})S:Cu	350	0.227
(Ca _{0.4} , Sr _{0.6})S:Cu	350	0.186
(Ca _{0.3} , Sr _{0.7})S:Cu	396	0.188
(Ca _{0.2} , Sr _{0.8})S:Cu	364	0.167
(Ca _{0.8} /Ba _{0.2})S:Cu	456	0.25
(Ca _{0.5} /Ba _{0.5})S:Cu	304	0.20
(Ca _{0.4} /Ba _{0.6})S:Cu	350	0.17
(Ca _{0.3} /Ba _{0.7})S:Cu	420	0.11

The values of W obtained by this method are slightly greater than those tabulated in Table 5.1. This is due to the higher slope of $\ln(\tau/\tau_0)$ vs $1/T$ curves. Here τ_0 is the extrapolated value of time constant. These results will be further discussed in chapter 6.

References:

1. H. Kusama, O. J. Sovers, and T. Yoshioka, *Jpn. J. Appl. Phys.*, **15**, 2349, (1976).
2. K. Wickershoim and R. Alves, *Ind Res. Dev.* **21**, 82 (1979).
3. R.R. Sholes and J. G. Small, *Rev Sci. Instrum.* **51**, 692, (1980).
4. T Samulski and P. K. Shrivastava, *Science*, **208**,193, (1980).
5. T Samulski and P. K. Shrivastava, *Phys. Med. Biol.* **27**,107, (1982).
6. J. S. McCormack, *Electron. Lett.*, **17**, 630 (1981).
7. J. R. Alcalá, E. Grattan, and D. M. Jameson, *Anal. Instrum.* **14**, 225 (1985).
8. J. R. Alcalá, E. Grattan, and F. G. Pendergast, *Biophys. J.* **51**, 587 (1987).
9. B. A. Feddersen, D. W. Piston, and E. Grattan, *Rev. Sci. Instrum.*, **60**, 2929 (1989).
10. J.R. Alcalá, *Rev. Sci. Instrum.* **62**, 1672 (1991).
11. J.R. Alcalá, C. Yu and G. J. Yeh, *Rev. Sci Instrum.* **64**, 1554 (1993).
12. B. A. Baukol, J. C. Hitt, P. D. Keir and J. F. Wager, *Appl. Phys. Lett.* **76**, 185 (2000).
13. N. E. Karsunskaya, T. V. Torchinskaya, B. R. Dzhumaev, B. R. Khomenkova, I. Yu, B. M. Bulakh, A. Many, Y. Goldstein, E. Savir, *Semiconductor conference*, **2**, 511 (2000).
14. D. C. Morton, E. W. Forsythe, S. S. Sun, M. C. Wood, M. H. Ervin and K. Kirchner, *Appl. Phys. Lett.* **78**, 1400, (2001).
15. C. S. Gupta, *Indian J. Phys A* , **75**, 535 (2001).
16. M. Gaft, R. Reisfeld, G. Panczer, G. Boulon, T. Saraidarov, S. Erlich, *Opt. Mater.*, **16**, 279 (2001).
17. B. L. Abrams, L. Williams, J. S. Bang, P. H. Holloway, *J. Electrochem. Soc.* **150**, H105 (2003).
18. J. C. Lee, D. H. Park, *Mater. Lett.*, **57**, 2872 (2003).
19. J. M. Fitzgerald, J. G. Hoekstra, R. K. Bansal, J. D. Fowlkes, P. D. Rack, *Mat. Res. Soc. Symp. Proc.*, **780**, Y1.4.1, (2003).
20. P. F. Smet, J. V. Gheluwe, D. Poleman, R. L. V. Meirhaeghe, *J. Lumin.* **104**, 145 (2003).
21. H. A. Klasens, *J. Phys. Chem. Solids*, **9**, 185 (1959).
22. F. A. Kroger, "Some aspects of luminescence of solids", Elsevier, Amsterdam, (1948).
23. M. M. Mishra and D. Sharma, *Indian J. Pure Appl. Phys.* **17**, 419 (1979).
24. H. Witzman & J. Baumann , *Z. Phys, Chem.*, **218**, 55 (1961).

25. J. Buhrow & G. Baumann , Z phys., 48, 3652 (1968).
26. D Curic, "Luminescence in Crystals", Methuen & Co. Lt., New York (1963).
27. K.T.V Grattan, Z. Y. Zhang, "Fiber Optic Fluorescence Thermometry, Chapman and Hall, London, (1995).

Chapter 6

Discussion and Conclusions

6.1 Introduction:

This chapter is devoted to the discussion and interpretation of all the results in the light of existing theories of luminescence. Some inferences have already been drawn and reported in the chapters dealing with specific investigations. Here an attempt has been made to summarize, correlate and discuss these results.

To recall, the aim of present investigation is to synthesize mixed alkaline earth sulphide phosphors activated by copper and study their fluoro-optic behavior to assess their suitability for thermographic applications.

Accordingly, the following studies have been carried out on all the series of phosphors: (i) Recording of X-ray diffraction spectra (ii) Recording of excitation spectra (iii) Recording of fluorescence spectra at RT (iv) Study of the variation of fluorescence intensity at λ_{max} (wavelength of maximum emission) with temperature (v) Recording of lifetime of fluorescence at λ_{max} at RT and (vi) Study of the variation of lifetime of fluorescence at λ_{max} with temperature.

Among the large class of alkaline earth sulphide phosphors, those with a mixed basic substance, namely (Ca,Sr)S, (Sr,Ba)S and (Ca,Ba)S, constitute an important group. These may be unactivated phosphors or ones activated with such elements as Cu, Ag or Au. Activation with copper yields phosphors which emit light in almost the entire visible range – from blue to red. Therefore, they are extensively used in the production of X-ray screen, color television screen, image intensifier, infrared sensor, OSL dosimeter and near infrared to visible converter [1-6]. Despite such important technical applications much less scientific research has been carried out on mixed alkaline earth sulphides.

When the composition of a phosphor is altered by the formation of solid solution with another compound, its emissive properties are likely to be altered. A good example of such a situation is furnished by the solid solution formed by ZnS and CdS [7,8]. In this case a gradual replacement of ZnS by CdS causes a smooth displacement of the maximum in the emission band towards the longer wavelength side. A further example of the same shift in the fluorescence maxima is exhibited by a combination of CdS and CdTe powders [9].

The solid solutions of alkaline earth sulphides have also been investigated by some researchers; (Ca,Sr)S doped with Cu and Nd [10,11], (Ca,Ba)S doped with Cu and Nd [12, 13] and (Sr,Ba)S doped with Cu [14]. Two methods of preparing good solid solutions of alkaline earth sulphides have been reported; one starting from alkaline earth carbonates [15-16], the other starting directly from sulphides [18]. In the present work we preferred to start with alkaline earth sulphates. Single or mixed alkaline earth sulphide phosphors were prepared by firing an intimate mixture of respective alkaline earth sulphates, reducing agent- carbon and the desired amount of activator compound (CuSO_4) in fused silica crucibles at 900°C for one hour. In order to compare the spectral properties of mixed sulphide phosphors with that of single sulphide phosphors, six series of phosphors have been synthesized. They are (i) SrS:Cu (ii) BaS:Cu (iii) CaS:Cu (iv) (Ca,Sr)S:Cu (v) (Sr,Ba)S:Cu and (vi) (Ca,Ba)S:Cu. The composition of these series of phosphor is given in Tables 2.1 to 2.6.

6.2 X-Ray Diffraction (XRD) Spectra:

In order to verify the conversion of sulphates to sulphide and also to ascertain the formation of mixed lattice, XRD spectra of all the series of phosphors have been recorded. The XRD spectra of individual alkaline earth sulphides activated by copper are presented in Figs. 3.6 to 3.8. Sharp lines of XRD demonstrate that the sulphates which are used as starting materials have been converted into respective sulphides. The position of the diffraction lines and related d_{hkl} values match very well with the standards [19]. Following the procedure illustrated by Khare [20], we have obtained the data from XRD of the three individual sulphides which is tabulated in Tables 3.2 to 3.4. This data clearly establishes that all the three sulphides crystallize in the cubic lattice form. Similar results have been reported by Tanaka et al. [21, 22] for copper activated SrS and CaS phosphor powders and thin films. In the powder form the diffraction pattern analogous to NaCl structure have been reported for these phosphors.

The XRD of (Sr,Ca)S:Cu and (Sr,Ba)S:Cu phosphors also exhibit sharp diffraction lines which means that these phosphors are well crystallized in the solid solution with a NaCl type structure. As the XRD is exhibiting only one phase in all the ratios of Ca/Sr and Ba/Sr, it is clear that the solid solution has been formed for the complete range from 0 to 100 mole % for these two series of phosphors. The lattice constant in both the cases increases linearly with increase in x (the fraction of Sr or Ba in the mixed lattice) of $(\text{Ca}_{(1-x)}\text{Sr}_{(x)})\text{S}:\text{Cu}$ and $(\text{Sr}_{(1-x)}\text{Ba}_{(x)})\text{S}:\text{Cu}$ respectively.

This means that these two solid solutions obey Vegard's law. Yamashita [11] has also reported similar results for (Sr,Ca)S:Cu phosphors.

The XRD of (Ca,Ba)S:Cu phosphors show the presence of both the phases for all ratios of CaS/BaS. However the intensities of diffraction lines vary with the change in the content of respective phases. This means that the solid solution of CaS and BaS is not formed. Mishra et al. [12] obtained the relation between lattice constant and concentration of BaS in (Ca,Ba)S:Cu phosphors, which deviates from Vegard's law. The authors have reported that the solid solution is formed within 12 mole % of the content of either phase.

6.3 Excitation and Emission Spectra:

The excitation spectra of single alkaline earth sulphides i.e SrS:Cu, BaS:Cu and CaS:Cu appear to consist of two peaks that are merged to form a single broad band peaking in the range from 0.30 to 0.40 μm . The peaks are not affected by change in concentration of activator; however the intensity changes. In the case of mixed sulphides, as expected, the peak wavelength varies with the change in the ratio of constituent sulphides. Consistent with these results, we have used the radiation of 0.3650 μm wavelength for excitation of fluorescence in all the samples.

The emission spectra of single sulphide phosphors are summarized in Table 6.1. These results have also been compared with that reported in the literature. One of the primary reasons for disagreement of results reported by different authors may be ascribed to the quality of host material and type of flux or co-activator used. Another probable reason is that the Cu ion in alkaline earth sulphides tend to aggregate and form different types of centres [11]

Table 6.1: Summary of emission spectra at RT of single alkaline earth sulphide phosphors activated by Cu

Sulphide	λ_{\max} (μm) observed in the present investigation	λ_{\max} (μm) as reported in the literature
SrS	0.520	0.466, 0.515 [23] 0.471, 0.517, 0.548 [24] 0.478 [25] 0.459, 0.528 [26] 0.490 [27] 0.510 [28] 0.530 [29] 0.520 [30] 0.485 [31] 0.510 [32] 0.520 [33] 0.475 [34]
BaS	0.610	0.585 [14] 0.568, 0.589 [35] 0.518 [36] 0.588 [37]
CaS	0.490	0.413 [25] 0.430 [38] 0.465 [39] 0.480 [28] 0.490 [40] 0.450 [41]

The emission bands in Cu- activated sulphides have been attributed to Cu^+ ions in the lattice and they have been thought to be due to a recombination process as is the case in the well known ZnS:Cu phosphors [42]. Such a model can easily explain two emission bands of SrS:Cu by two different acceptor levels within the SrS band gap due to the coexistence of Cu^+ and some co-activator such as halogenide ions or vacancies[30]. However, in the work done by Yamashita [25], the lightly doped SrS:Cu powder was found to have a broad band emission located at 513 nm at 80 K and it was attributed to the emission from isolated Cu^+ centre. Moreover there is a well established model for Cu^+ doped alkali halides [43] where the luminescence mechanism is based on $3d^{10} \rightarrow 3d^9 4s$ transition of Cu^+ ion. Most of the alkali halides also have same crystal structure as SrS. Fig 6.1 illustrates the energy level diagrams of Cu^+ as a free ion and in the octahedral crystal field. With such model, however, it is difficult to explain the thermal quenching of fluorescence. As discussed in the next section, all the series of phosphors in the present investigation exhibited strong thermal quenching. Therefore, Schon Klasens Model [44] for sulphide appears more applicable in our case. This has been further discussed in the next section.

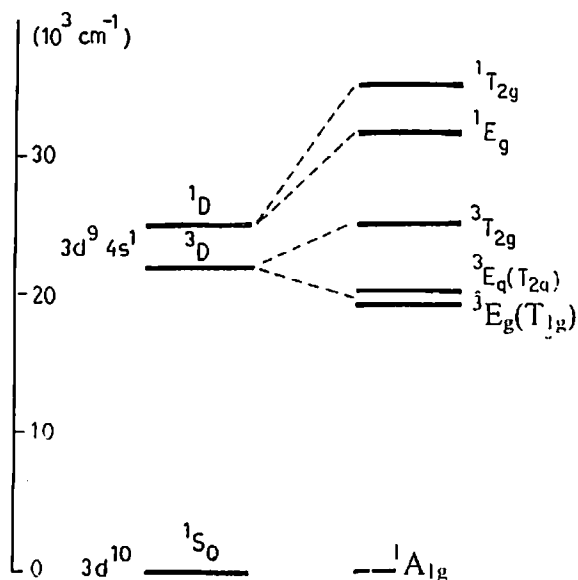


Fig 6.1: Energy level diagrams of a free Cu^+ ion and a Cu^+ ion in octahedral crystal field.

As expected, in the case of $(\text{Sr}_x\text{Ca}_{(1-x)})\text{S}:\text{Cu}^+$ phosphors, as the value of x varies from 0 (for pure $\text{CaS}:\text{Cu}^+$) to 1 (for pure $\text{SrS}:\text{Cu}^+$), the emission peak monotonously shifts from $0.49 \mu\text{m}$ (for pure $\text{CaS}:\text{Cu}^+$) to $0.52 \mu\text{m}$ (for pure $\text{SrS}:\text{Cu}^+$) [see Fig 4.19]. Similarly in the case of $(\text{Ba}_x\text{Sr}_{(1-x)})\text{S}:\text{Cu}^+$ phosphors, as the value of x varies from 0 to 1, the emission peak shifts from $0.52 \mu\text{m}$ to $0.61 \mu\text{m}$ (see Fig 4.20). This behavior further confirms the formation of the mixed lattice in these two cases. The shift in the emission peak may be attributed partially to a change in the band gap and partially to a change in the crystal structure. **This property of these two series of phosphors is interesting from the point of view of tuning of the emitted fluorescence by simply varying the relative fraction of the constituent sulphides.**

The third series of phosphors, namely, $(\text{Ca,Ba})\text{S}:\text{Cu}$ shows phase dominated fluorescence (see Fig 4.21). Thus phosphors with higher fraction of CaS emit $0.49 \mu\text{m}$ whereas those with higher fraction of BaS emit $0.61 \mu\text{m}$. This behavior also shows that the mixed lattice has not been formed. Mishra *et al* [12]. assume that in the case of $(\text{Ca,Ba})\text{S}:\text{Cu}$ phosphors, Cu^+ gives rise to acceptor like levels and S^{2-} vacancies to donor – like levels and that they are associated.

6.4 Temperature Dependence of Fluorescence:

We have already seen in chapter 5 that the fluorescence intensity at λ_{max} (the wavelength of maximum intensity at RT) decreases with increase in all the series of phosphors (refer to Figs. 5.2 to 5.4 for single sulphides and Figs. 5.5 to 5.7 for mixed alkaline earth sulphides). This fall in intensity with temperature is related to the fluorescence efficiency η of the phosphors. The latter is given by

$$\eta = \frac{P_r}{P_r + P_{nr}} \quad (5.1)$$

where P_r is the probability of radiative transitions and the P_{nr} is probability of non-radiative transitions. It is assumed that P_r is almost independent of temperature while P_{nr} rises rapidly with temperature. The latter is given by

$$P_{nr} = s \exp (-W/kT) \quad (5.2)$$

where s is called the frequency factor, W is the thermal activation energy, k is Boltzmann constant and T is temperature (K).

Combining Eq. (5.1) and (5.2), we get

$$\eta = \frac{1}{1 + C \exp\left(-\frac{W}{kT}\right)} \quad (5.3)$$

where $C(=s/P_r)$ is a constant. We have calculated the values of W and C for all the six series of phosphors and these are listed in Table 5.1. The value of C has been found to approximately 25 for all the phosphors but W varies from phosphor to phosphor.

The generally accepted Schon -Klasens Scheme [44] of Fig 6.2 furnishes a simple and interesting explanation of thermal quenching in these phosphors.

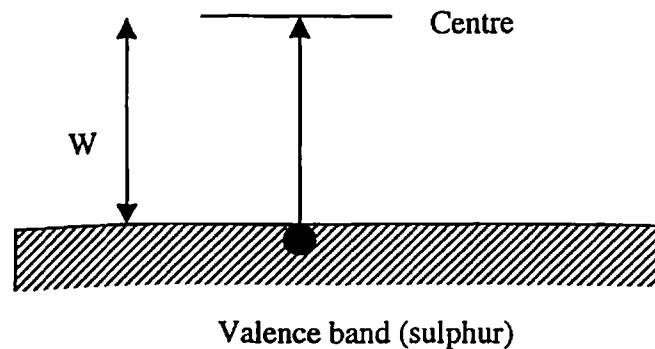


Fig 6.2: Schon -Klasens model for thermal quenching of luminescence in sulphide phosphors

An electron in the valence band can enter a luminescence center by a thermal activation of energy W . The electron previously removed from the center by optical excitation cannot now return and after diffusing in the conduction band for a while will finally recombine via some defect or other non radiative transition.

The temperature dependence of life time τ is also adequately described by the equation

$$\eta = \frac{\tau}{\tau_0} = \frac{1}{1 + C \exp\left(-\frac{W}{kT}\right)} \quad (5.12)$$

where τ_0 is the life time at zero degree Kelvin and other symbols have their usual meaning. In chapter 5 we have used these equations to calculate the value of W , where its order of magnitude has been found to be almost the same as that calculated using equation (5.3).

6.5 Conclusions:

Fiber optic fluorescence thermometry utilizes two properties of the phosphor viz (i) variation of fluorescence intensity with temperature and (ii) variation of life time of fluorescence with temperature. From this point of view, mixed alkaline earth sulphide (Cu) phosphors, synthesized and studied in the present work seem to be the potential candidates for fluorescence thermometry because (i) their fluorescence intensity varies markedly with temperature (at least in the range of investigation from RT to about 150 °C) and (ii) their lifetime also varies with temperature. Furthermore, the peak wavelength of emission can be tuned in $(\text{Sr}_x\text{Ca}_{(1-x)})\text{S}:\text{Cu}$ and $(\text{Ba}_x\text{Sr}_{(1-x)})\text{S}:\text{Cu}$ phosphors by varying the fraction x . The following composition phosphors have been found to be most appropriate for thermographic application (1) $(\text{Sr}_{(0.8)}\text{Ca}_{(0.2)})\text{S}:\text{Cu}(0.003\text{M})$ (2) $(\text{Sr}_{(0.6)}\text{Ba}_{(0.4)})\text{S}:\text{Cu}(0.003\text{M})$ These phosphors may be used in the variety of thermographic applications. Some of these are summarized as follows:

6.5.1 Electrical Machinery:

The immunity of optical signals to electromagnetic interference makes phosphor thermometry very useful in diagnostic studies of electrical machinery. A thermographic phosphor based technique for monitoring the temperature of the rotor in a large turbogenerator may be developed. The motivation for doing this is to seek out any "hot spots" that might develop in the rotor of the generator as a result of several possible causes, including overheated insulation. A pulsed optical source may be used and the light conveyed along an all-silica optical fiber having a larger core diameter (Silica fibers are generally preferred over plastic-clad fibers because of their higher pulsed-power damage threshold and their superior transmission characteristics in the ultraviolet.) A plastic-clad fiber can collect the fluorescence and convey it to a photomultiplier tube. A custom-designed data analysis system may be used to determine the fluorescence decay times. A silicone binder, mixed 50% by weight with phosphor, may be painted in a 5- 10 cm wide stripe around the circumference of the rotor.

Hot spots are also developed in electrical transformers, and fluoro- optic thermometers have been used to determine the temperatures of the windings, the leads and the transformer tank. Other

applications that call for the sensor to function in the presence of large electromagnetic fields include fiber optic thermometry-based measurements of microwave power and rf susceptibility.

6.5.2 Flow Tracing:

Phosphor particles may be used as tracer to aid in visualizing the flows of liquids. Both continuous ultraviolet lamps and the nitrogen laser may serve as sources of illumination for different configuration of this method. ZnS, CdS and CaS phosphors and their combinations have already been used in this technique [45, 46]. Longer lifetimes of alkaline earth sulphide making them particularly well suited for measuring the flow of slowly moving liquids.

6.5.3 Gas Centrifuges:

These phosphors may be used for making non-contact temperature measurement on the gas centrifuges. These devices are large right circular cylinders driven at very high speed. Their function is to separate U^{235} from the natural isotopic distribution in UF_6 gas to create enriched fuel for nuclear power reactors. The flow pattern inside the machine and, hence, the separative efficiency of the centrifuge are affected by thermal variations on the rotor surface. The goal of maximizing separative work performance provided the impetus for developing a remote thermometry system compatible with a high speed mechanism of this type.

6.5.4 Heat Flux:

The determination of heat flux through a surface is important in a variety of scientific and engineering applications. The method may consist of an array of discrete circular and triangular spots of phosphor on the surface to be mounted. The alkaline earth sulphide phosphor may be used for the development of several embodiments of the thermal phosphor-based heat flux gauges.

6.5.5 Particle Beam Characteristics:

Phosphors and other scintillating materials can be used to study the structure of high energy ion and electron beams, indicating the position, profile, and flux density of the beam as a function of phosphor brightness. Also, if the beam current is large enough to heat the material, then an appropriate method of phosphor-based thermometry can be used to diagonalise the beam. Over time, as a significant dose accumulates the phosphors efficiency will deteriorate due to radiation damage. This process, which manifests itself as a decrease in brightness, was first noted

by Birks and Black [47, 48]. They established the relationship between phosphor intensity, I and total accumulated dose, N :

$$I/I_0 = 1 / [1 + (N/N_{1/2})] \quad (6.1)$$

Here, I_0 is the original zero-dose brightness and $N_{1/2}$ is the characteristic dose at which the brightness decreases to one half of the original level. Hence, $N_{1/2}$ is an indicator of phosphor's susceptibility to radiation damage. In recent work, Hollerman *et al* [49, 50] studied the proton-beam induced damage of several common phosphor materials at 3 and 60 MeV, and found that the dose associated with one half decay ranged from $(1-20) \times 10^{15}$ proton/cm². One of the interesting results was that raising the temperature from ambient to 150 °C actually increased $N_{1/2}$ somewhat. Evidently, the higher temperatures promoted some healing of atomic level damage sites. Such information may be of significance in assessing the use of phosphors in nuclear reactor as well as particle beam application. The present set of phosphors can also be used for such an application

6.6 Suggestions for Further Research:

- (i) As new applications for phosphor thermometry arise, there will be a concomitant need for target materials that have luminescence characteristics appropriate to the measurement being undertaken. For instance, although many of the phosphors that have been studied to date emit at the longer visible wavelengths, i.e., at the yellow to red end of the spectrum, some color-sensitive applications might call for a phosphor that emits at shorter wavelengths, near the blue- to- violet end of the spectrum.
- (ii) At higher temperatures, the fluorescence lifetimes of virtually all phosphors are very short. Once the lifetime drops below about 100 μ s, the speed, resolution, and accuracy requirements placed on the data acquisition system typically call for the use of sophisticated transient digitizers and fast pulse analyzers. Equipment of this type is used routinely in nuclear, particle, and laser physics laboratories. If more research is done to adapt it for use in phosphor thermometry systems, then the range over which temperature measurements could be made with this technique might be extended.
- (iii) Improvement in the methods of phosphor bonding would also be welcome. A particularly valuable advance would arise from the development of a technique that would produce thin,

durable, spray-on coatings like those created by flame and plasma deposition, but without the need for high temperature combusting gases and expensive apparatus.

- (iv) Finally, the potential of thermographic phosphors to sense still other physical quantities should be explored.

References:

1. S. Jutamulia, G. Storti, J. Lindmayer, and W. Seiderman, Proc. SPIE, **1151**, 83 (1990)
2. P. Soltani, D. Brower, and G. Storti, Proc SPIE, **1243**, 114 (1990).
3. M. Yoshida, K. Tanaka, K. Taniguchi, T. Yamashita, Y. Kakihara and T. Inoguchi, in Digest 1980 SID International Symposium, San Diego, Society for Information Display, Los Angeles, 106 (1980).
4. T. Suyama, N. Sawara, K. Okamoto and Y. Hamakawa, Jpn. J. Appl. Phys. Suppl. **21**, 383 (1982).
5. S. Tanaka, Y. Mikami, H. Deguchi and H. Kobayashi, Jpn. J. Appl. Phys. **23**, L225 (1986).
6. L. Junjun, Z. Maisheng, Acta. Opt. Sin., **23**, 604, (2003).
7. T. Lukaszewicz, Acta Phys. Polo.; **42**, 515 (1972).
8. T. Lukaszewicz, Acta Phys. Polo.; **43**, 65 (1973).
9. M. A. Santana-Aranda, M. M. Lira, Sociedad Mexicana de Ciencia de Superficies y de Vacío, **10**, 36 (2000).
10. A.M Rastogi, and S.L Mor Phys. Stat. Sol. (b), **63**, 75 (1981).
11. N. Yamashita, K. Ebisumori, and K Nakamura, J. Lumin., **62**, 25 (1994).
12. U.K Mishra, S.L Mor and J.D Ranade; Ind. J. Pure & Appl. Phys., **18**, 6 (1980).
13. A.M Rastogi and S.L Mor; Ind. J. Pure & Appl. Phys., **19**, 1019 (1981).
14. B.B Laud and V.W Kulkarni; Phys. Stat. Sol. (a), **51**, 269 (1979).
15. K. Kato and F. Okamoto, Jpn. J. Appl. Phys. **22**, 76 (1983)
16. F. Okamoto, K. Kato, J. Electrochem. Soc. **130**, 432, (1983).
17. H. Yamamoto, K. Megumi, H. Kasano and O. Kanehisa, J. Electrochem. Soc. **134**, 1571 (1987).
18. H. Kasano, K. Megumi and H. Yamamoto; J. Electrochem. Soc. **131**, 1953 (1984).
19. National Bureau of Standards (USA), Circ 539, 7, 8 & 52 (1957)
20. R. P. Khare, "Analysis Instrumentation: An Introduction, (CBS, New Delhi), 135 (1993).
21. H. Kobayashi, S. Tanaka, V. Shanker, M. Shiiki and H. Deguchi, J. Cryst. Growth, **72**, 559 (1985).
22. S. Tanaka, J. Cryst. Growth, **101**, 958 (1990).
23. W. Lehmann, J. Lumin., **5**, 87 (1972).
24. B. B. Laud and V. W. Kulkarni, J. Phys. Chem. Solids, **39**, 555 (1978)

25. N. Yamashita, *Jpn. J. Appl. Phys.*, **30**, 3335, (1991)
26. F. Altukhova, K. Piir, F. Savikhin, , *Trudy. Inst. Fiz, Akad. Nauk Est. SSR* **54**, 188 (1983).
27. F. Urbach, D. Pearlman and H. Hemmendingr, *J. Opt. Soc. Am.* **36**, 372 (1946).
28. D. Sharma and A. Singh, *Ind. J. Pure &Appl. Phys.* **9**, 810 (1971).
29. N. Singh, G. L. Marwaha and V.K. Mathur, *Phys. Status Solidi A*, **66**, 761 (1981).
30. W. M. Li, M. Ritala M. Leskela, L. Niinisto, E. Soininen, S. S.Sun ,W. Tong and C.J.Summers, *J. Appl. Phys.*, **86**, 5017 (1999).
31. J. Youngchore, S. M. Blomqno, D. C. Morton, *Appl. Phys. Lett.*, **80**, 4124 (2002).
32. D. Wruck, R. Boyn, M. Wienecke, F. Henneberger, U. Troppenz, B.huttl, W.Bohne, B. Reinhold, and H.E. Mahnke *J. Appl. Phys.* **91**, 2847, (2002).
33. K. Ohmi, K. Yamable, H. Fukada, T. Fujiwara, S. Tanaka, and H. Kobayashi, *Appl. Phys. Lett.* **73**, 1889, (1998).
34. W. Park, T. C. Jones and C. J. Summers, *Appl. Phys.Lett.* **74**, 1785 (1999)
35. M. L. Yu Allsalu, E. P. Efanova, A. I. Lebedeva, V. V. Lebedeva, V. V. Mikhailin, E. Yu Pedak and A.A. Plachev, *J. Appl. Spectros*, **31**, 1441(1979).
36. V. L. Rabotkin an, T. N. Stroganova, *Bull, Acad. Sci. USSR, Phys. Scr. (USA)* **30**, 1575 (1966).
37. W. Lehmann, *J. Electrochem.Soc.* **117**, 1389 (1970).
38. A. Wachtel, *J. Electrochem. Soc.*, **107**, 199 (1960).
39. M. Avinor, A. Carmi and Z. Weinberger, *J. Chem. Phys.* , **35**, 1978, (1961).
40. A.K. Uppal, S.N. Chaturvedi, and N. Nath, *Ind. J. Pure. & Appl. Phys.*, **25**, 72, (1987).
41. 39. C.S. Gupta, *Ind. J.Pure Appl. Phys.* **36**, 765 (1998).
42. R.Pandey, and S. Sivaraman, *J. Phys.Chem. Solids*, **52**, 211 (1991).
43. D. S. McClure and S.C. Weaver, *J. Phys. Chem. Solids* **52**, 81 (1991).
44. H. A. Klasens, *J. Phys. Chem. Solids*, **9**, 185 (1959).
45. N. Nakatani, K. Fujiwara, M. Matsumoto, and T. Yamada, *J. Phys. E* **8**,1042 (1975).
46. N. Nakatani and T. Yamada, in *Flow Visualization II: Proceedings of the Second International Symposium on Flow Visualization*, edited by W. Merzkirch, Hemisphere, New York, , 215 (1980).

47. J. B. Birks and F. A. Black, Proc. Phys. Soc. London, Sec. A **64**, 511 (1951).
48. J. B. Birks, Theory and Practice of Scintillation Counting (Macmillan, New York, (1964).
49. W. A. Hollerman, J. H. Fisher, G. A. Shelby, L. R. Holland, and G. M. Jenkins, IEEE Trans. Nucl. Sci. **38**, 184 (1991).
50. W. A. Hollemlan, J. H. Fisher, G. A. Shelby, L. R. Holland, and G. M. N. Jenkins, IEEE Trans. Nucl. Sci. **39**, 2295 (1992).

List of Publications

Part of this work has been communicated for publication in the following journals:

1. Spectrally tunable and temperature sensitive fluoro-optic behavior of $[\text{Sr}_x\text{Ba}_{(1-x)}]\text{S}:\text{Cu}$ Phosphors: K. C. Sati & R. P. Khare
Smart Materials and Structures (USA)
2. Thermographic properties of $[\text{Sr}_x\text{Ca}_{(1-x)}]\text{S}:\text{Cu}$ phosphors: K. C. Sati & R. P. Khare
Journal of Materials Science (USA)
3. Phase- dominated temperature sensitive fluorescence of $(\text{Ca},\text{Ba})\text{S}:\text{Cu}$ phosphors: K. C. Sati & R. P. Khare
Physica Status Solidi (a) (Germany)

Biography

R. P. Kharę is presently Professor of Physics/Instrumentation at Birla Institute of Science and Technology, Pilani. A PhD in Optical Materials, he has published several research papers in Indian and International journals and has 27 years of teaching and research experience. He has authored two books, namely i) Analysis Instrumentation An Introduction (CBS) and ii) Fiber Optics and Optoelectronics (Oxford University Press).

K. C. Sati is presently Scientist 'B' in Gas Dynamic Laser Section of Laser Science and Technology Center (Ministry of Defense, Govt. of India). Earlier he was Lecturer at BRCM, College of Engineering and Technology, Bahal. He has done M. Tech in Laser Science and its application from Devi Ahiliya University Indore and M. Sc. in physics with the specialization in Electronics from D. S. B Campus Kumoun, University Nainital. He has completed his PhD work from BITS, Pilani.